

AD-752 249

DIVERSITY TECHNIQUES FOR AIRBORNE
COMMUNICATIONS IN THE PRESENCE OF GROUND
REFLECTION MULTIPATH

Henry Berger, et al

Massachusetts Institute of Technology

Prepared for:

Air Force Systems Command

September 1972

DISTRIBUTED BY:

NTIS

National Technical Information Service
U. S. DEPARTMENT OF COMMERCE
5285 Port Royal Road, Springfield Va. 22151

MASSACHUSETTS INSTITUTE OF TECHNOLOGY
LINCOLN LABORATORY

DIVERSITY TECHNIQUES FOR AIRBORNE COMMUNICATIONS
IN THE PRESENCE OF GROUND REFLECTION MULTIPATH

H. BERGER
J. E. EVANS

Group 44

TECHNICAL NOTE 1972-27

8 SEPTEMBER 1972

Approved for public release; distribution unlimited.

ib

LEXINGTON

MASSACHUSETTS

The work reported in this document was performed at Lincoln Laboratory, a center for research operated by Massachusetts Institute of Technology, with the support of the Department of the Air Force under Contract F19628-73-C-0002.

This report may be reproduced to satisfy needs of U.S. Government agencies.

DIVERSITY TECHNIQUES FOR AIRBORNE COMMUNICATIONS
IN THE PRESENCE OF GROUND REFLECTION MULTIPATH*

ABSTRACT

The signal power reduction due to multipath fading is an important design consideration in the development of air-air and ground-air communication links at L-band. A first order mathematical model of ground reflection multipath is used to predict the relationship between the depth of fading and environmental parameters such as surface roughness and the terminal positions relative to earth. The model is then used to investigate two techniques for reducing the loss in received signal power: frequency diversity and antenna height diversity. A measurement program to experimentally evaluate the applicability of antenna height diversity is outlined.

Accepted for the Air Force
Nicholas A. Orsini, Lt. Col., USAF
Chief, Lincoln Laboratory Project Office

* This study was conducted in support of the program of the Communications Development Division, Deputy for Planning and Technology of the USAF Electronic Systems Division.

TABLE OF CONTENTS

	<u>Page</u>
Abstract.....	iii
I. INTRODUCTION AND SUMMARY.....	1
II. DIVERSITY TECHNIQUES.....	6
2.1 Interference Model.....	7
2.2 Analysis of Diversity Techniques.....	17
2.2.1 Variation in Surface Reflections.....	17
2.2.2 The Effect of Terrain Curvature.....	21
2.2.3 Antenna Height Diversity.....	27
2.2.4 Frequency Diversity.....	30
2.2.5 Coverage.....	32
2.3 Assessment of Fade Margin Selection on Spatial Regions of Usefulness of Diversity Techniques.....	35
2.4 Assessment of Ground Roughness on Benefits from Diversity Techniques.....	43
2.5 Communication Between a High Altitude Transmitter and Low Altitude Receivers.....	59
2.6 Limitations of the Analysis.....	67
2.6.1 Atmospheric Effects.....	67
2.6.2 Geometric Effects.....	67
2.6.3 Propagation Effects.....	69
2.6.4 Antenna Effects.....	69
2.6.5 Diffuse Reflection Effects.....	70
2.6.6 Some Other Effects.....	72
III. A MEASUREMENT PROGRAM TO EVALUATE ANTENNA HEIGHT DIVERSITY.....	73
3.1 Measurements Required.....	73
3.2 Receiver Measurement Equipment.....	79
3.3 Transmitter Measurement Equipment.....	85
3.4 Topics to be Addressed.....	95

TABLE OF CONTENTS (Cont.)

	<u>Page</u>
APPENDIX A Fresnel Zone Considerations	97
APPENDIX B Optimum Spacing of Antennas (Frequencies) in a Height (Discrete Tone) Diversity System.....	101
APPENDIX C Statistical Aspects of Estimating the Resultant Signal Power	106
APPENDIX D A First-Order Model of Multipath Reflections From Nonsmooth Surfaces	114
APPENDIX E Combining of Diversity Outputs.....	134
REFERENCES.....	138

LIST OF FIGURES

<u>Figure</u>		<u>Page</u>
1	Ray geometry for curved earth.	8
2	Specular scattering coefficient vs apparent surface roughness.	11
3	The fraction F of airspace for which fades are equal to or greater than 3 db and 10 db vs. reflection coefficient of scattering surface.	14
4	The received signal power (in arbitrary units) vs. the vertical receiving antenna altitude (in feet) at two distances (measured along the earth's surface) of the transmitting from the receiving antenna. The transmitter altitude is taken as 10 miles, and the magnitude of the specular reflection coefficient is taken as 1.0.	16
5	The magnitude of the reflection coefficient, R, of smooth flat terrain vs. the angle of incidence, θ , for dry soil and sea water.	18
6	Antenna and frequency diversity limits, terrain reflection and divergence limits for 3 db fades in the presence of smooth terrain illustrated in the space of reflection angle (α_r) - receiver altitude above a curved earth (h_r) when $r_1 = r_2$.	20
7	Antenna and frequency diversity limits, terrain reflection and divergence limits for 10 db fades in the presence of smooth terrain illustrated in the $\alpha_r - h_r$ space when $r_1 = r_2$. Unlike the case of 3 db fades the numerical values are 2^2 such that the terrain reflection and divergence must be combined into a single set of curves.	22
8	Antenna and frequency diversity limits, terrain reflection and divergence limits for 3 db fades in the presence of smooth terrain illustrated in the space of reflection angle (α_r) - receiver altitude above a curved earth (h_r) when $r_2 \gg r_1$.	24
9	Antenna and frequency diversity limits, terrain reflection and divergence limits for 10 db fades in the presence of smooth terrain illustrated in the $\alpha_r - h_r$ space when $r_2 \gg r_1$.	26
10	The geometry of the direct and reflected electric fields (a) at the first antenna (b) at the second antenna.	29

<u>Figure</u>		<u>Page</u>
11	Space coverage in h_r -d space by four antenna spatial diversity system. The dotted lines are those for which Eq. (34) is exactly satisfied.	34
12	Antenna and frequency limits, smooth terrain reflection and divergence limits for 3 db fades illustrated in h_r -d space when $r_1=r_2$.	40
13	Antenna and frequency diversity limits, smooth terrain reflection and divergence limits for 10 db fades illustrated in the h_r -d space when $r_2=r_1$.	41
14	Antenna and frequency diversity limits, smooth terrain reflection and divergence limits for 3 db fades illustrated in h_r -d space when $r_2 \gg r_1$.	44
15	Antenna diversity limit, terrain reflection and divergence limits for the 10 db case in the presence of smooth terrain illustrated in h_r -d space when $r_2 \gg r_1$.	45
16	Antenna and frequency diversity limits, non-smooth terrain reflection and divergence limits for the 3 db case with $\sigma=4$ feet illustrated in α_r - h_r space when $r_2 \gg r_1$.	48
17	Antenna and frequency diversity limits, non-smooth terrain reflection and divergence limits for the 10 db case with $\sigma=4$ feet illustrated in α_r - h_r space when $r_2 \gg r_1$.	49
18	Antenna and frequency diversity limits, non-smooth terrain reflection and divergence limits for the 3 db case with $\sigma=4$ feet illustrated in α_r - h_r space when $r_2=r_1$.	50
19	Antenna and frequency diversity limits, non-smooth terrain reflection and divergence limits for the 10 db case with $\sigma=4$ feet illustrated in α_r - h_r space when $r_2=r_1$.	51
20	Antenna and frequency diversity limits, non-smooth terrain reflection and divergence limits for the 3 db case with $\sigma=4$ feet illustrated in h_r -d space when $r_2=r_1$.	53
21	Antenna and frequency diversity limits, non-smooth terrain reflection and divergence limits for the 3 db case with $\sigma=4$ feet illustrated in h_r -d space when $r_2 \gg r_1$.	55

<u>Figure</u>		<u>Page</u>
22	Antenna diversity limits, non-smooth terrain reflection and divergence limits for the 10 db case with $\sigma=4$ feet illustrated in h_r -d space when $r_2=r_1$.	57
23	Antenna diversity limits, non-smooth terrain reflection for the 10 db case with $\sigma=4$ feet illustrated in h_t -d space when $r_2 \gg r_1$.	58
24	Receiver altitude vs. interaircraft separation measured along smooth curved ground for 3 db fades when the transmitter altitude is 50,000 feet.	60
25	Receiver altitude vs. interaircraft separation measured along rough ($\sigma=4$ ft.) curved ground for 3 db fades when the transmitter altitude is 50,000 ft.	61
26.	Receiver altitude vs. interaircraft separation measured along smooth curved ground for 10 db fades when the transmitter altitude is 50,000 ft.	62
27	Receiver altitude vs. interaircraft separation measured along rough ($\sigma=4$ ft.) curved ground for 10 db fades when the transmitter altitude is 50,000 ft.	63
28	In-flight received signal processing prior to recording.	81
29	In-flight received signal power monitoring.	82
30	Generation of tones for frequency diversity.	82
31	Post-flight signal processing.	82
32	Block Diagram of Transmitter.	86
A-1	First Fresnel zone geometry for a flat reflecting plane.	98
B-1	Region of diversity usefulness vs. generalized transmitter-receiver geometry.	104
B-2	Region of diversity usefulness vs. generalized transmitter-receiver geometry with logarithmic separations.	104
C-1	Receiver to estimate the resultant signal power.	107
D-1	A representation of rough surface scattering.	118

<u>Figure</u>	<u>Page</u>
D-2	Roughness factor as a function of roughness and elevation angle. 125
D-3	The specular scattering coefficient vs. apparent ocean roughness. 127
D-4	The RMS value of diffuse scattering coefficient vs. apparent ocean roughness (from data in [5]). 130
D-5	The scattering coefficient of diffuse power reflected vs. apparent surface roughness. 131
D-6	The scattering coefficient model for specular $ \rho_s ^2$ and diffuse $ \rho_r ^2$, power reflection. 133
D-7	The diffuse scattering coefficient vs. apparent surface roughness for satellite-aircraft geometries. The data from fig. 11 of reference 9 was used to construct the smooth curve. The model is from Eq. 21. 133
E-1	The geometry of direct and reflected electric fields at the lowest antenna and at a higher antenna. 136
E-2	Possible antenna diversity combining scheme. 136

SECTION 1 INTRODUCTION AND SUMMARY

The signal power reduction due to multipath fading is an important design consideration in the development of air-air and ground-air communication links at L-band. A first order mathematical model of ground reflection multipath is used to predict the relationship between the depth of fading and environmental parameters such as surface roughness and the terminal positions relative to earth. The model is then used to investigate two techniques for reducing the loss in received signal power: frequency diversity and antenna height diversity.

The results suggest that significant reductions in fading due to reflection multipath can be obtained by both diversity techniques, but that antenna height diversity is substantially better for low altitude receivers. A measurement program to experimentally evaluate the applicability of antenna height diversity is outlined.

The first order mathematical model is based on assuming that the field strength E at the receiving antenna is given by

$$E = E_d \{1 + DR_0 \rho_s e^{j(\phi_s + \phi_L)}\}$$

where

E_d = direct ray field strength

R_0 = classical reflection coefficient magnitude for the polarization used.

ϕ_s = classical reflection coefficient phase shift for the polarization used

ϕ_L = phase lag of the reflected signal with respect to the direct signal

D = divergence factor which takes into account the effect of the curved surface of the earth on the amplitude of reflection

ρ_S = specular scattering coefficient due to surface roughness
= $\exp [- \{ (4\pi\sigma \sin \alpha_r / \lambda)^2 / 2 \}]$

and σ is the rms height of the surface irregularities, λ the wavelength, with α_r the reflection angle. The above model in the absence of surface roughness is the "classical" ray picture of electromagnetic energy propagation [1]. The curvature of the ray paths due to vertical variations of the refractive index is taken into account by considering the ray paths as straight lines, but replacing the earth's radius R_E in any calculation by an effective earth's radius of $(4/3) R_E$. In addition, we assume that the antenna gain patterns are isotropic and that the lengths of the direct and indirect ray paths are comparable so that the normal signal strength attenuation due to distance is comparable for rays traversing the two paths.

The reflected energy from a non-smooth surface may be decomposed into specular and diffuse constituents [2]. Significant multipath fading occurs only when the specular component is by far the greater of the two constituents (e.g., at very low reflection angles). In Appendix D it is shown that when the specular component is large, theory and experiment indicate that to a good degree of approximation the specular component is given by the classical expression with R_0 replaced by $\rho_S R_0$.

In Table 1, we summarize a few representative cases when vertical polarization is used. Also shown in Table 1 is the improvement obtained by using frequency diversity and antenna diversity.* Clearly fading due to the destructive interference caused by ground reflection multipath is predominately a low altitude phenomena. For the cases presented it is apparent that at receiver altitudes in excess of 1 kft fades in excess of 10 db should not be experienced except over smooth dry soil.

The vertical antenna separation required for use of antenna height diversity on an aircraft can be realized in a variety of ways, e.g., locating one antenna at the top of the tail and another under the aircraft. With suitable diversity combining of the antenna outputs, this configuration can significantly reduce fading due to both aircraft shielding and reflection multipath. For cases presented in the Table it is clear that a mere 9 ft. of vertical antenna separation suffices to significantly reduce the maximum receiver altitude at which fades greater than 10 db can be experienced. As indicated, roughly comparable results can be realized with frequency diversity.

For frequency diversity to be effective in combating multipath fading, the bandwidth must at least be comparable to the reciprocal of the differential time delay between the direct and the specularly reflected path. For

* The analysis of the diversity systems is based on assuming the signals to be discrete tones. Although the frequency diversity improvement shown strictly applies only to systems using several discrete tones, the results are comparable to what would be obtained using other good bandspread waveforms [15]. An interesting subsidiary result of our analysis (see Appendix B) was that the "optimal" distribution of vertical separations (discrete tones) in a height(frequency) diversity system is to generate separations that are logarithmically spaced (i.e., the k th separation = maximum separation / F^{k-1} where F depends on the depth of fade to be alleviated).

Table 1. Maximum Receiver Altitude With Possible Fades in Excess of 10 db (at 1 GHz).

Environmental Parameters		Maximum Receiver Altitude for Fades Exceeding 10 db (in K ft)			
Terrain	RMS Roughness (ft.)	No Diversity	Antenna Diversity (9' or Vertical Separation)	Frequency Diversity (10 MHz Spread Spectrum)	
Transmitter Altitude Much Greater Than Receiver Altitude	Dry Soil	5.0	0.1	0.5	
	Sea	0.5	0.1	0.4	
	Dry Soil	0.7	0.1	0.5	
	Sea	0.2	0.1	0.2	
Transmitter and Receiver at the Same Altitude	Dry Soil	10.0	1.0	1.0	
	Sea	0.8	0.7	0.7	
	Dry Soil	1.0	0.7	0.9	
	Sea	0.5	0.4	0.5	

a ground or near ground located antenna this is often an impractical technique for combating ground reflection multipath because of the small differential delay between the direct path and the multipath return. Antenna height diversity can offer significant improvement with omnidirectional antennas. The improvement would be less spectacular if the ground based antenna used directivity to suppress the multipath return.

The remainder of this report is organized as follows: Section 2 provides a more complete discussion of the ground multipath reflection interference as well as an extensive graphical description of the usefulness of the two diversity techniques. Two aspects are studied at length. The first is fade margin selection. This is considered here to be the selection of the maximum reduction in signal below the free space value which the system parameters chosen will permit. The fade margin selection will affect the spatial regions of diversity usefulness. The 3 dB and 10 dB cases are used for numerical results. The second aspect studied at length theoretically is the limiting effect of ground roughness on the need for diversity techniques.

Some of the critical parameters used in assessing the practical utility of antenna height diversity cannot be satisfactorily assessed with the data at hand (e.g., airframe effects on the antenna pattern, spatial variations in refractive index, the non-stationary character of real terrain). Section 3 (together with Appendices A and C) outlines a measurement program to experimentally evaluate the application of antenna height diversity. The measurements required are discussed in terms of:

- (1) The nature of the transmitter-receiver link
- (2) Flight profile
- (3) Numbers of antennas and frequencies

SECTION 2

DIVERSITY TECHNIQUES

The diversity techniques to be considered involve:

- (1) Two or more frequencies received at one antenna for frequency diversity, and
- (2) Two or more antennas spatially separated some non-zero distance for spatial diversity.

The primary concern in this work is vertical spatial diversity for airborne and ground antennas but frequency diversity is considered for the sake of comparison. Although the general ideas are old (e.g., see [1] for some early experiments), the frequency band and the frequency spread considered (10 MHz) apparently have not been considered previously and the manner in which the results are expressed appears to be new. This section will cover:

- (1) The theoretical model of the multipath interference.
- (2) Analytical and graphical description of the above diversity techniques.
- (3) An assessment of the fade margin selection on the spatial regions of diversity usefulness.

- (4) An assessment of the effect of ground roughness on the spatial regions of diversity usefulness.
- (5) A discussion of the limitations of the analysis.

2.1 INTERFERENCE MODEL

For simplicity, the ray picture of electromagnetic energy propagation will be used in the discussion of the interference model. This represents a simplification of the exact wave theory and supposes that electromagnetic energy radiates outward along trajectories whose geometry is determined by the variation of refractive index according to the laws of geometric optics. Thus, in free space the ray paths are straight lines while in the atmosphere they are curved lines. The effect of the lower atmosphere can be taken into account [1] in an approximate but convenient fashion by considering the ray paths as straight lines but replacing the earth's radius R_E in any calculation by an effective earth's radius R_e which is usually taken as $(4/3)R_E$. Interference takes place at a receiving antenna, between a direct ray from the transmitting antenna and an indirect ray which emanated from the transmitter and was reflected off the earth's surface toward the receiving antenna.

When the surface is smooth, the area of the surface from which the received rays have been reflected is primarily the 1st Fresnel zone [2], an elliptically shaped area whose dimensions and orientation are determined by geometry of the locations of the transmitting and receiving antennas relative to the curved earth. This antenna geometry is illustrated in Figure 1, and the details

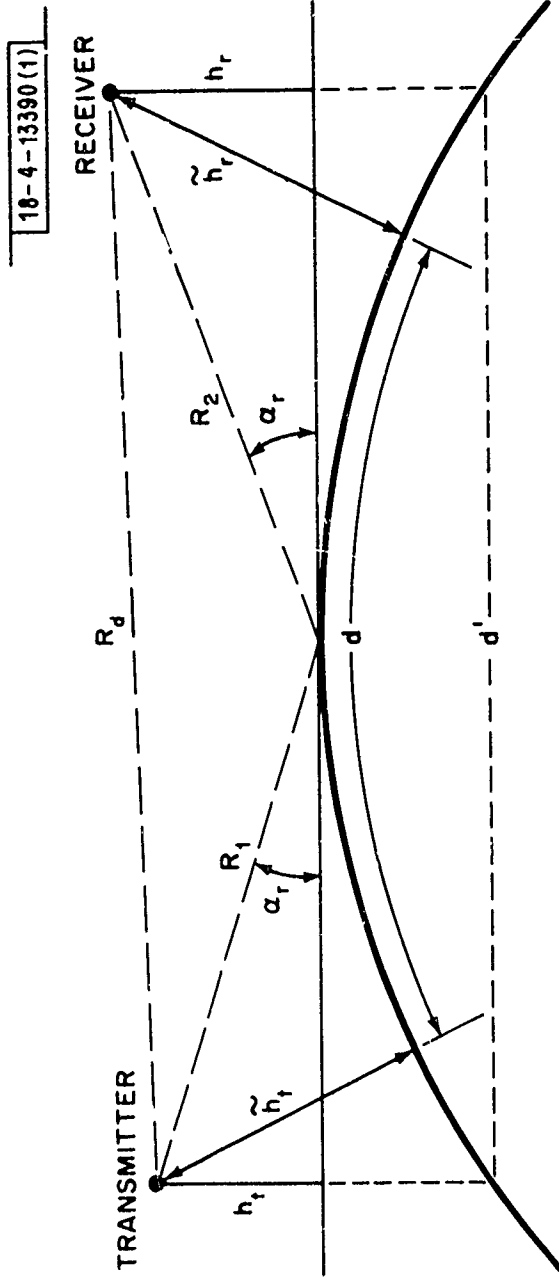


Fig. 1. Ray geometry for curved earth.

of the Fresnel zone size and orientation are discussed in Appendix A. Using the law of cosines, it can be shown that the height of an antenna above the curved earth \tilde{h} , is approximately

$$\tilde{h} = h + h^* \quad (1)$$

where h is the height above the tangent plane shown in Figure 1 and the distance

$$h^* = \frac{1}{2R_e} (h/\sin \alpha)^2 \quad (2)$$

which can in turn be shown to be the distance of the tangent plane above the curved earth at the radio horizon as illustrated in Figure 1. One direct ray which emits from the antenna intersects the curved earth at a distance $d_r = h/\sin \alpha$ as a tangent line. The point of intersection is called the radio horizon. The radio horizon ray is sometimes called the "line of sight." From Eq. (2) $d_r = \sqrt{2R_e h^*}$. The error in $\tilde{h} \approx h + h^*$ is less than 3% for $\alpha \leq 8^\circ$, $\tilde{h} \leq 55,000$ ft, and $\theta \leq 28^\circ$.

The electric field strength E at the receiving antenna is given by

$$E = E_d + E_r \quad (3)$$

where E_d and E_r represent the direct and reflected rays as measured at the receiving antenna. By the use of further simplifying assumptions Eq. (3)

can be converted into a more useful form. It will be assumed that

- (1) The antenna gain patterns are isotropic.
- (2) The direct and indirect ray paths, r_d and $r_1 + r_2$ (see Figure 1), are comparable so that the normal inverse distance signal strength attenuation is comparable for rays traversing the two paths.

Then, Eq. (3) may be written

$$E = E_d \{1 + R \exp[j(\varphi_s + \varphi_L)]\} \quad (4)$$

where R is the amplitude of the effective reflection coefficient of the reflecting area, φ_s is the phase change introduced by the reflection process, and φ_L is the phase lag of the reflected signal with respect to the direct signal.

The reflected energy from a general curved non-smooth surface is usually decomposed into specular and diffuse constituents [2,3]. At very low angles of reflection, the specular constituent is by far the greater of the two (see Figure 2) and it is in this situation (when the direct and reflected rays are of comparable amplitude and have the potential of cancelling each other at the receiver) that there would be interest in applying antenna diversity techniques. Thus, the R for specular scattering is used here. Theory and experiment indicate that to a good degree of approximation, R is given by [2,3]

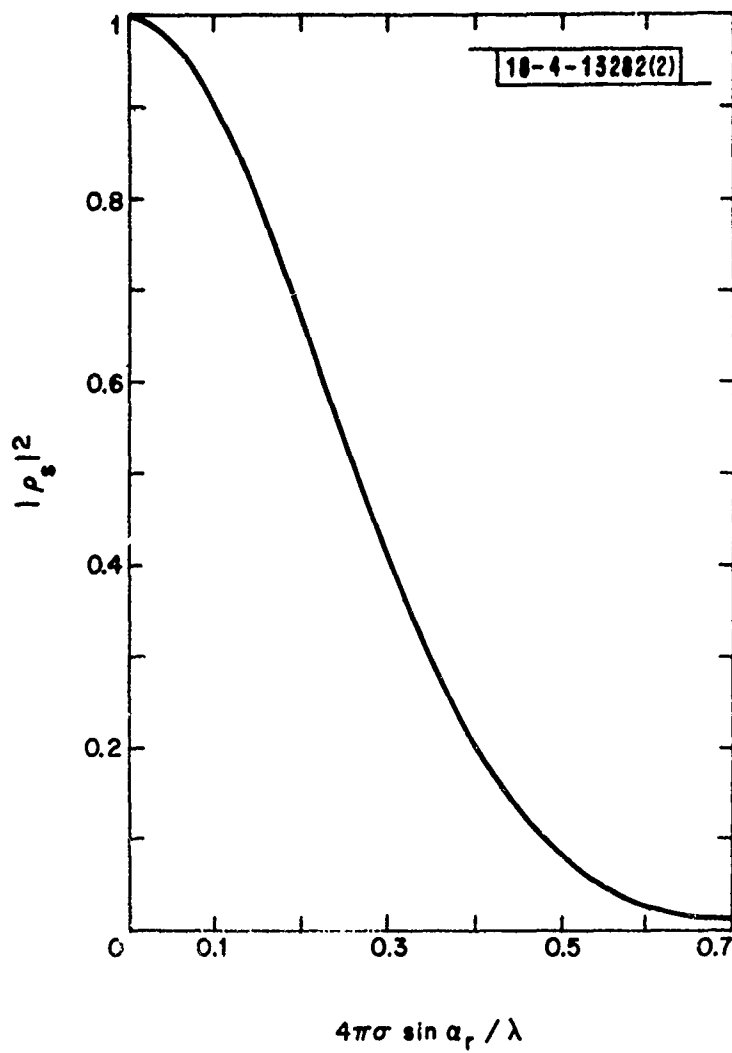


Fig. 2. Specular scattering coefficient vs apparent surface roughness.

$$R = |R_0^{\pm}| D \rho_s \quad (5)$$

Here R_0^{\pm} are the classical reflection coefficients with the "+" and "-" superscripts indicating vertical and horizontal wave polarization. The divergence factor D takes into account the effect of the curvature of the curved surface on the amplitude of the reflection and is given by [2,3]:

$$D = \left\{ 1 + \frac{2r_1 r_2}{R_e (r_1 + r_2) \sin \alpha_r} \right\}^{1/2} \quad (6)$$

where [3] $r_1 r_2 \ll R_e$ and α_r is the angle between the incident (or reflected) ray and the tangent line at point of reflection. The length of the major axis of the 1st Fresnel zone X becomes DX for a curved surface. ρ_s is the specular scattering coefficient which theory and experiment [2,3] indicate is accurately given by

$$\begin{aligned} \rho_s &= \exp(-g/2) \\ g &\equiv (4\pi\sigma \sin \alpha_r / \lambda)^2 \end{aligned} \quad (7)$$

where σ is the rms height of the surface irregularities and λ is the wavelength. Eq. (7) is illustrated in Figure 2.

When $\phi = \phi_s + \phi_L$ is an odd multiple of π (see Eq. (4)), then the interference between the direct and reflected rays causes a power loss in total received signal of $20 \log_{10}(1-R)$. The resulting fading is only significant when ϕ is "sufficiently" close to an odd multiple of π . For $1.3 \geq R \geq 0.7$, the fraction (P)

of airspace for which fades equal to or greater than 10 db will occur is given by

$$P(\geq 10 \text{ db fade}) = \frac{1}{\pi} \cos^{-1} \left\{ \frac{0.91 + R^2}{2R} \right\} \quad (8)$$

which is illustrated in Figure 3a. For $1.7 \geq R \geq 0.3$, the fraction of airspace for which fades equal to or greater than 3 db will occur is given by

$$F(\geq 3 \text{ db. fade}) = \frac{1}{\pi} \cos^{-1} \left\{ \frac{0.5 + R^2}{2R} \right\} \quad (9)$$

which is illustrated in Figure 3b.

The crucial quantity ϕ_L is given by $\phi_L = 2\pi \delta / \lambda$ where the physical path length difference

$$\delta \equiv R_1 + R_2 - R_d \quad (10)$$

With reference to Figure 1, this may be written

$$\delta = \sqrt{(d')^2 + (h_t + h_r)^2} - \sqrt{(d')^2 + (h_t - h_r)^2} \quad (11)$$

which, when

$$h_t, h_r \ll d' \approx d$$

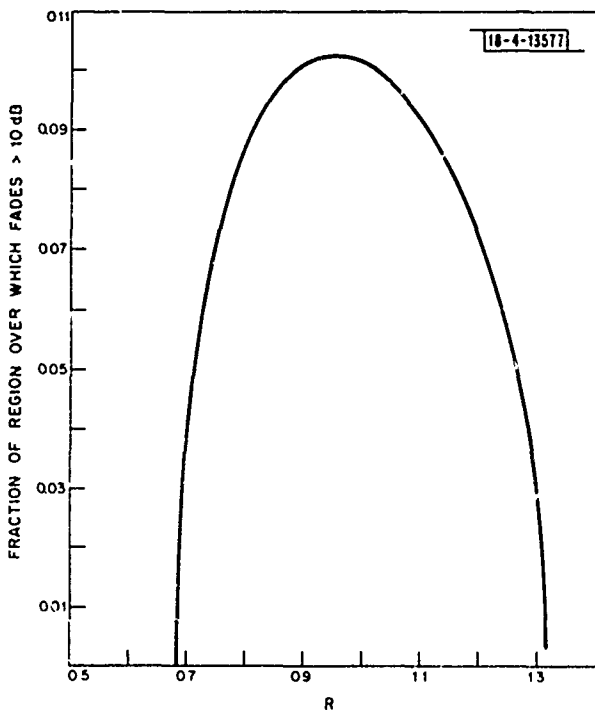
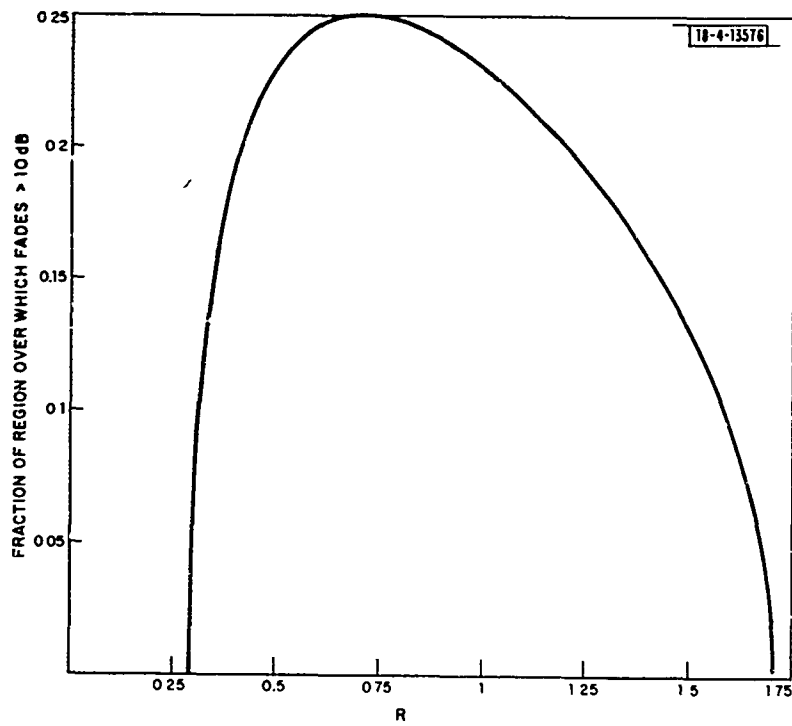


Fig. 3. The fraction F of airspace for which fades are equal to or greater than 3 dB and 10 dB vs reflection coefficient of scattering surface.

reduces with great accuracy to

$$\delta \approx \frac{2h_r h_t}{d^2} \quad (12)$$

so that

$$\varphi_L = \frac{4\pi h_r h_t}{\lambda d} \quad (13)$$

From Eqs. (4) and (13), the received signal power vs. receiver antenna vertical altitude can be determined as a periodic function and is illustrated in Figure 4 for receivers at distances (as measured along the surface of the earth) of 50 and 100 miles from the transmitting antenna. The periodicity clearly permits the application of vertical spatial diversity, although the precise way that fixed spatial separations can be used over a broad spectrum of distances from the transmitter is not immediately obvious and will be discussed briefly later in the text and in greater detail in Appendix C. The spatial regions in which the interference model, using the ray optic description of propagation, is applicable, is from the transmitting antenna approximately up until the radio horizon. Numerous experiments bear this out. If the altitude h^* is given in feet and $R_e = (4/3)R_E$, then the distance to the radio horizon, given in Section 2.1, reduces to

$$d_r = \sqrt{2h^*} \quad (\text{in miles}). \quad (14)$$

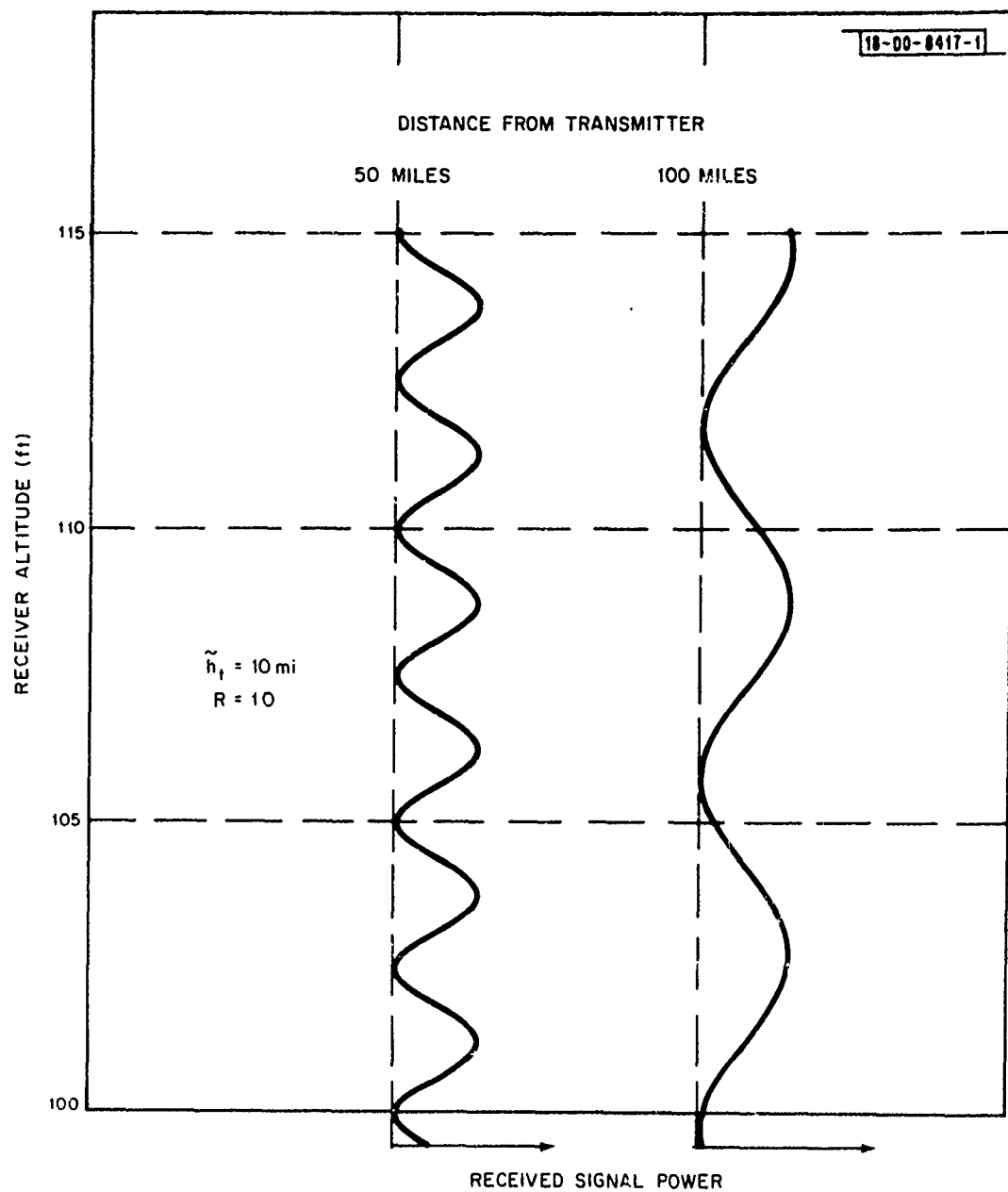


Fig. 4. The received signal power (in arbitrary units) vs the vertical receiving antenna altitude (in feet) at two distances (measured along the earth's surface) of the transmitting from the receiving antenna. The transmitter altitude is taken as 10 miles, and the magnitude of the specular reflection coefficient is taken as 1.0.

The equations presented in this subsection provide the basis for the analysis to follow.

2.2 ANALYSIS OF DIVERSITY TECHNIQUES

Eqs. (4) and (12) can be used as a basis for analyzing spatial and frequency diversity. After some preliminary analysis of surface reflections and the effects of curved terrain, these techniques will be examined in the above order and then a number of observations and interrelationships will be briefly noted.

2.2.1 Variation in Surface Reflections

Suppose at one antenna of the set it is assumed that the worst phase condition occurs (i.e., E_d is π radians out of phase with E_r) and it is specified that the maximum fade is 3 db, i.e., $20 \log_{10}(1-R)=3$ db maximum. Then, $(1-R)^2=0.5$ and thus R must satisfy $R \approx 0.3$. Consulting the reflection coefficient curves in Figure 5, it can be found that for a vertically polarized wave incident on a smooth, flat surface, $R_0 \approx 0.3$ is obtained for a reflection angle* α_r of:

$$\text{For dry soil: } \alpha_{r1} \approx 9.5^\circ, 32^\circ$$

$$\text{For sea water: } \alpha_{r2} \approx 4^\circ, 8^\circ \quad (15)$$

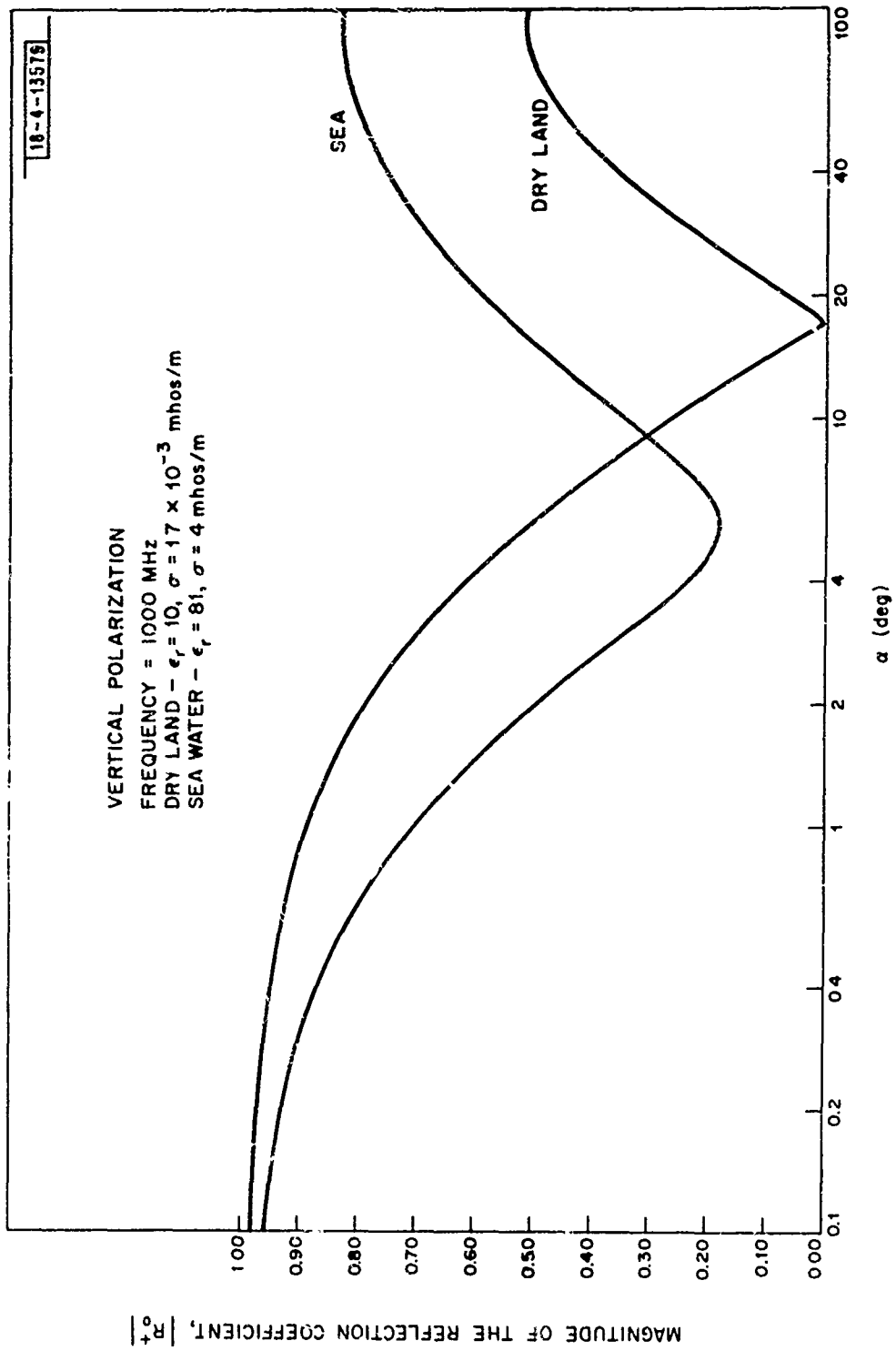


Fig. 5. The magnitude of the reflection coefficient, R , of smooth flat terrain vs the angle of incidence, θ , for dry soil and sea water.

These results may be plotted (as shall often be done later in this section) as horizontal lines on a graph of α_r vs. receiving antenna altitude (\tilde{h}) above the curved earth surface. (See Figure 6.) The angles in Eq. (14) are double valued because vertical polarized waves are being considered, and R for these waves goes from unity (at $\phi=0$) monotonically down to a minimum (at the pseudo-Brewster angle) and then increases monotonically to a non-unity maximum (at $\phi=90^\circ$). Within the area bounded by $\alpha_r=9.5^\circ$ and 32° in Figure 6, the interference-caused fades are less than 3 db below a direct signal received in free space (with no reflected signal interference) when the scattering surface is flat, smooth dry soil. A similar statement may be made for the case of interference from waves reflected from a flat, smooth sea.* Thus, it may be noted that no special techniques are required to combat multipath fading of 3 db or more within the above boundaries. However, some technique is required for combating multipath reflection outside these regions.

If the fade margin is selected as 10 db, i.e., $20 \log_{10}(1-R)=-10$ db maximum, then $R_0 \approx 0.7$ which is obtained from a smooth flat surface for a reflection angle** of:

$$\begin{aligned} \text{for dry soil: } & \alpha_{r3} \approx 3^\circ \\ \text{for sea water: } & \alpha_{r4} \approx 1^\circ, 28^\circ \end{aligned} \quad (16)$$

* These results will be generalized later to include curved, rough surfaces.

** The absence of a second angle is due to the fact that past the pseudo-Brewster angle, R_0 does not climb up to 0.7 again.

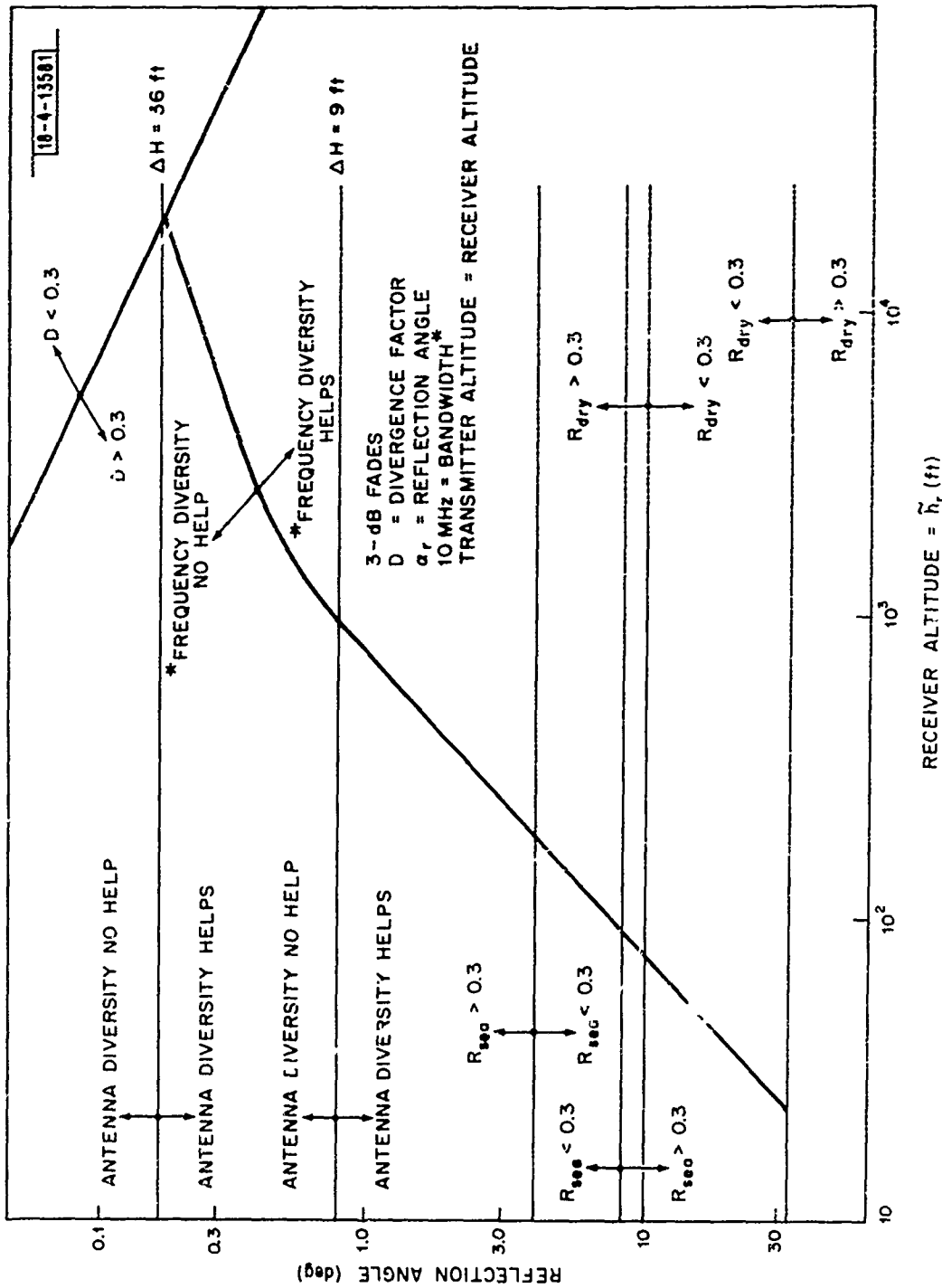


Fig. 6. Antenna and frequency diversity limits, terrain reflection and divergence limits for 3 dB fades in the presence of smooth terrain illustrated in the space of reflection angle (α_r) - receiver altitude above a curved earth (\tilde{h}_r) when $r_1 = r_2$.

Below these horizontal lines* in Figure 7, the received signal power reduction due to interference is 10 db or less, so that special techniques are required to get 10 db or less fades above these angles. Due to the magnitude of the numerical values in this case, these lines must be calculated taking into account divergence which is discussed at greater length in the subsection 2.2.2. (The effect of the terrain's curvature, as given by the divergence factor D, provides some aid but not to a practical degree in all cases).

2.2.2 The Effect of Terrain Curvature

The effect of terrain curvature on signal reflection is taken into account in (4), (5) and (6) by the use of the divergence factor D. Not only α_r , but also h_t and h_r must be considered. For a 3 db fade margin assuming the other terms in the right hand side of Eq. (5) are practically unity, $D \approx 0.3$ would be required. This leads, from Eq. (6), to

$$\sin \alpha_r \approx \frac{r_1 r_2}{5R_e(r_1 + r_2)} \quad (16)$$

* Except for sea water in which the trouble free area is bounded in the $\alpha_r - h_r$ diagram by $\alpha_r \approx 1^\circ$ and $\alpha_r \approx 28^\circ$.

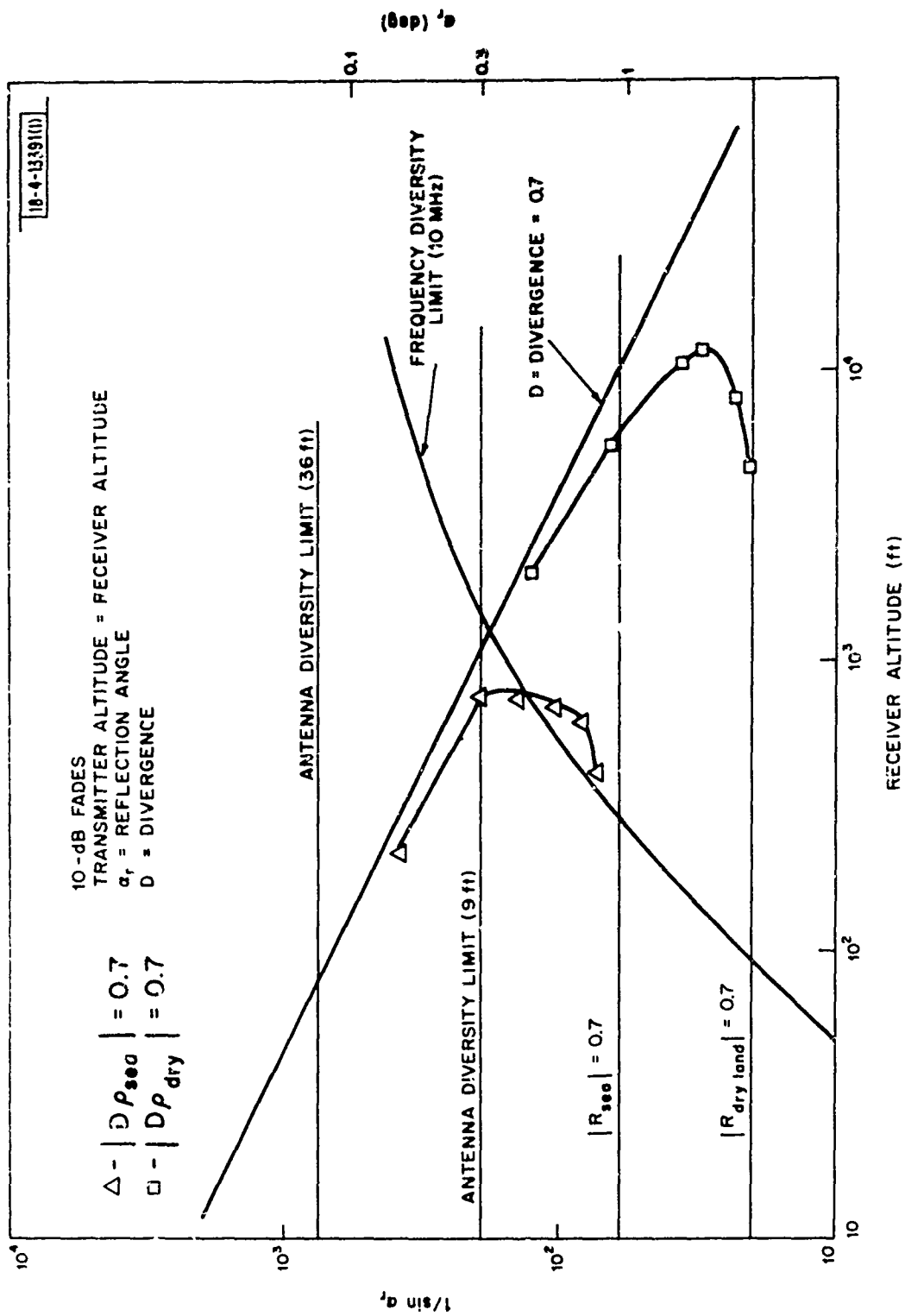


Fig. 7. Antenna and frequency diversity limits, terrain reflection and divergence limits for 10 dB fades in the presence of smooth terrain illustrated in the $\alpha_r - h_r$ space when $r_1 = r_2$. Unlike the case of 3 dB fades the numerical values are such that the terrain reflection and divergence must be combined into a single set of curves.

In general, $1/2 \leq r_1 r_2 / (r_1 + r_2) \leq 1$ so that;

$$\frac{r_1}{10R_e} \leq \sin \alpha_r \leq \frac{r_1}{5R_e} \quad (17)$$

$$\text{When } r_1 = r_2 \quad \tilde{h}_r = h_r^* + 10R_e \sin^2 \alpha_r. \quad (18)$$

$$\text{When } r_2 \gg r_1 \quad \tilde{h}_r = \tilde{h}_r^* + 5R_e \sin^2 \alpha_r. \quad (19)$$

In these special cases, algebraic manipulation leads to the time-saving result; when $r_1 = r_2$ then $h_r^* = 5h_r$, and when $r_2 \gg r_1$ then $\tilde{h}_r^* = 2.5 h_r$. Thus;

$$\text{when } r_1 = r_2 \quad : \quad \tilde{h}_r = 6(10R_e \sin^2 \alpha_r) \quad (20)$$

$$\text{when } r_2 \gg r_1 \quad : \quad \tilde{h}_r = 3.5(5R_e \sin^2 \alpha_r) \quad (21)$$

These boundaries are illustrated in Figures 6 and 8. Above and to the right of these boundaries, the terrain curvature insures that the fade margin of 3 db is met. Below and to the left of these boundaries, some technique is required to reach the fade margin until the limiting reflection angle for reduced surface reflection is the reflection angle of operation. Although D

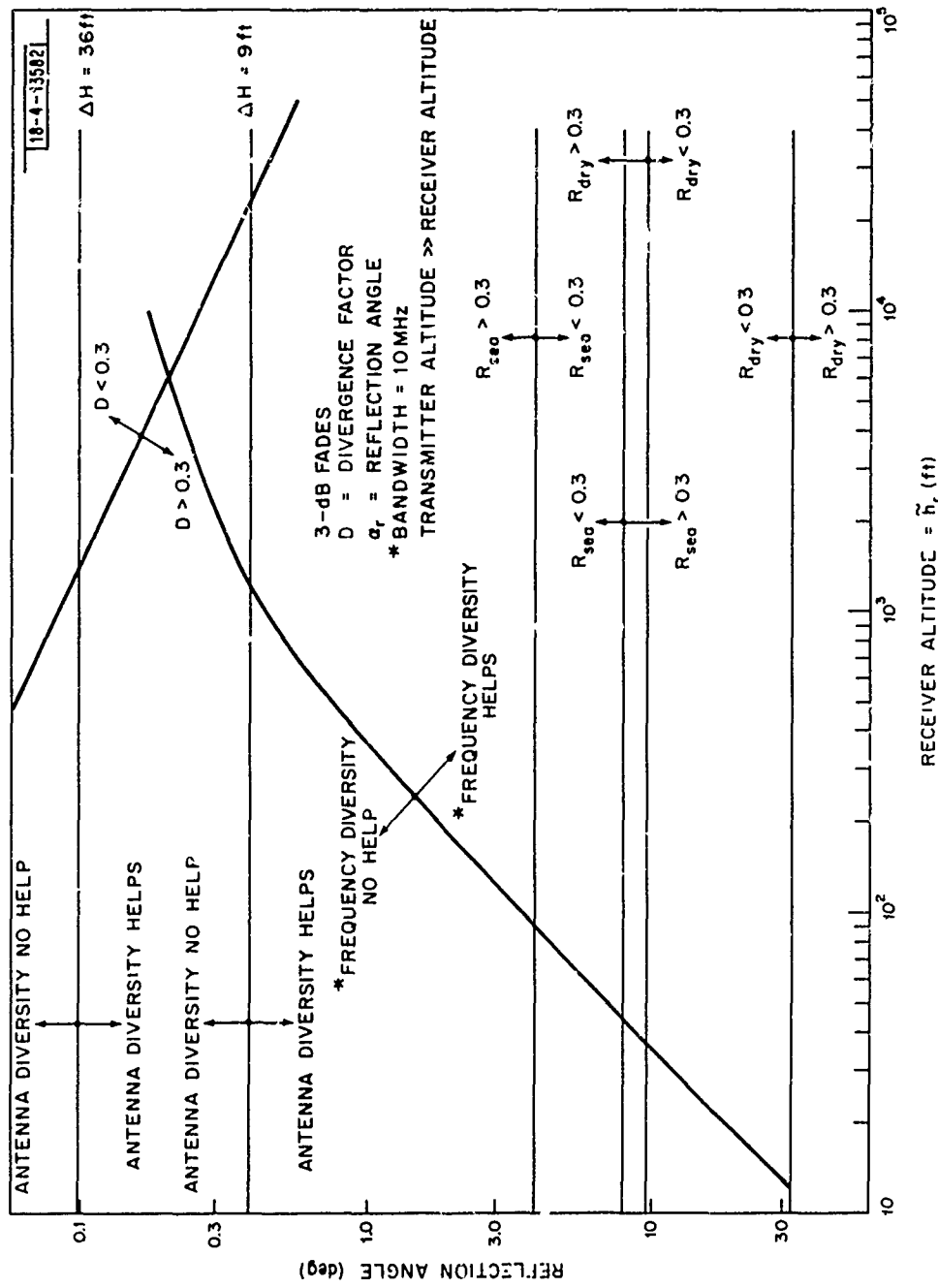


Fig. 8. Antenna and frequency diversity limits, terrain reflection and divergence limits for 3 dB fades in the presence of smooth terrain illustrated in the space of reflection angle (α_r) - receiver altitude above a curved earth (\tilde{h}_r) when $r_2 \gg r_1$.

and R_0 are multiplicative terms in Eq. (5), each is essentially unity when the other is about 0.3 in the portion of the α_r - \tilde{h}_r space shown in the figures for 3 db fades. Thus, they may be plotted as separate lines. This is not true for the 10 db fade margin discussed next.

For a 10 db fade margin, if the other terms in the right hand side of Eq. (5) are essentially unity, $D \approx 0.7$ is required. This leads, from Eq. (6), to

$$\sin \alpha_r \approx \frac{2r_1 r_2}{R_e (r_1 + r_2)} \quad (22)$$

In general,

$$\frac{r_1}{R_e} \leq \sin \alpha_r \leq \frac{2r_1}{R_e} \quad (23)$$

With the time-saving results that here, $h_r^* = (1/2) h_r$ for $r_1 = r_2$ and $h_r^* = (1/4) h_r$ for $r_2 \gg r_1$; it follows from Figure 1 and Eq. (1) that

$$\text{when } r_1 = r_2 : \tilde{h}_r \approx 1.5 (R_e \sin^2 \alpha_r) \quad (24)$$

$$\text{where } r_2 \gg r_1 : \tilde{h}_r \approx 1.25 (0.5 R_e \sin^2 \alpha_r) \quad (25)$$

These boundaries are illustrated in Figure 7 and 9. The same comments apply as were made for the 3 db case immediately following Eq. (21) with an important exception. That is, there is a portion of the α_r - \tilde{h}_r diagram which D and R_0 must be simultaneously accounted for as shown by the extra curved

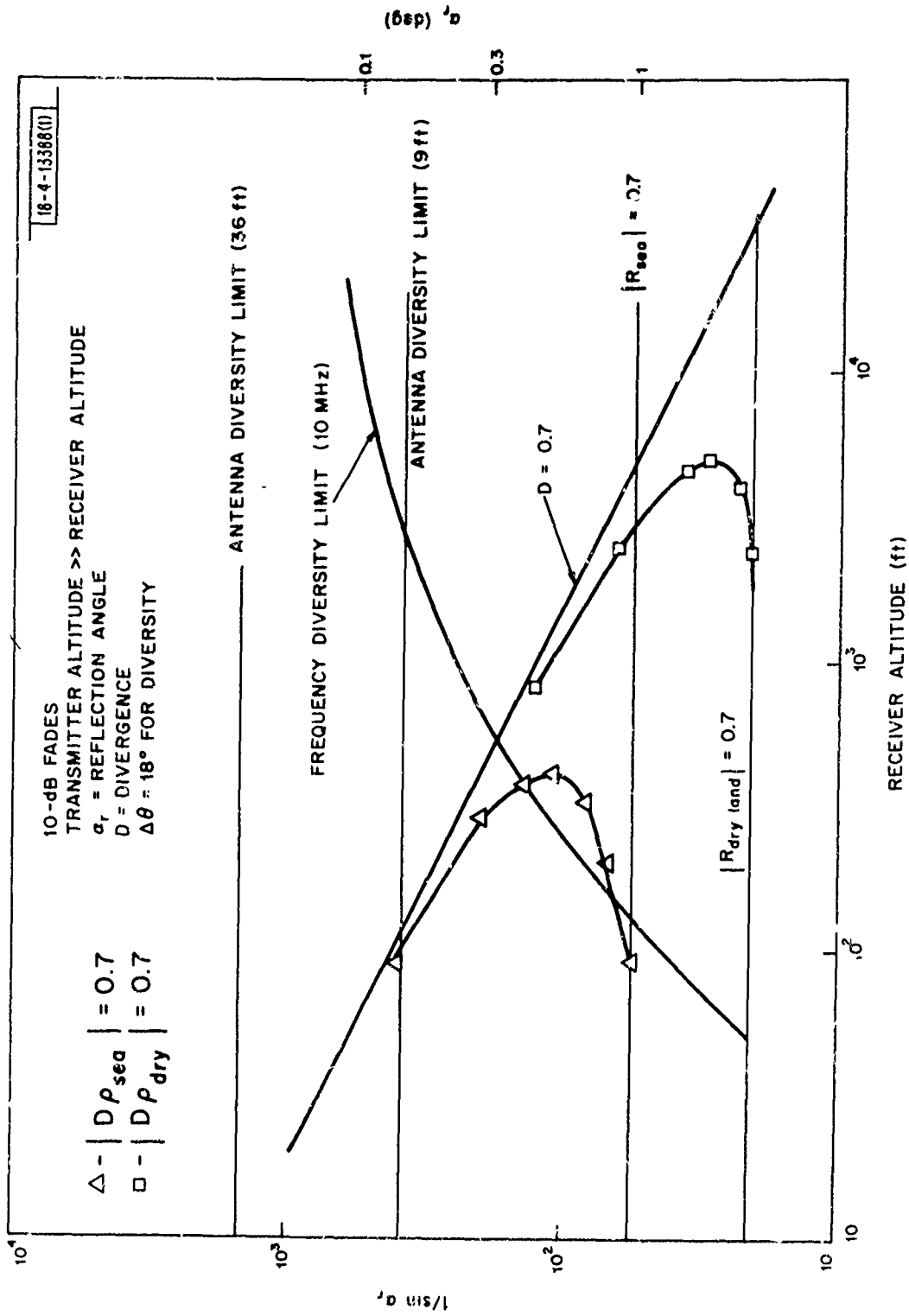


Fig. 2. Antenna and frequency diversity limits, terrain reflection and divergence limits for 10 dB fades in the presence of smooth terrain illustrated in the $\alpha_r - \tilde{h}_1$ space when $r_2 \gg r_1$.

lines shown in Figures 7 and 9. The calculation of this follows from setting $DR_0 = 0.7$ and deriving from Eq. (6) the equation

$$\tilde{h}_r = h_r^* + R_e \sin^2 \alpha_r \{2R_0^2(\alpha_r) - 1\}/2$$

Because the reflection angle, α_r , cannot be significantly altered during the time spans of interest, diversity must be employed to alter ϕ_L (see Eq. (4)) in regions where aid is required in minimizing the effect of multipath reflections. We now discuss two methods of obtaining the change in ϕ_L : vertical height diversity which changes h_r in (4) and frequency diversity where one changes λ in (4).

2.2.3 Antenna Height Diversity

It was found that the minimal required horizontal antenna separations required to obtain a significant change in ϕ_L by changing d in Eq. (4) are generally too large for practical airborne application at L-band frequencies or lower. The minimal required vertical separations will be shown to be of practical interest at L-band but of considerably less interest at UHF.

This section analytically describes a technique of analyzing vertical height diversity for antennas. It is only assumed that the antenna gain variations with direction is the same for each antenna involved, an assumption which will be reconsidered in Section 2.5.

Suppose at one antenna, and at one frequency f_0 , E_d and E_r are in phase opposition and comparable in magnitude. Then, deep fading will take place at that antenna. At another antenna, located vertically above or below the first, it is desired to limit the fading to a maximum of F db below the

signal. A practical way to do this is to obtain a change in ϕ_L (the phase lag between the direct and reflected signals) written $\Delta\phi_L$, so that E_r lies outside or tangent to a circle about the tip of E_d (see Figure 10) of radius ρ where $20 \log_{10}(1-\rho) = -F$ db. Several things can be noted from Figure 10:

- (1) For $\Delta\phi_L \geq \Delta\phi_{L0}$ the angle of the tangent line, E_r may be of any magnitude and the maximum fade at the second antenna will still be F db.
- (2) $\Delta\phi_{L0}$ is the smallest angle for which this is true.

Therefore, $\Delta\phi_{L0}$ is chosen as the desired angular lag between E_d and E_r at the second antenna. A more detailed discussion of the diversity combining technique assumed and the relevance of $\Delta\phi_{L0}$ as estimated from Figure 10 appears in Appendix E.

The vertical separation Δh_r , required to obtain the desired phase lag can be determined from Eq. (13) by the relation

$$\Delta\phi_{L0} = \frac{4\pi}{\lambda} \left(\frac{h_t}{d_t} \right) \Delta h_r \quad (26)$$

When $r_1 = r_2$, then $\sin \alpha_r = h_t / r_1 \approx h_t / d_t \approx 2h_t / d$ and the required separation is given by

$$\Delta h_r = \left(\frac{\lambda}{2\pi} \right) \frac{\Delta\phi_{L0}}{\sin \alpha_r} \quad (27)$$

When $r_2 \gg r_1$, then $\sin \alpha_r = h_t / r_1 \approx h_t / d_t \approx h_t / d$ and then

$$\Delta h_r = \left(\frac{\lambda}{4\pi} \right) \frac{\Delta\phi_{L0}}{\sin \alpha_r} \quad (28)$$

18-4-13583

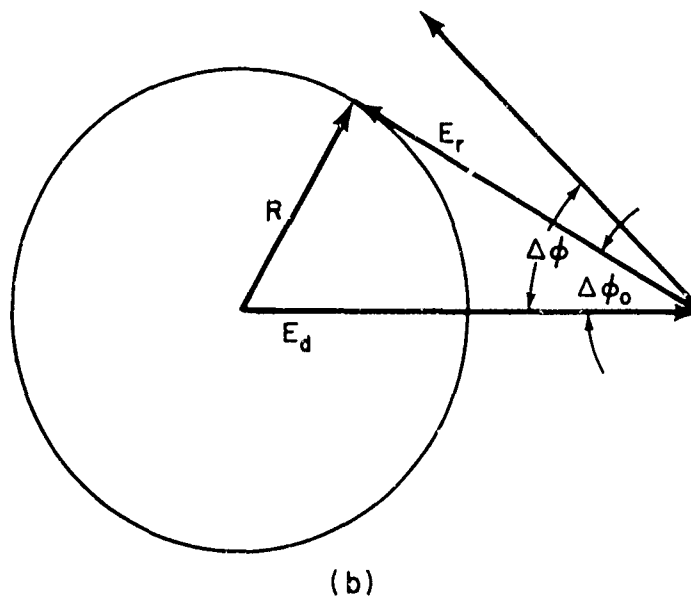
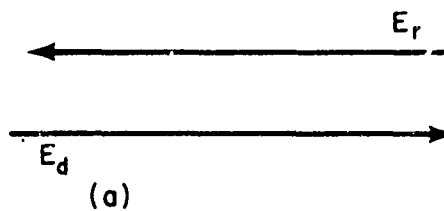


Fig. 10. The geometry of the direct and reflected electric fields (a) at the first antenna, (b) at the second antenna.

From Eqs. (26), (27), and (28) it may be observed that:

- (1) Spatial diversity is increasingly practical as λ gets small.

It will be seen in the next section that for frequencies around 1 GHz, i.e., $\lambda \approx 1$ ft, the method is practical even for small present-day aircraft.

- (2) For a fixed value of h_t/d , the required antenna separation Δh_r is independent of the receiving antenna altitude.
- (3) For a given Δh_r and $\Delta\phi_{L0}$ (which in turn means a given fade margin) Eqs. (27) and (28) describe the smallest multipath reflection angle α_r for which a fade margin F can be maintained. They are

$$\alpha_r \geq \sin^{-1} \left\{ \frac{\lambda}{\Delta h_r} \frac{\Delta\phi_{L0}}{2\pi} \right\}$$

from Eq. (27) and $\alpha_r \geq \sin^{-1} \{ (\Delta\phi_{L0}/4\pi)(\lambda/\Delta h_r) \}$ from Eq. (28)

2.2.4 Frequency Diversity

This section reconsiders the situation described in the prior section but effects a change $\Delta\phi_{L0}$ at a single antenna by using frequencies f_0 and $f_0 + \Delta f$. From Eq. (13), the required frequency difference satisfies

$$\Delta\phi_{L0} = 4\pi \left(\frac{\Delta f}{C_0} \right) h_r \left(\frac{h_t}{d} \right) \quad (29)$$

where $C_0 = 3 \times 10^8$ meters/sec. $\approx 10^9$ ft./sec.

Similar to the previous discussion when $r_1=r_2$

$$\Delta f = (\Delta\phi_{L0}/2\pi)(C_0/h_r)/\sin \alpha_r \quad (30)$$

and when $r_2 \gg r_1$

$$\Delta f = (\Delta\phi_{L0}/4\pi)(C_0/h_r)/\sin \alpha_r \quad (31)$$

From the above, it may be observed that

- (1) For a given fade margin (and hence a given $\Delta\phi_{L0}$) and a given reflection angle as the receiving antenna height decreases, the minimum frequency spread Δf must increase. Thus, for a fixed spread, increasingly deep fades occur as h_r decreases.
- (2) For fixed values of h_r and $\Delta\phi_{L0}$, the minimum reflection angles that are acceptable vary with Δf . In particular, for $r_1=r_2$

$$\alpha_r \geq \sin^{-1}\{(\Delta\phi_{L0}/2\pi)(C_0/h_r)/\Delta f\}$$

and for $r_2 \gg r_1$ a similar result with 2 replaced by 4 applies.

- (3) For a given $\Delta\phi_{L0}$, h_t/d , and λ

$$\frac{\Delta h_r}{h_r} = \frac{\Delta f}{f_0} \quad .$$

Thus, when frequency and spatial diversity are available, spatial diversity will be more useful for

$$h_r < (\Delta h_{\max})(f_o / \Delta f_{\max}) \quad (32)$$

and frequency diversity will be more useful for

$$f_o < (\Delta f_{\max})(h_r / \Delta h_{\max}) \quad (33)$$

Figures 6,7,8, and 9 illustrate result (32) quantitatively and these figures will be discussed in detail in Section 2.3.

2.2.5 Coverage

Sections 2.3 and 2.4 will discuss in detail the spatial coverage obtained by the use of spatial and frequency diversity and the other effects previously mentioned. Appendix B will give a quantitative theory for the optimum spacing of antennas in a linear array used for spatial diversity (as well as a related theory for the optimum separation of frequencies in a multiple tone frequency diversity technique). In this subsection, a simple brief discussion will be given of coverage and antenna spacing to obtain some initial insight into the topic.

Suppose, for example, four antennas can be used in a spatial diversity system. Further, suppose the first two antenna are separated by $\Delta h_1=5$ feet; a third antenna is separated from the second $\Delta h_2=10$ feet, and the fourth

antenna is separated from the third by $\Delta h_3=20$ feet. From these then, there exist other spatial diversity separations:

$$\Delta h_4 = \Delta h_1 + \Delta h_2 = 15 \text{ feet}$$

$$\Delta h_5 = \Delta h_2 + \Delta h_3 = 30 \text{ feet}$$

$$\Delta h_6 = \Delta h_1 + \Delta h_2 + \Delta h_3 = 45 \text{ feet}$$

From these six values of Δh_r , Eq. (26) yields six lines in h_t -d space (independent of h_r) for which

$$(h_t/d)_i = (\lambda/\Delta h_i) (\Delta\phi_{L0}/4\pi) \quad (i=1,\dots,6) \quad (34)$$

shown as dotted lines in Figure 11. For $\Delta\phi_{L0}=\pi/2$, which is used in obtaining Figure 11, it is seen from Figure 10 that $|E/E_d|=1$ so that no fading occurs. As $\Delta\phi_{L0}$ is decreased from $\pi/2$, fades of increasing magnitude occur. Thus, if a range of fades up to some selected maximum value F are permitted, the previous lines in Figure 11 become sides of triangles in the h_t -d space within which fades no deeper than F can occur. Thus, in Figure 11 a given portion of the airspace is covered by these triangles. Outside of these triangles, fades of undesirable magnitude occur. The best "covering of this h_t -d space by a minimal number of antennas is discussed in Appendix B.

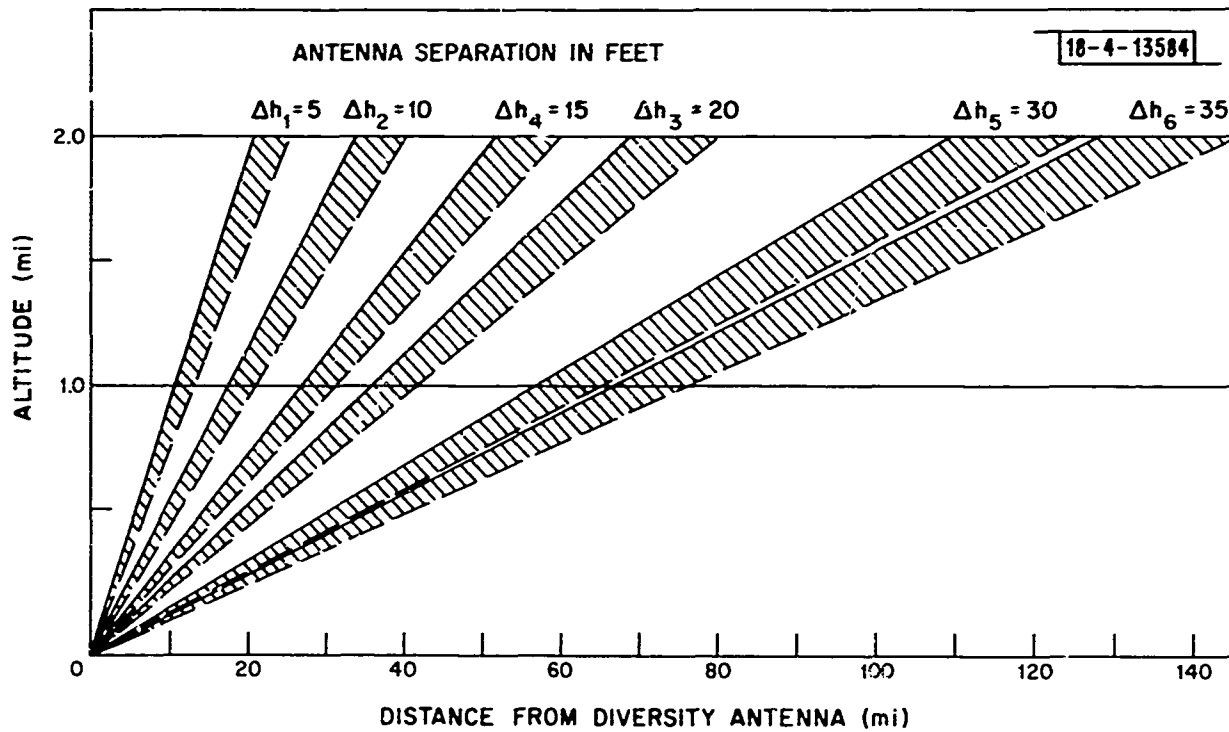


Fig. 11. Space coverage in h_t - d space by four antenna spatial diversity system. The dotted lines are those for which Eq. (34) is exactly satisfied.

2.3 ASSESSMENT OF FADE MARGIN SELECTION ON SPATIAL REGIONS OF USEFULNESS OF DIVERSITY TECHNIQUES

The relative effects on the range of diversity technique effectiveness due to the selection of 3 db and 10 db fade margins are compared in this section for smooth scattering surfaces. The boundary lines in $\alpha_r - \tilde{h}_r$ space due to ground reflection and divergence as individual and simultaneous factors for 3 db and 10 db fades are discussed in subsections 2.2.1 and 2.2.2.

For 3 db fades, it follows from the graphical construction in Figure 10 that $\Delta\phi_{L0} = \pi/4$. For $r_1 = r_2$, it follows from Eq. (27), with $\lambda = 1$ ft., that

$$\Delta h_r = 1/8 \sin \alpha_r \quad (r_1 = r_2; F = -3 \text{ db}) \quad (35)$$

and hence $\Delta h_r = 9$ ft. implies $\sin \alpha_r = 1/72$, while $\Delta h_r = 36$ ft. implies $\sin \alpha_r = 1/288$, both of which are shown in Figure 6. For $r_2 \gg r_1$, it follows from Eq. (28), with $\lambda = 1$ ft., that

$$\Delta h_r = 1/16 \sin \alpha_r \quad (r_2 \gg r_1; F = -3 \text{ db}). \quad (36)$$

In this case, $\Delta h_r = 9$ ft. implies $\sin \alpha_r = 1/144$, while $\Delta h_r = 36$ ft. requires that $\sin \alpha_r = 1/576$, both of which are shown in Figure 8. For frequency diversity when $r_1 = r_2$, it follows from Eq. (30) and the choice of $\Delta f = 10$ MHz that

$$\tilde{h}_r = h_r^* + 100/8 \sin \alpha_r \quad (r_1 = r_2; F = -3 \text{ db}) \quad (37)$$

However, when $r_2 \gg r_1$, it follows from Eq. (31) and the choice of $\Delta f = 10 \text{ MHz}$ that

$$\tilde{h}_r = h_r^* + 100/16 \sin \alpha_r \quad (r_2 \gg r_1; F = -3 \text{ db}) \quad (38)$$

Eq. (37) is plotted in Figure 6 and Eq. (38) is plotted in Figure 8. The above information is summarized in Table 2 below.

Table 2. Results Corresponding to 3 db Fade Margins.

$r_2 = r_1$	$r_2 \gg r_1$	
$\sin \alpha_r = 1/8 \Delta h_r$	$\sin \alpha_r = 1/16 \Delta h_r$	Spatial Diversity
$\sin \alpha_r = 100/8 h_r$	$\sin \alpha_r = 100/16 h_r$	Freq. Diversity ($\Delta f = 10 \text{ MHz}$)

In a similar manner, 10 db fades may be considered. From the use of Figure 10, $\Delta \phi_{LO} \approx \sin^{-1}\{0.3\} \approx 0.3$. The results for $\Delta h_r = 9 \text{ ft.}$, 36 ft. , and $\Delta f = 10 \text{ MHz}$ are plotted in Figures 7 and 9 and the equations are summarized in Table 3 below.

Table 3. Results Corresponding to 10 db Fade Margins.

	$r_2 = r_1$	$r_2 \gg r_1$
Spatial Diversity	$\sin \alpha_r \approx 0.3/2\pi \Delta h_r$	$\sin \alpha_r \approx 0.3/4\pi \Delta h_r$
Freq. Diversity ($\Delta f = 10 \text{ MHz}$)	$\sin \alpha_r \approx 30/2\pi h_r$	$\sin \alpha_r \approx 30/4\pi h_r$

Comparing Figure 6 (3 db fade margin) and Figure 7 (10 db fade margin), a number of general observations may be made.

- (1) The reflection angle α_r at which frequency or antenna diversity is of aid is numerically larger for the 3 db case (Figure 6) than for the 10 db case (Figure 7).
- (2) Frequency diversity is potentially of considerable usefulness in the 3 db case and of little value in the 10 db case (for $\Delta f=10$ MHz).
- (3) The range of angles, α_r , (within which antenna diversity with $\Delta h_r=9$ ft. is of use) is greater in the 3 db case than in the 10 db case.

When $r_1=r_2$, then

- (1) In the absence of frequency diversity, antenna diversity with $\Delta h_r=9$ feet is useful, for 3 db fade margins for all practical receiver altitudes roughly:
 - (a) Between α_r equal about 1° and 4° and α_r greater than 8° for sea water.
 - (b) Between α_r equal about 1° and 9.5° and α_r greater than 32° for dry soil.
- (2) In the absence of frequency diversity, antenna diversity with $\Delta h_r=9$ feet is useful for 10 db fade margins up to a maximum receiving antenna altitude of:
 - (a) 12,000 ft. above dry land, and
 - (b) 800 ft. above sea water.

These upper bounds are imposed by the DR_0 curves shown in Figure 6.

The range of reflection angles α_r for which the above applies are:

- (a) Between about 0.3° and about 1° for sea water.
 - (b) Between about 0.3° and about 3° for dry land.
- (3) If frequency diversity ($\Delta f=10$ MHz) is already in use, antenna diversity is only additionally useful:
- (a) Up to a maximum receiving antenna altitude of about 1000 feet for the 3 db case (which occurs at about $\alpha_r=1^\circ$).
 - (b) In the 10 db case, up to a maximum receiving antenna altitude of:
 - (i) About 1300 feet above dry land (which occurs at about $\alpha_r \approx 3^\circ$).
 - (ii) About 800 feet above sea water (which occurs at about $\alpha_r \approx 0.3^\circ$).

Comparing Figure 8 (3 db fade margin) and Figure 9 (10 db fade margin), a number of observations, analogous to the above ones, may be made when $r_2 \gg r_1$

- (1) In the absence of frequency diversity, antenna diversity with $\Delta h_r=9$ feet is useful, for 3 db fade margins, up to a receiving antenna altitude of about 23,000 ft. above the curved earth (at about $\alpha_r=0.4^\circ$) and higher altitudes for larger α_r . For $\tilde{h}_r \geq 23,000$, antenna diversity is useful for reflection angles:
- (a) Between α_r equal about 0.4° and about 4° and α_r greater than about 9° for sea water.
 - (b) Between α_r equal about 0.4° and about 10° and α_r greater than about 30° for dry land.

(2) In the absence of frequency diversity, antenna diversity with $\Delta h_r = 9$ feet is useful, for 10 db fade margins, up to a maximum receiving antenna altitude of:

- (a) About 5,000 feet above dry land.
- (b) About 400 feet above sea water.

The range of reflection angles α_r for which the above applies are:

- (a) Between about 0.15° and about 1° for sea water.
- (b) Between about 0.15° and about 3° for dry land.

(3) If frequency diversity (frequency spacing $\Delta f = 10$ MHz) is already in use, antenna diversity is only additionally useful:

(a) Up to a maximum receiving antenna altitude of about 1,300 feet for the 3 db case (which occurs at about $\alpha_r = 0.4^\circ$).

(b) In the 10 db case, up to a maximum receiving antenna altitude of:

(i) About 550 feet above dry land (which occurs at about $\alpha_r = 0.3^\circ$).

(ii) About 37 feet above sea water (which occurs at about $\alpha_r = 0.4^\circ$).

Some of the implications of the preceding observations may appear clearer, when applying some simple geometric relations to obtain Figures 12 and 13. For example, in Figure 12 it may be seen for the 3 db case that for $r_1 = r_2$, $\tilde{h}_r = 10,000$ feet $= \tilde{h}_t$, antenna diversity with $\Delta h_r = 9$ feet combats multipath inter-

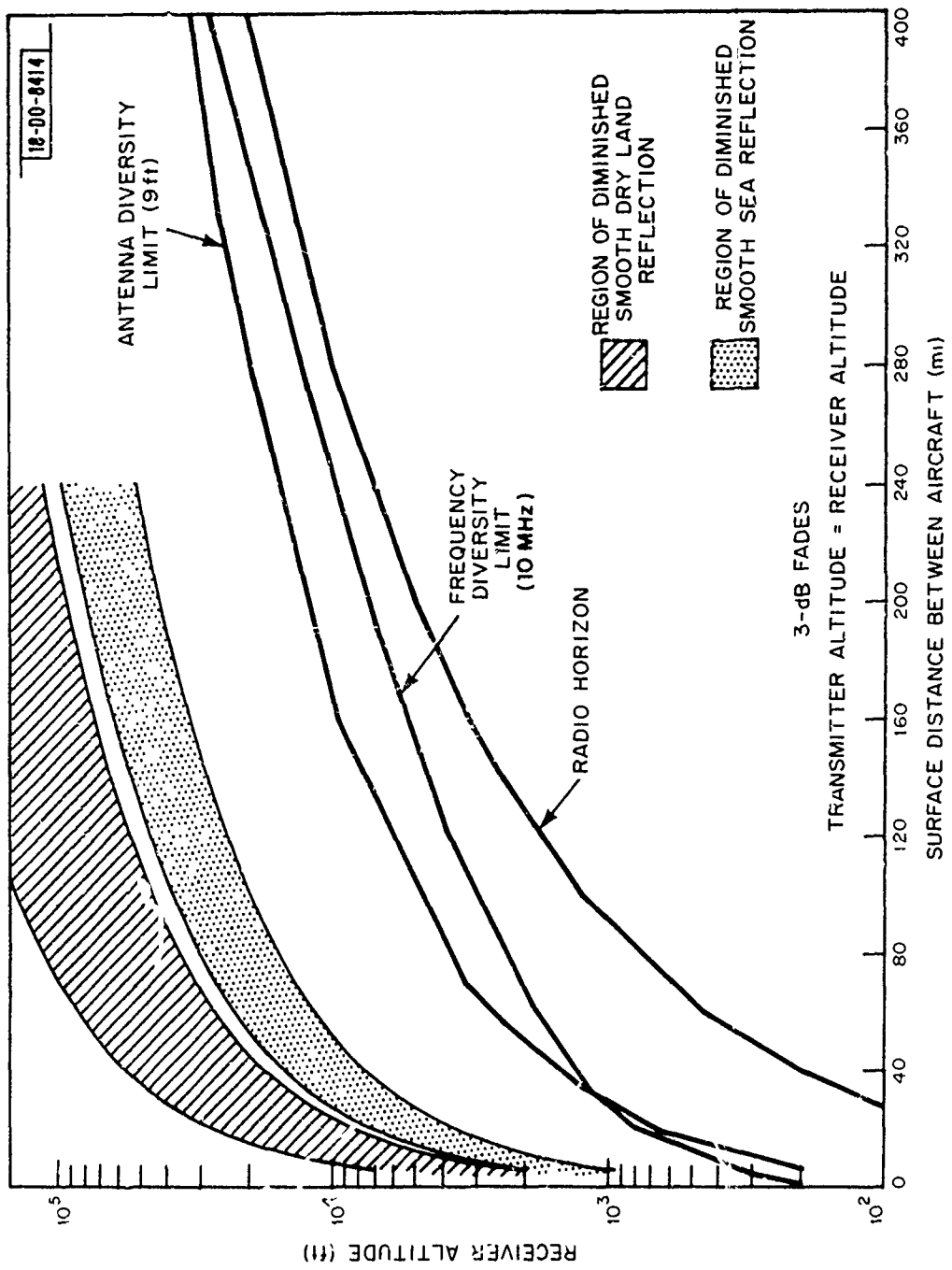


Fig. 12. Antenna and frequency limits, smooth terrain reflection and divergence limits for 3 dB fades illustrated in h_r - d space when $r_1=r_2$.

ference so that an extra distance between aircraft of 144 miles (from $d=24$ miles out to $d=168$ miles) is added to that resulting from reduced ground reflection from dry soil in which $F_{\geq -3\text{db}}$. In the identical case for sea water, an extra distance between aircraft of 116 miles (from $d=52$ miles out to $d=168$ miles) is added. The preceding neglects the extra 28 miles for the sea water case, and the extra 8 miles for the dry soil case obtained to the left of the bounded area of diminished reflection shown in Figure 12. The use of frequency diversity (with $\Delta f=10$ MHz) would add an extra 76 miles (from $d=168$ miles out to $d=244$ miles) of permissible aircraft separation (for $F_{\geq -3\text{db}}$) which is only 36 miles short of the radio horizon for that altitude ($\tilde{h}_r=10,000$ feet). Below about $\tilde{h}_r=1,000$ feet and closer than $d=28$ miles, the antenna diversity (with $\Delta h_r=9$ feet) technique becomes superior to the frequency diversity technique (with $\Delta f=10$ MHz), as shown in Figure 12.

In sharp contrast to the above, Figure 13 illustrates the 10 db case for $r_1=r_2$. Here, $\tilde{h}_r=10,000$ feet is excluded from consideration with respect to the diversity system because the DR_0 factor provides the desired antimultipath aid over a substantial portion of the space. Rather, at $\tilde{h}_r \approx 800$ feet and below, the antenna diversity (with $\Delta h_r=9$ feet) provides a small amount of extra permissible aircraft separation when $F_{\geq -10}$ db. The maximum extra distance (40 miles) is obtained at about $\tilde{h}_r \approx 800$ feet when compared to the dry soil limit and reduces rapidly as \tilde{h}_r decreases. The maximum extra distance, obtained below $\tilde{h}_r=800$ feet, when compared to the sea water limit is about 15 miles. Here again, in sharp contrast to the 3 db case, frequency diversity yields small benefits and only over a segment which falls near a portion of the sea water limit.

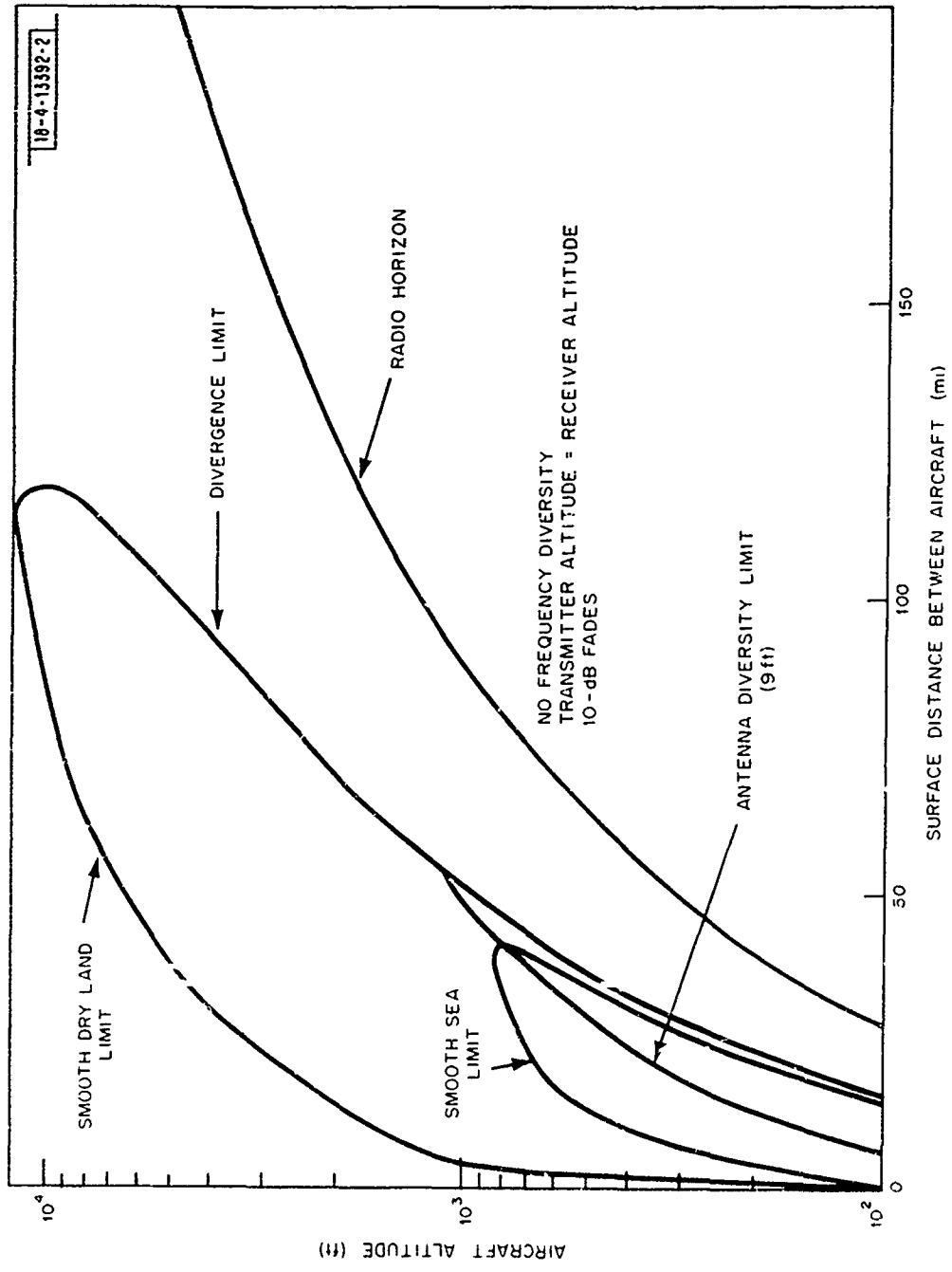


Fig. 13. Antenna and frequency diversity limits, smooth terrain, reflection and divergence limits for 10 dB fades illustrated in the h_t - d space when $r_2=r_1$.

Now consider the 3 db case when $r_2 \gg r_1$; more precisely, assume that the receiving antenna is quite close to the ground (say, $\tilde{h}_r \leq 50$ feet). Suppose $\Delta h_r = 9$ feet and $\tilde{h}_t = 10,000$ feet. Then from Figure 14, antenna diversity will add 86 miles (from $d=26$ miles out to $d=112$ miles) to that obtained from reduced sea water reflections, and will add 100 miles (from $d=12$ miles out to $d=112$ miles) to that obtained from reduced dry soil reflection. This neglects the 14 miles and 8 miles on the left of the regions of reduced reflection from sea water and dry soil respectively. At $\tilde{h}_t = 10,000$ feet, the antenna diversity outer limit (for $\Delta h_r = 9$ feet) is only 28 miles from the radio horizon. Note for the receiver antenna very close to the ground, frequency diversity is not useful.

Figure 15 illustrates the 10 db case when $r_2 \gg r_1$, and say $\tilde{h}_r \leq 50$ feet. As above, frequency diversity yields no benefits in this case. However, antenna diversity with $\Delta h_r = 9$ feet, and $\tilde{h}_t = 10,000$ feet above sea water for example, yields an additional aircraft separation of 50 miles (from $d=80$ miles out to $d=130$ miles). Above dry soil, an additional 100 miles is obtained (from $d=30$ miles out to $d=130$ miles). This is quite similar to the 3 db case, and the $\tilde{h}_r = 9$ feet antenna diversity limit is quite close to the radio horizon.

2.4 ASSESSMENT OF GROUND ROUGHNESS ON BENEFITS FROM DIVERSITY TECHNIQUES

Perfectly smooth terrain over a significant distance is relatively rare. Commonly, natural surfaces have some roughness, one effect of which is to attenuate the waves scattered from it. It is usually convenient to model

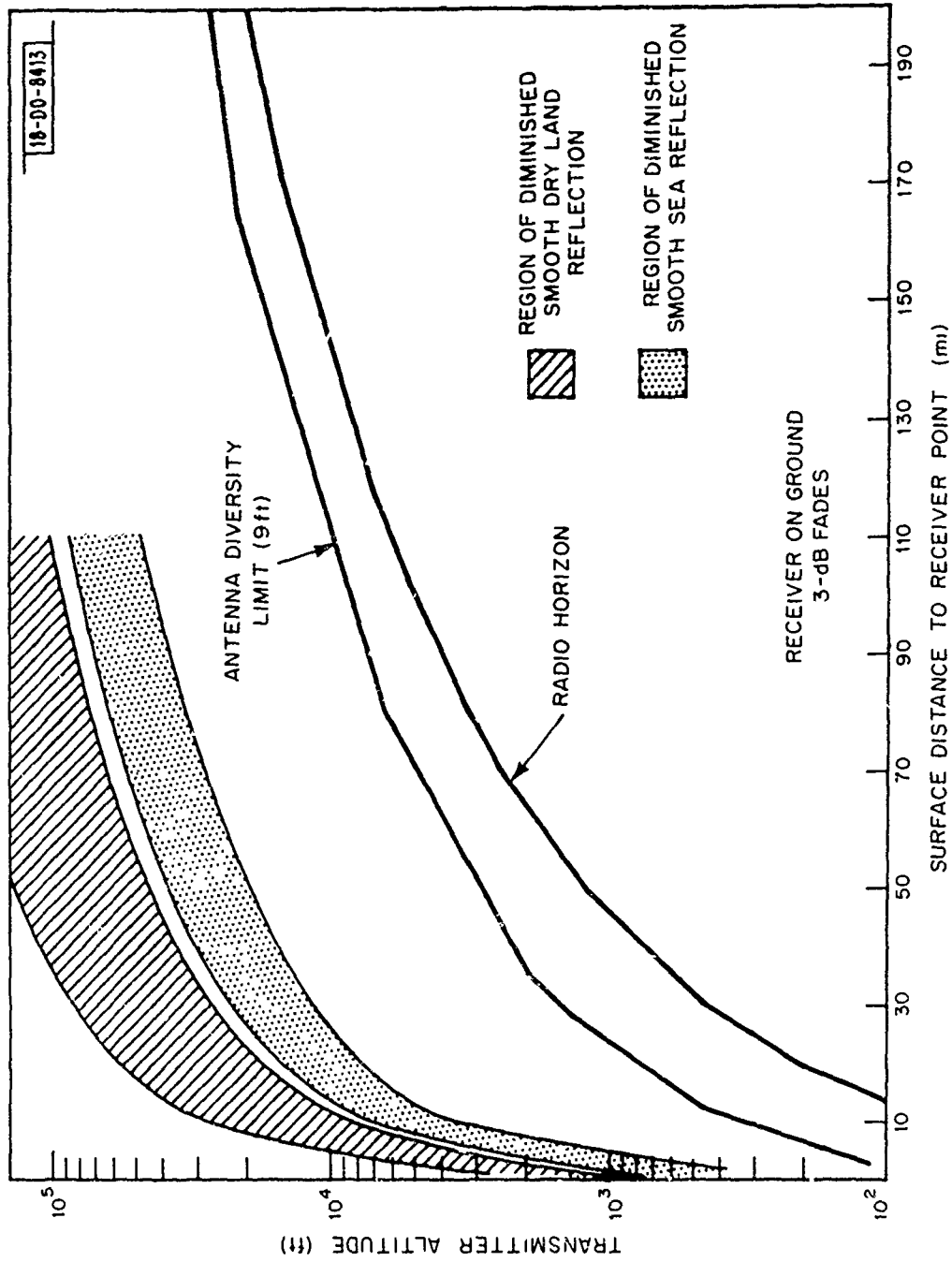


Fig. 14. Antenna and frequency diversity limits, smooth terrain reflection and divergence limits for 3 dB fades illustrated in h_r - d space when $r_2 \gg r_1$.

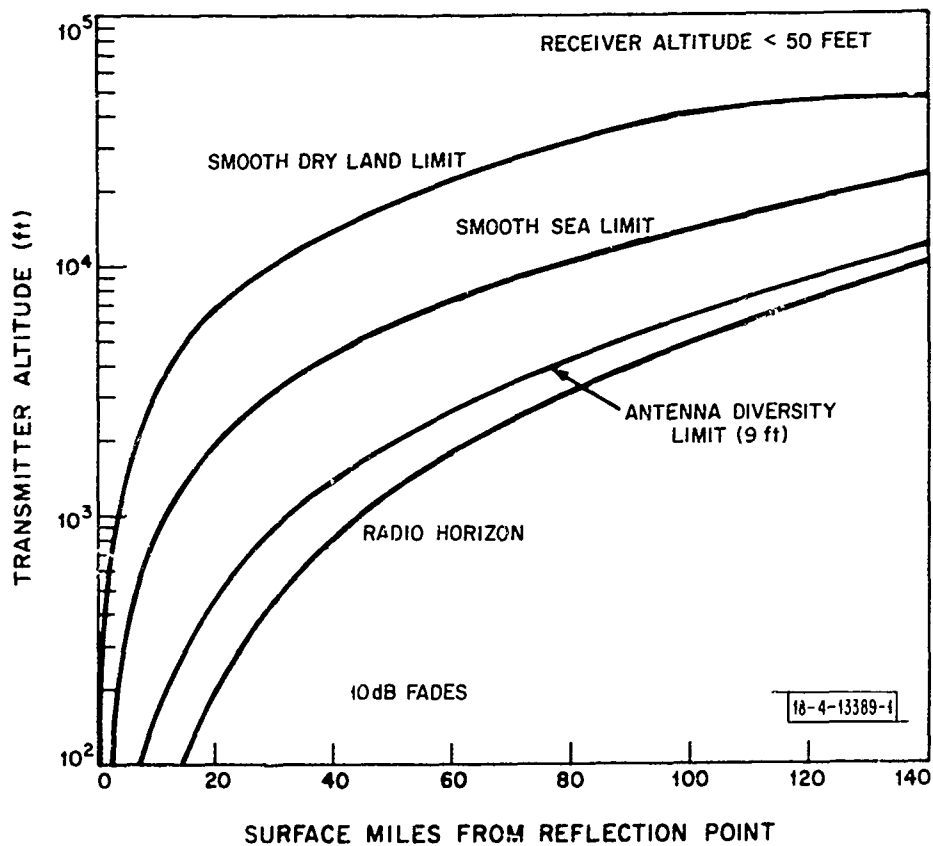


Fig. 15. Antenna diversity limit, terrain reflection and divergence limits for the 10 dB case in the presence of smooth terrain illustrated in \tilde{h}_r -d space when $r_2 \gg r_1$.

non-smooth surfaces as a sample function of a Gaussian random process [2,3]. If the surface state varies with time, as it does for the ocean, or if the transmitter and/or receiver are in relative motion over the non-smooth surface, then the received signal may be conveniently decomposed into specular and diffuse components [2,3]. The specular component may be conveniently modeled as a deterministic signal for which the angle of incidence of the incident rays with respect to a reference or datum surface equals the angle of reflection of the reflected rays with respect to that reference surface [3]. At the low grazing angles of interest in the present work, the specular component completely dominates the diffuse component [2,3]; and it is that component which is considered in the interference model. The reflection coefficient R of the non-smooth surface is given by Eq. (5)* with the specular scatter coefficient ρ_s approximated by Eq. (7). Both theory and experiment indicate that Eq. (7) is a fairly accurate mathematical model for ρ_s . For a smooth surface, $\rho_s=1$ and for non-smooth surfaces with σ (the RMS height of the surface irregularities) greater than zero, then $0 < \rho_s < 1$. Eq. (7) for ρ_s is illustrated in Figure 2.

To obtain some reasonable numerical results, a tabulation of the presently-known statistics of ocean roughness [4] was consulted. From this, it was observed that ocean wave height was greater than or equal to 4 feet about half the time. Thus, $\sigma=4$ feet was chosen as a reasonable median value with which to numerically evaluate Eq. (7). From Eqs. (5), (6), and (7) and $\sin \alpha_r = h/r$, results for $\tilde{h}_r = \tilde{h}_r(\alpha_r)$ were obtained for the combined effects from

* $R = |R_0^+| D \rho_s$

smooth surface reflection, surface roughness, and curvature. When $r_2 \gg r_1$ then, for the 3 db case

$$\tilde{h}_r = h_r^* + R_e \sin^2 \alpha_r \{10R_0^2(\alpha_r) \exp[-128\pi^2 \sin^2 \alpha_r] - 1\} / 2 \quad (39)$$

while for the 10 db case

$$\tilde{h}_r = h_r^* + R_e \sin^2 \alpha_r \{2R_0^2(\alpha_r) \exp[-128\pi^2 \sin^2 \alpha_r] - 1\} / 2 \quad (40)$$

These have been plotted in Figures 16 (3 db case) and 17 (10 db case).

Comparing these figures with the corresponding figures for smooth terrain, it is clear that the benefits from frequency and antenna diversities, beyond those provided by the electromagnetic properties of the media and curvature of the terrain surface, are substantially less when the terrain is non-smooth. This is also seen to be true in the $r_2=r_1$ case illustrated in Figures 18 (3 db case) and 19 (10 db case). In addition, the double-valued angle effect from R_0 (arising from the pseudo-Brewster angle effect) is absent in the rough terrain cases. The frequency and spatial antenna diversity limit curves shown in Figures 16 to 19 are unchanged from the corresponding curves in Figures 6 to 9 because terrain roughness does not enter the equations developed to describe the effect of these techniques.

To examine the reduction in benefits from diversity techniques when the terrain is rough with $\sigma=4$, consider first the comparisons in the 3 db case. In general, the range of angles α_r (within which antenna diversity with

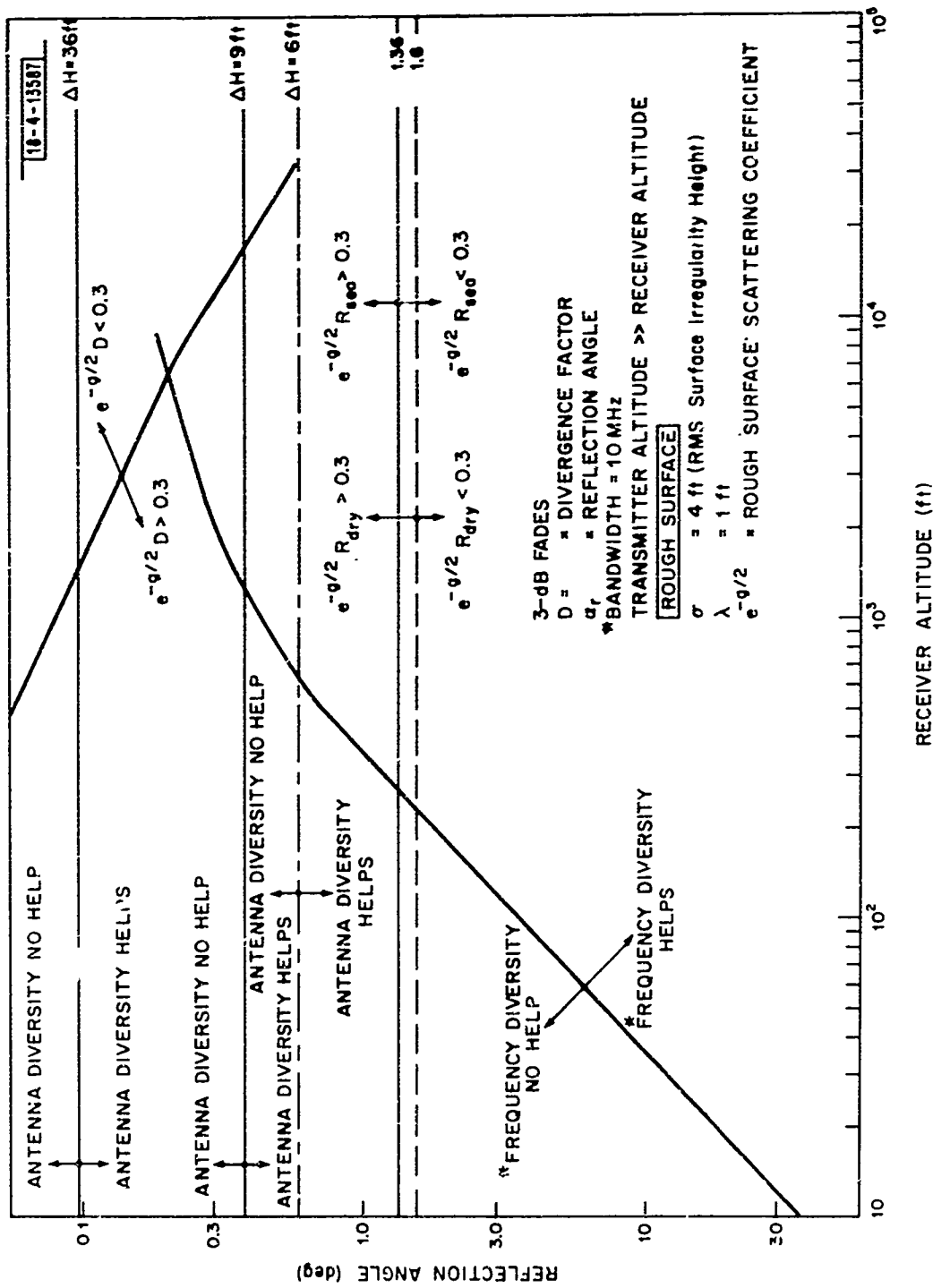


Fig. 16. Antenna and frequency diversity limits, non-smooth terrain reflection and divergence limits for the 3 dB case with $\sigma = 4$ feet illustrated in $\alpha_r - h_r$ space when $r_2 \gg r_1$.

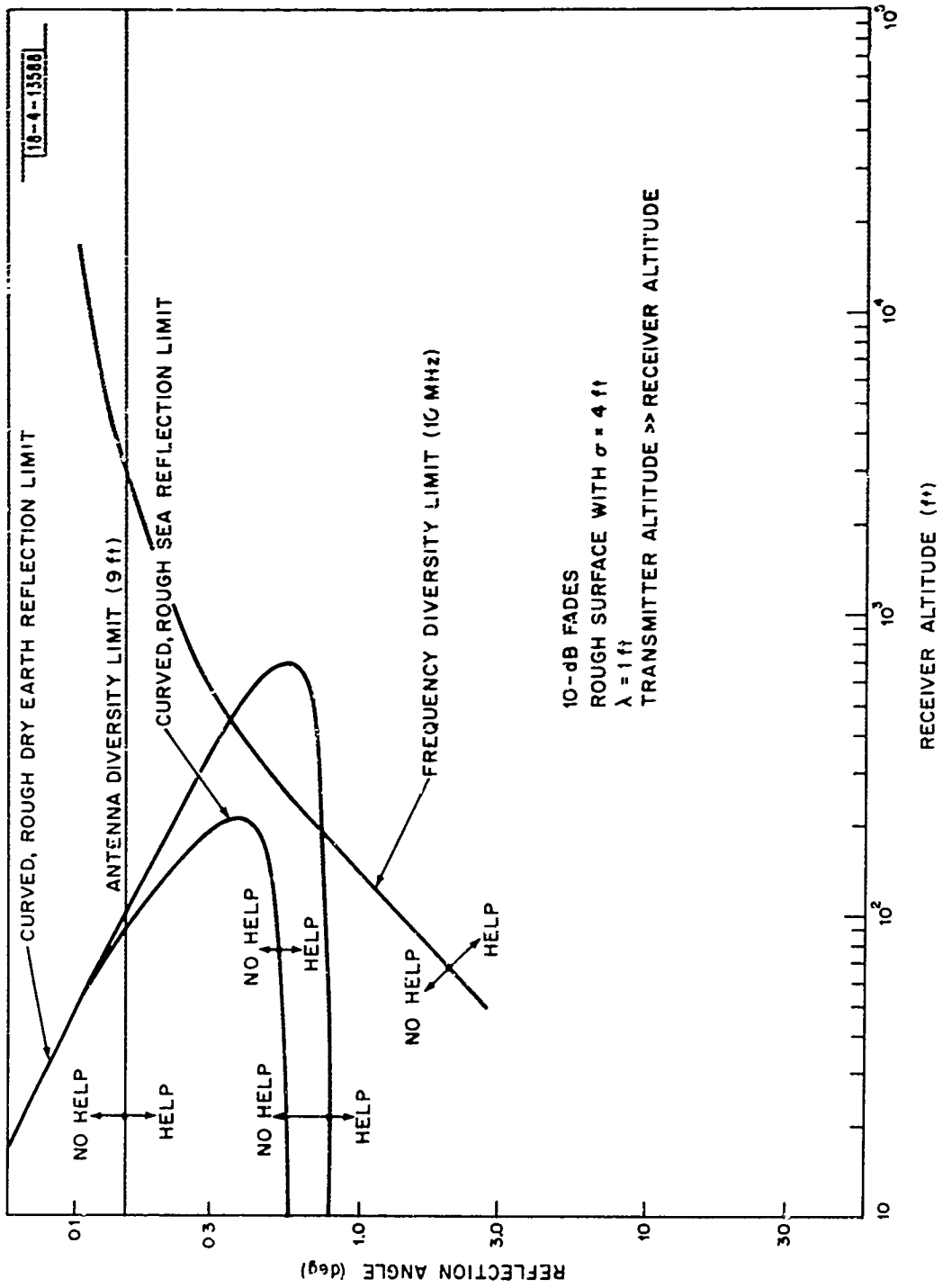


Fig. 17. Antenna and frequency diversity limits, non-smooth terrain reflection and divergence limits for the 10 dB case with $\sigma=4$ feet illustrated in α_r-h_r space when $r_2 \gg r_1$.

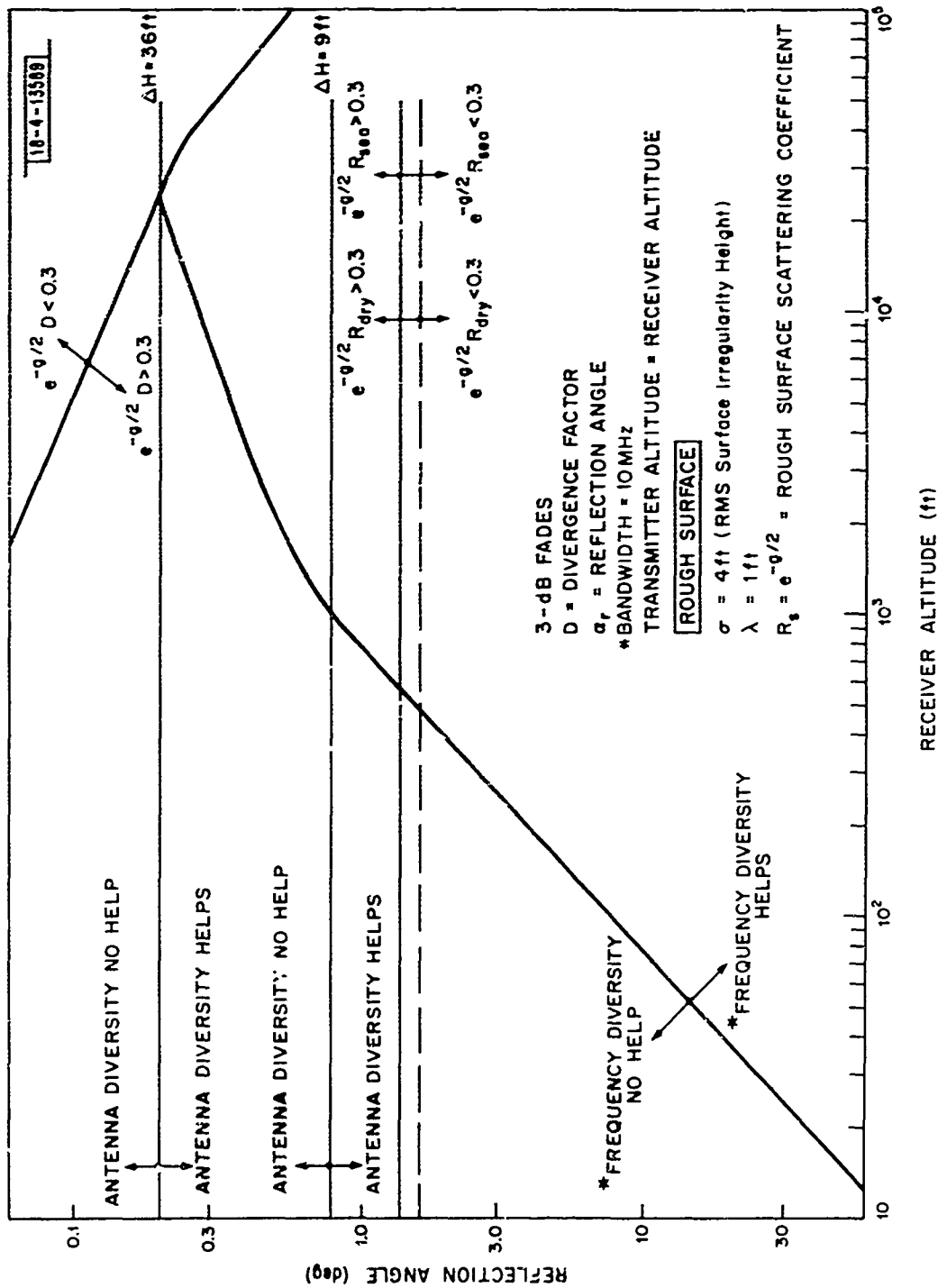


Fig. 18. Antenna and frequency diversity limits, non-smooth terrain reflection and divergence limits for the 3 dB case with $\sigma = 4$ feet illustrated in $\alpha_r - h_r$ space when $r_2 = r_1$.

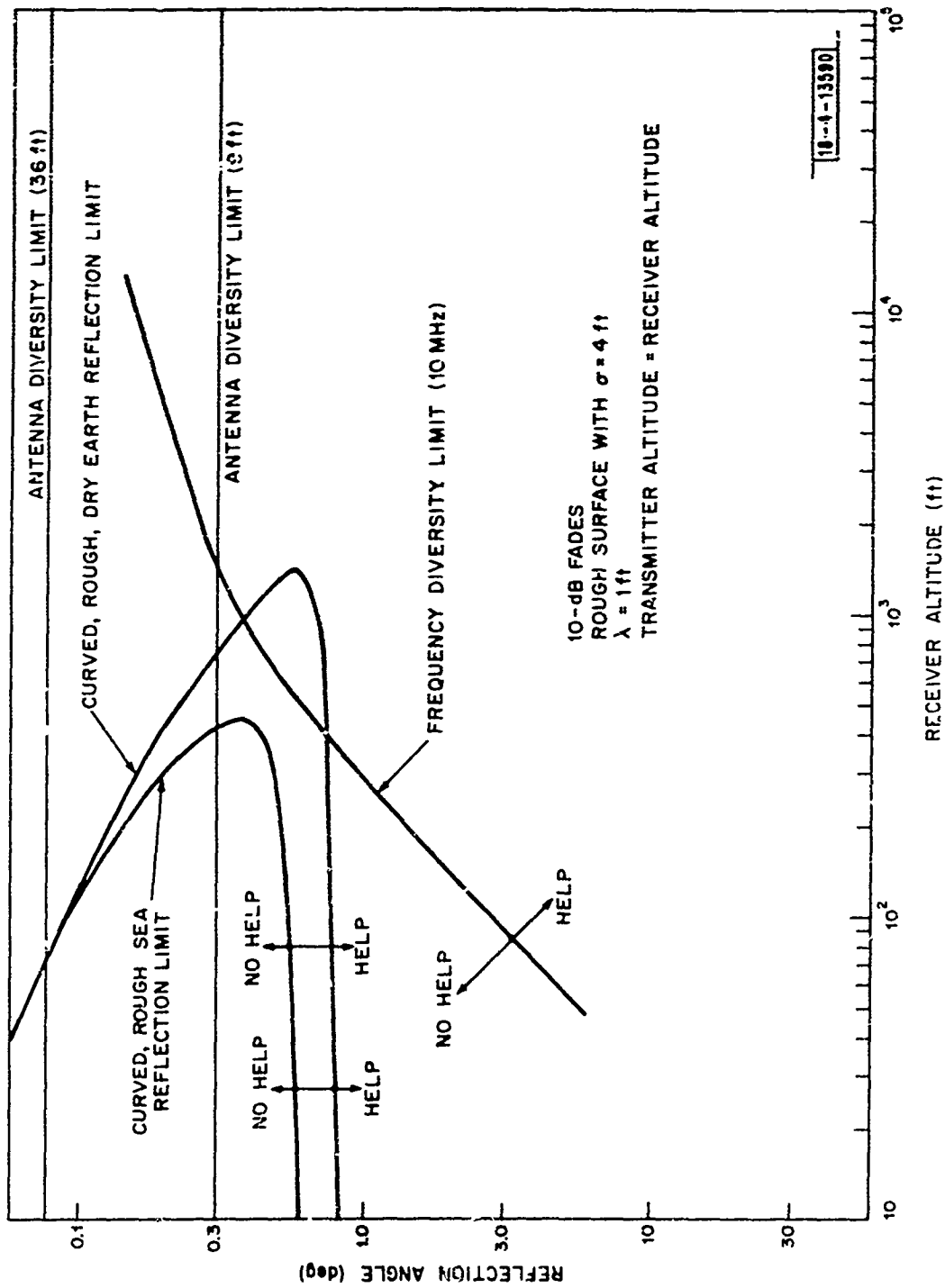


Fig. 19. Antenna and frequency diversity limits, non-smooth terrain reflection and divergence limits for the 10 dB case with $\sigma = 4$ feet illustrated in $\alpha_r - h_r$ space when $r_2 = r_1$.

$\Delta h_r = 9$ feet is of use) is much less in the 3 db non-smooth terrain case than in the 3 db smooth terrain case. When $r_2 = r_1$ and $r_2 \gg r_1$ the band of angles for naturally reduced terrain reflection changes to a single boundary where:

- (1) The range of α_r changes from about 4° through 8° to the single value of about 1.5° for sea water.
- (2) The range of α_r changes from about 9.5° through 32° to the single value of close to 1.5° .

When $r_2 = r_1$, the minimum receiver altitude at which frequency diversity ($\Delta f = 10$ MHz) is needed.

- (1) Is raised from about $\tilde{h}_r \approx 200$ feet to about 700 feet for sea water.
- (2) Is raised from about $\tilde{h}_r \approx 80$ feet to about 600 feet for dry soil.

Comparing Figure 20 with Figure 14, it is seen that the extra inter-aircraft distance for $\tilde{h}_r = 10,000$ feet for which $F \geq 3$ db obtained by spatial diversity is reduced:

- (1) From 144 miles in the smooth terrain case to 55 miles in the non-smooth dry soil case.
- (2) From 116 miles to 48 miles in the non-smooth sea water case.

The comparison is even sharper when the distances to the left of sea water and dry soil curves in Figure 20 are taken into account.

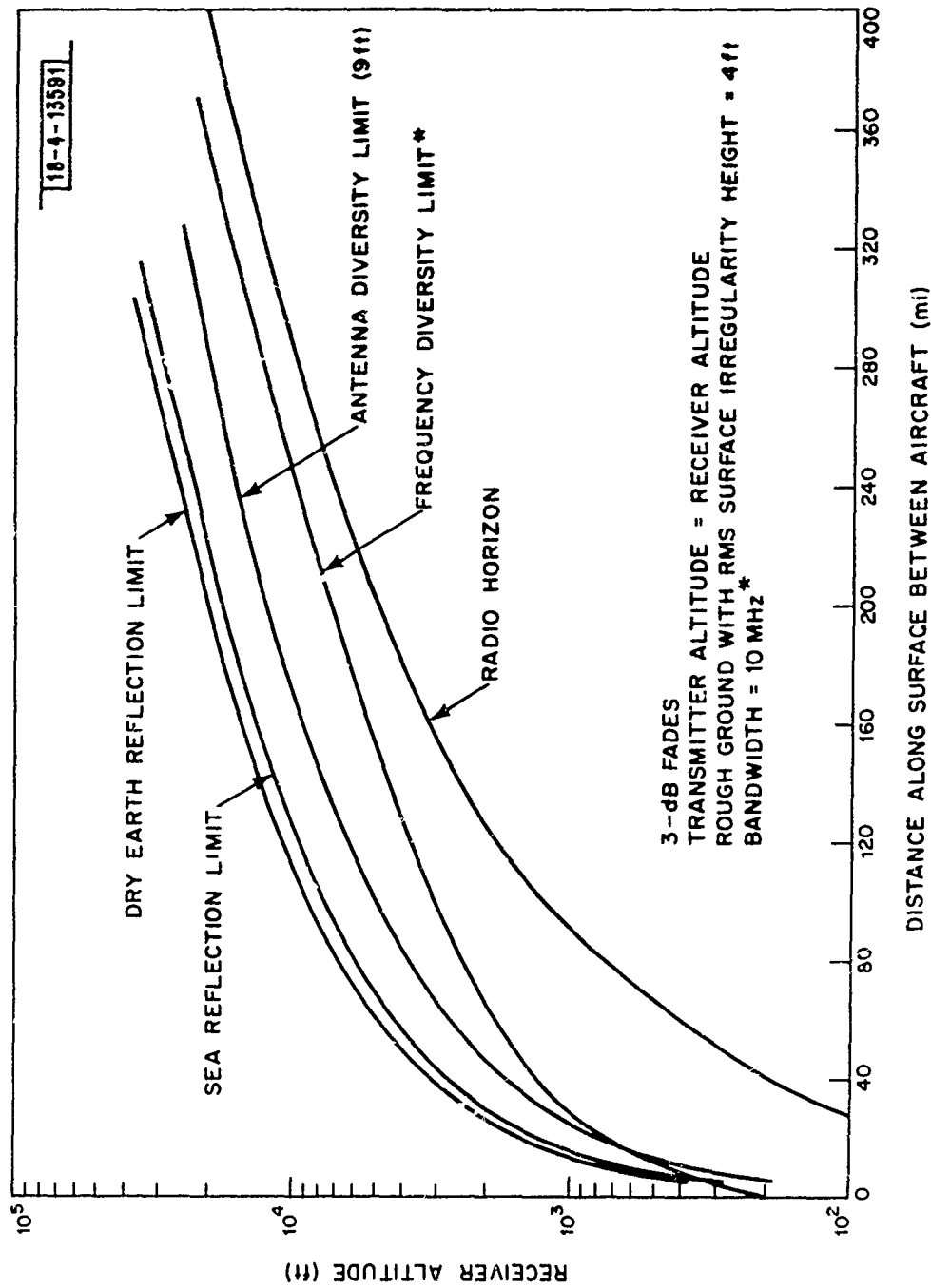


Fig. 20. Antenna and frequency diversity limits, non-smooth terrain reflection and divergence limits for the 3 dB case with $\sigma=4$ feet illustrated in \tilde{h}_r -d space when $r_2=r_1$.

In the 3 db case, with $\sigma = 4$ feet, and $r_2 \gg r_1$, Figure 21 should be compared with Figure 15. It may be seen that the minimum altitude at which frequency diversity ($\Delta f = 10$ MHz) is needed:

- (1) Is raised from about $\tilde{h}_r = 100$ feet to about 280 feet for sea water.
- (2) Is raised from about $\tilde{h}_r = 38$ feet to about $\tilde{h}_r = 240$ feet for dry soil.

Comparing Figure 21 with Figure 14, it is seen that the extra interaircraft distance from $\tilde{h}_r = 10,000$ feet (for which $F \geq -3$ db) obtained by spatial diversity is reduced:

- (1) From 86 miles in the smooth sea water case to 51 miles for non-smooth sea water.
- (2) From 100 miles in the smooth dry soil case to 67 miles for non-smooth dry soil.

In the 10 db case, the effect of non-smooth terrain with $\sigma = 4$ is again considered. As in the 3 db case, the band of angles in the smooth terrain case for reduced terrain reflection from sea water due to decreased R_0 (and D) as a function of α_r is changed to a single boundary line when the terrain is non-smooth. The dry soil reflection case is a single boundary for (in the 10 db case) both smooth and non-smooth terrain. Considering Figures 17, 19, 13, and 15, in general:

- (1) The range of angles α_r (within which antenna diversity with $\Delta h_r = 9$ feet is of use) is much less in the 10 db non-smooth terrain case than in the 10 db smooth terrain case.
- (2) The frequency diversity technique (with $\Delta f = 10$ MHz) is of little use in both smooth and non-smooth terrain cases.

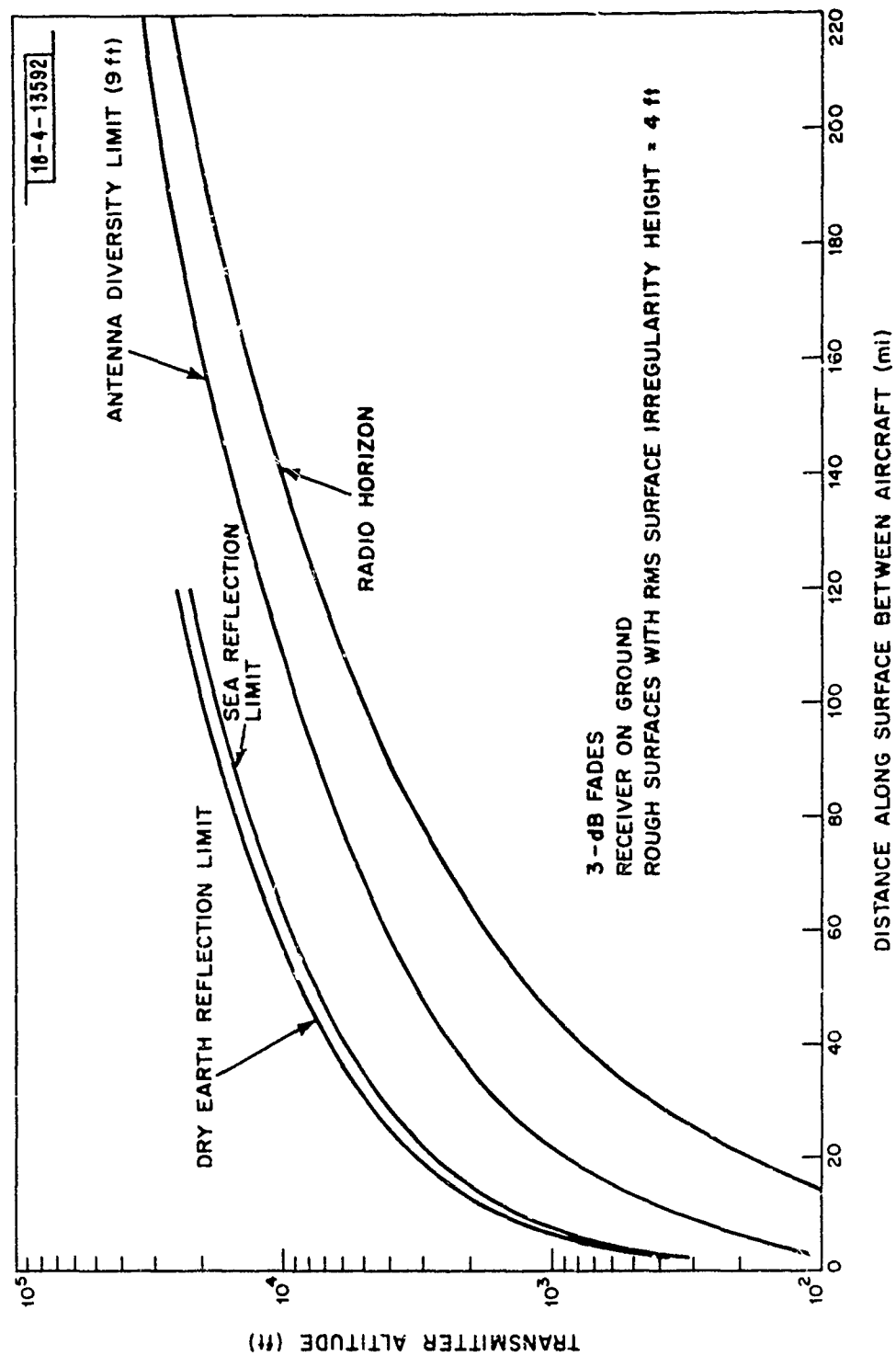


Fig. 21. Antenna and frequency diversity limits, non-smooth terrain reflection and divergence limits for the 3 dB case with $\sigma=4$ feet illustrated in h_r - d space when $r_2 \gg r_1$.

When $r_1 = r_2$, then comparing Figures 22 and 13, it is clear that antenna diversity (with $h_r = 9$ feet) is of use in a smaller range of h_r when the terrain is rough. Thus, in Figure 13 (with smooth terrain) the maximum receiver altitude above sea water for which height diversity is of use, is about 800 feet while in Figure 22 it can be seen that the maximum useful receiver altitude above sea water is about 450 feet. For the preceding sea water case, the maximum useful inter-aircraft separation is typically about 12 miles when the terrain is smooth, and about 3 miles when the terrain is non-smooth. For dry soil, in this case the maximum useful interaircraft separation is typically about 40 miles when the terrain is smooth, and typically less than 10 miles when the terrain is non-smooth.

When $r_1 \gg r_2$ then comparing Figures 23 and 15 it is again clear that non-smooth terrain reduces the usefulness of antenna diversity. For example with $\Delta h = 9$ feet, and a transmitter altitude above the curved earth of 5,000 feet antenna diversity "buys" a bit less than 50 miles when the surface is a smooth sea while antenna diversity "buys" a bit less than 30 miles for a nonsmooth sea. For the same conditions antenna diversity "buys" a bit more than 90 miles over smooth dry earth, but only buys approximately 40 miles over nonsmooth dry earth.

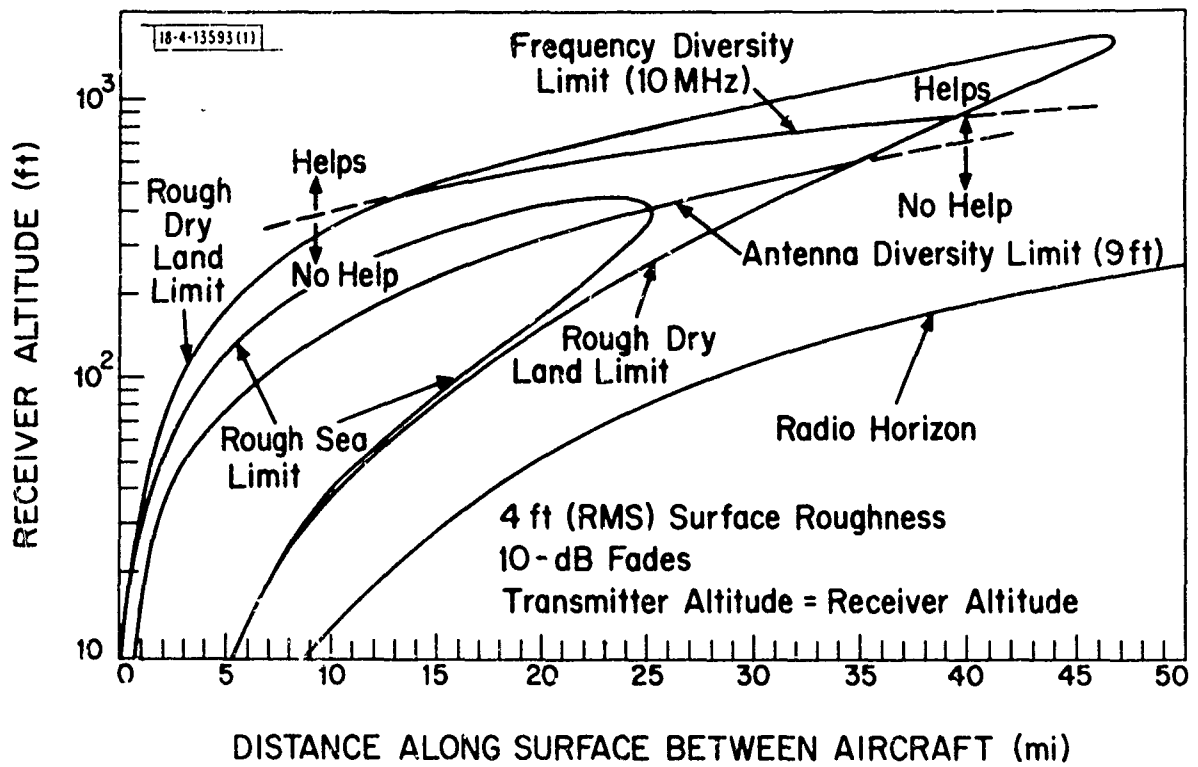


Fig. 22. Antenna diversity limits, non-smooth terrain reflection and divergence limits for the 10 dB case with $\sigma=4$ feet illustrated in \tilde{h}_r -d space when $r_2=r_1$.

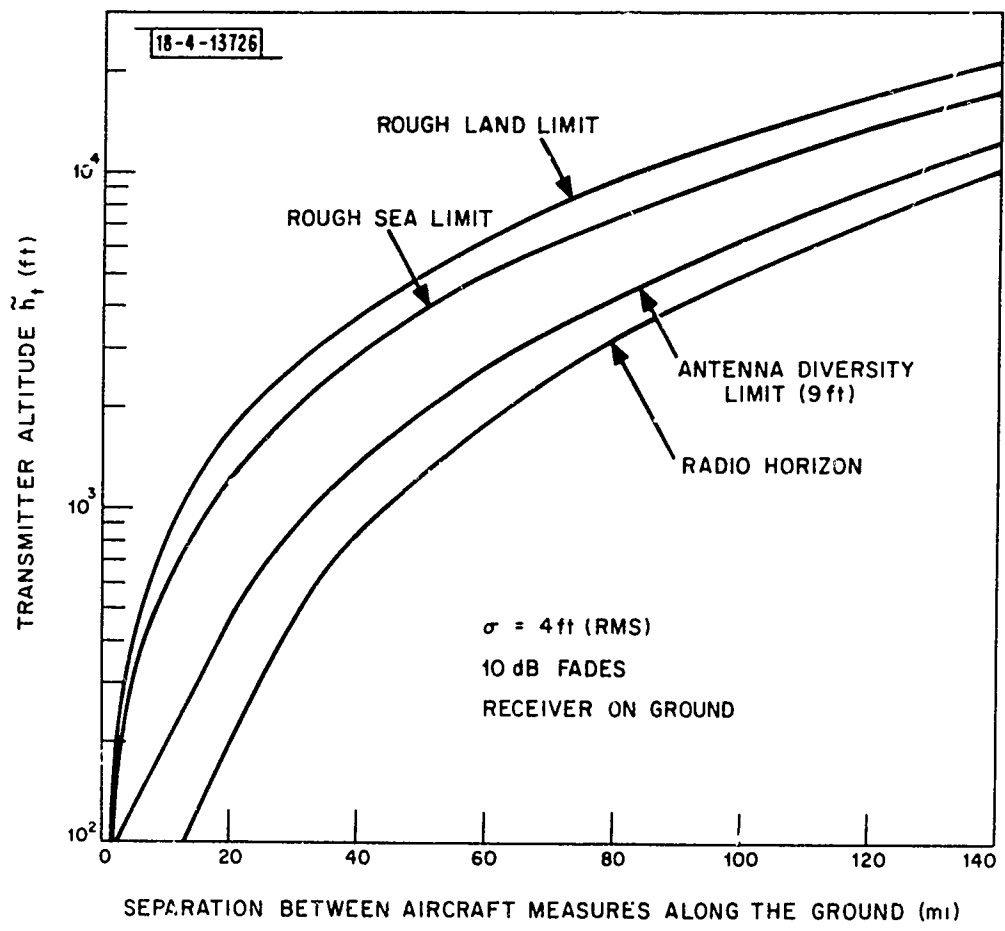


Fig. 23. Antenna diversity limits, non-smooth terrain reflection for the 10 dB case with $\sigma=4$ feet illustrated in \tilde{h}_t - d space when $r_2 \gg r_1$.

2.5 COMMUNICATION BETWEEN A HIGH ALTITUDE TRANSMITTER AND LOW ALTITUDE RECEIVERS

Antenna diversity can overcome severe multipath problems when communication is attempted between a high altitude transmitter (possibly a drone relay) and low flying aircraft. However, this useful effect is substantially reduced when the surface is not smooth.* The reason for this reduction is that the rough surface produces much less severe multipath reflection than the case of the comparable smooth surface and hence there is much less to be "bought" by the use of antenna diversity.

The calculations in this section are all based on the theory presented in prior sections for vertically polarized waves. To be specific, it will be assumed that the high flying transmitter is at an altitude of 50,000 feet above the curved earth with $\Delta h = 9$ feet and $\Delta f = 10$ MHz. The two fade margins of 3 db and 10 db are selected for illustrative examples. The commentary here will center on four figures which should illustrate all the points of interest, Figures 24, 25, 26 and 27. The vertical coordinate is receiver altitude (in feet) and the horizontal coordinate is interaircraft separation (in miles) as measured along the curved surface of the earth.

In Figure 24, a 3 db case for a smooth earth, two regions of diminished surface reflection are indicated, one for smooth sea reflections and one for smooth dry earth reflections. Within these regions in $\tilde{h}_r - d$ space the fading is less than 3 db due to sufficiently low surface reflection. The fact that each region is bounded by two lines can be attributed to

* As in Section 2.5 a value of 4 feet RMS will be used for σ in the numerical examples.

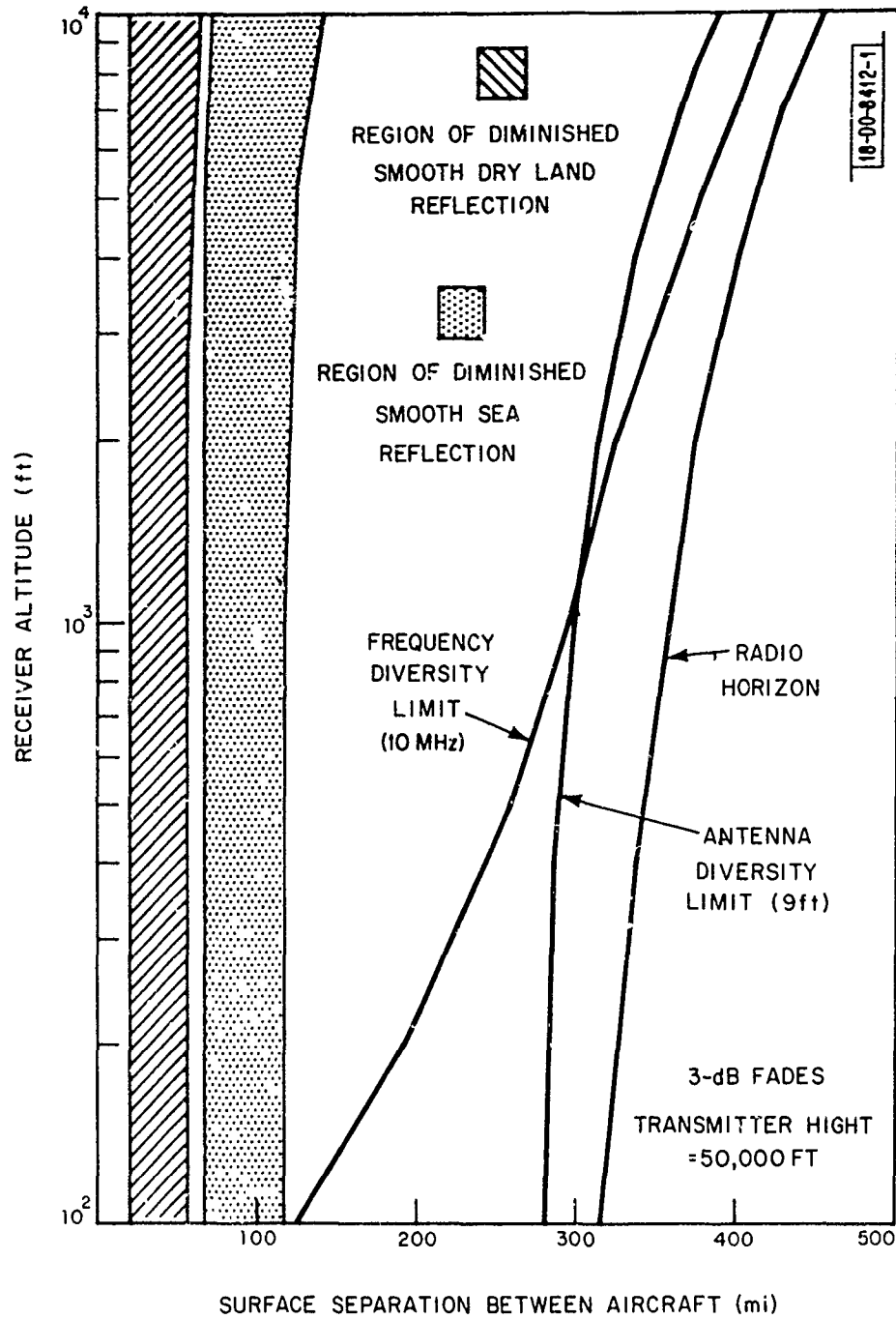


Fig. 24. Receiver altitude vs interaircraft separation measured along smooth curved ground for 3 dB fades when the transmitter altitude is 50,000 feet.

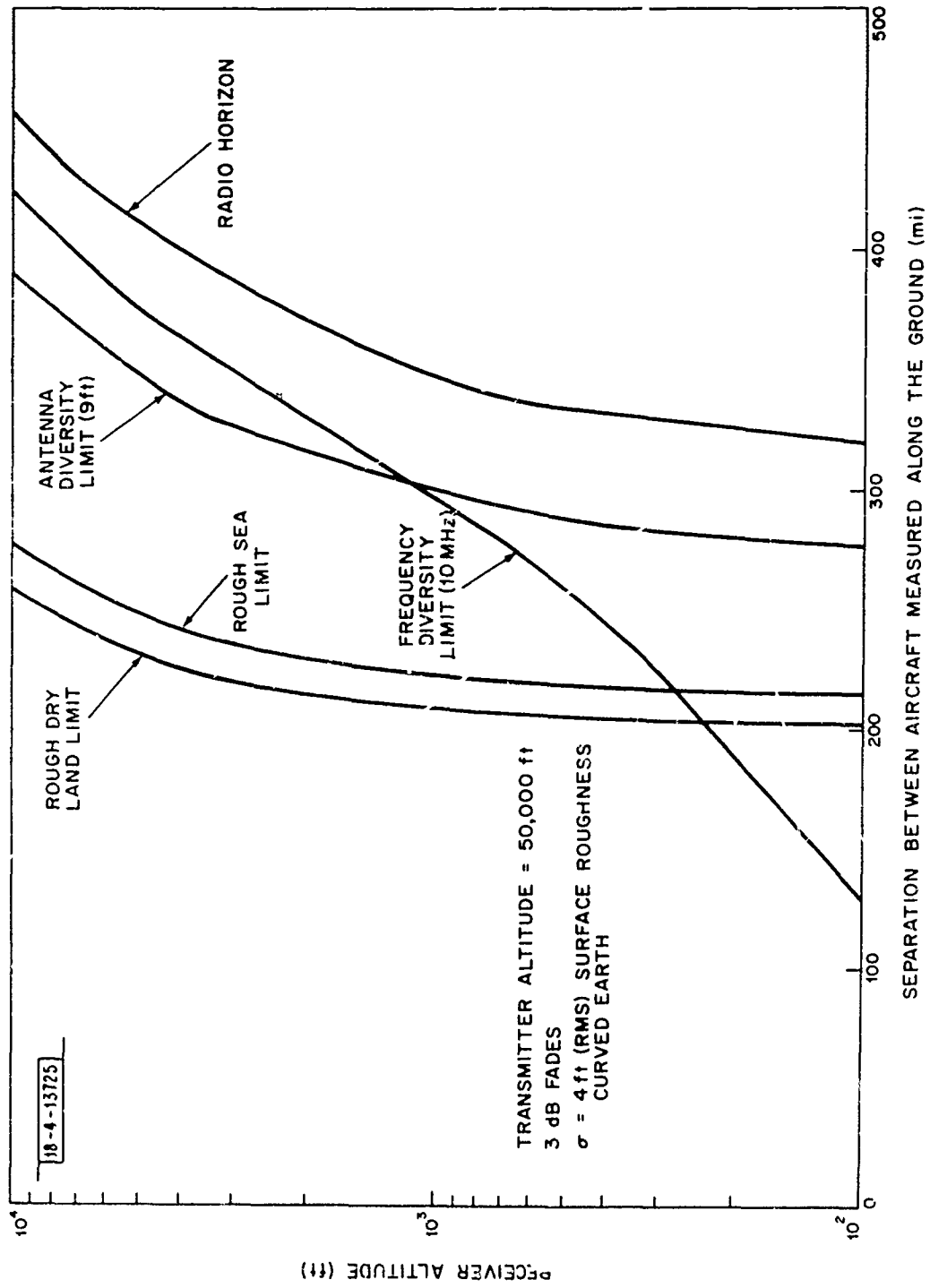


Fig. 25. Receiver altitude vs interaircraft separation measured along rough ($\sigma=4$ feet) curved ground for 3 dB fades when the transmitter altitude is 50,000 feet.

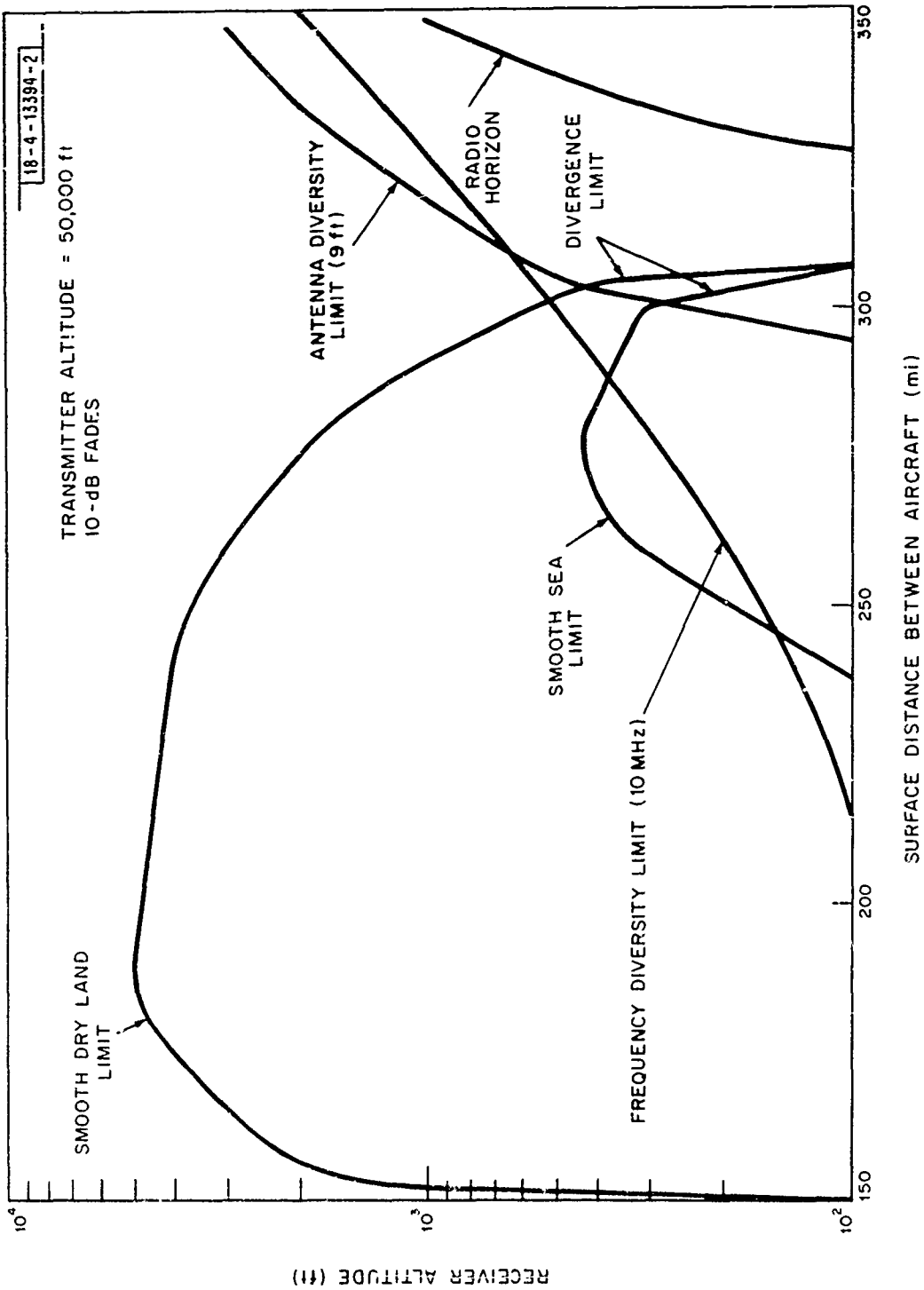


Fig. 26. Receiver altitude vs interaircraft separation measured along smooth curved ground for 10 dB fades when the transmitter altitude is 50,000 feet.

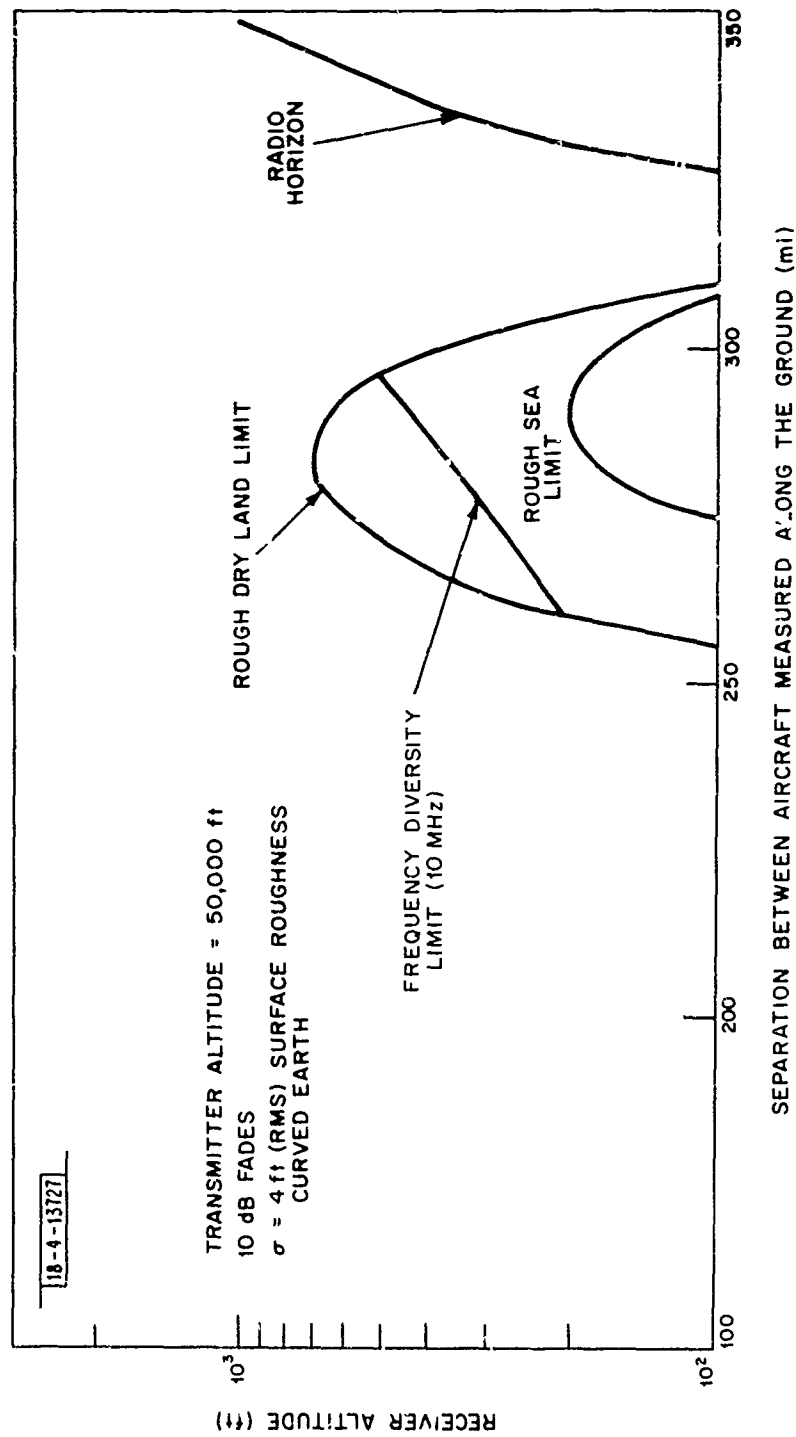


Fig. 27. Receiver altitude vs interaircraft separation measured along rough ($\sigma=4$ feet) curved ground for 10 dB fades when the transmitter altitude is 50,000 feet.

the Brewster angle effect (this type of double boundary has shown up on earlier graphs). Outside these regions the fading will be equal to or greater than 3 db in the absence of the use of any antifading technique. The use of frequency diversity in the manner described in earlier sections limits the region of 3 db or greater fading everywhere to the right of the curve shown in Figure 24 up to the edge of the usable space demarked by the radio horizon. Frequency diversity prevents unacceptable fades over increasing interaircraft distances as the receiver altitude increases. The use of spatial diversity (with $\tilde{h} = 9$ feet) is more effective than frequency diversity below about $\tilde{h}_r = 10^3$ feet yielding as much as an additional 150 miles of usable separation at $\tilde{h}_r = 10^2$ feet. The amount of extra usable space "bought" by the use of spatial diversity over frequency diversity decreases monotonically as \tilde{h}_r increases until about 10^3 feet. Above this "crossover" altitude, frequency diversity "buys" a larger usable separation, the amount of which increases to about 70 additional miles when $\tilde{h}_r = 10^4$ feet.

Figure 25 shows a situation similar to Figure 24 for the 3 db case and applies to communication over rough surfaces. The frequency diversity limit, antenna diversity limit and radio horizon lines are the same as in Figure 24. As in previous figures for the non-zero ground roughness case, the Brewster angle effect does not show up in the curves and only single lines demark the region where fades are greater than 3 db (to the right of the lines in Fig. 25). The other major effect is that illustrated by the "inner" boundary of the region of diminished reflection from the sea. This is fairly vertically oriented in Figures 24 and 25 but begins at an interaircraft distance (d) of 120 miles

at $\tilde{h}_r = 10^2$ feet in Figure 24; and the single line begins in Figure 25 at a d of 215 miles for $\tilde{h}_r = 10^2$ feet. Similarly, for smooth dry land reflections, the inner boundary begins at about $d = 60$ miles for $h_t = 10^2$ feet and the single boundary for rough dry land reflections in Figure 25 begins at about $d = 202$ miles for $\tilde{h}_r = 10^2$ feet. Figures 24 and 25 illustrate the general statement made at the beginning of this section that for the high transmitter-low receiver case, frequency and spatial diversity can "buy" a great deal of usable space but the extent of this space is greatly reduced by terrain roughness.

In order to complete the calculations in the 3 db case above, and in the 10 db case to follow, certain simple geometric transformations were required. Thus, in earlier curves, $\alpha - \tilde{h}_r$ or $\tilde{h}_r - d$ was plotted. These earlier curves could be used to generate the curves in Figures 24 to 27 by using the relations

$$h \approx d \sin \alpha$$

$$\tilde{h} \approx h + \frac{1}{2R_e} \left(\frac{1}{\sin \alpha} \right)^2$$

which combine to give

$$\tilde{h} \approx d \sin \alpha + d^2 / 2R_e$$

or its inverse

$$d = \sqrt{R_e^2 \sin^2 \alpha + 2h R_e} - R_e \sin \alpha$$

For $h_t \gg h_r$ this yields the distance from the transmitter (or receiver) to the point of ray reflection (as measured along the ground), given the altitude \tilde{h} above the curved surface and α .

Figures 26 and 27 show the usefulness of the two diversity techniques in alleviating 10 db fades over smooth and rough terrain. The concave curves "smooth dry land limit" and "smooth sea limit" in Figure 26 delineate those regions (in \tilde{h}_r -d space) where 10 db fades may be experienced over the respective smooth terrains. We see that antenna diversity alleviates 10 db fades in almost all of the \tilde{h}_r -d space where such fades occur for either terrain. Frequency diversity is of substantial aid over dry land, but is of little help in alleviating 10 db fades over sea.

Figure 27 shows the rough surface case for 10 db fades. Again the frequency diversity, spatial diversity, and radio horizon lines are from the smooth surface case, shown in Figure 26. However, the concave boundaries (for greater than 10 db fades) for the rough land and rough sea case are greatly reduced. For example, for the dry land case, the concave curve in Figure 26 goes from $d \approx 150$ miles to $d \approx 310$ miles at $\tilde{h}_r = 10^2$ feet. The corresponding curve in Figure 27 goes from $d \approx 255$ miles to $d \approx 310$ miles at $\tilde{h}_r = 10^2$ feet. Thus, there is a much smaller interaircraft distance in which the use of diversity is needed to alleviate severe fades.

The preceding should not obscure the observation that over smooth terrain, spatial diversity can be used to prevent severe fading from occurring (when proper signal combining is used) over a significant region of \tilde{h}_r -d space.

2.6 LIMITATIONS OF THE ANALYSIS

There are many assumptions and approximations in the preceding four sections of analysis, most of which were noted at the appropriate points of the discussion. This section will briefly recall some of the most crucial ones and then indicate a number of others which were not mentioned earlier.

2.6.1 Atmospheric Effects

The text uses the convenient and commonly used "4/3-earth radius" approximation to take into account the curvature of the electromagnetic ray paths in the lower atmosphere due to changes of atmospheric refractive index n . However, there are a great variety of profiles of n with altitude which are usually possible. These are dependent upon the geographic location of interest, the weather, the time of day, and many other factors [5]. The idea of height-error correction by accounting for the refractivity* N and the initial gradient of N at the surface of the site of interest has had considerable discussion [5] but cannot be applied to designing a system which must be utilized in a wide variety of situations. Further, there exist atmospheric phenomena which involve "anomalous propagation" which are not at all anomalous (i.e., rare) at many geographic locations. Some of these are radio holes, anti-radio holes, and elevated ducts [6].

2.6.2 Geometric Effects

The condition

$$h_r, h_t \ll d \quad (41)$$

* $N \equiv (n-1.0) \times 10^6$

given in subsection 2.1.1 is crucial to all that follows, but can be expected to hold for the majority of situations in which the diversity techniques might be applied. Special cases have been considered, e.g., $\tilde{h}_t \gg \tilde{h}_r$, but these conditions do not replace Eq. (41). Rather, they are in addition to it.

Eq. (6), for the divergence factor D , is sometimes said in the literature to hold for "sufficiently small" angles but it is shown in [3] that it holds so long as $r_1, r_2 \ll R_e$ (which should hold in all practical applications of the diversity techniques) and may be confidently used for all values of the reflection angle α_r .

It has been implicitly assumed in the interference model analysis that the problem may be treated with a scalar theory. However, the directions of propagation of the direct and reflected rays are not exactly coincident. Rather, the rays meet at an angle θ radians, and the projection of the field strength vector associated with one ray onto the field strength vector associated with the other ray must be taken into account. The phasor character used in the analysis involves physically different effects and does not account for the preceding effect. Fortunately for the cases considered, i.e., $\tilde{h}_t = \tilde{h}_r$ and $\tilde{h}_t \gg \tilde{h}_r$, the angle θ is exactly equal to or close to α_r so that when the ray projection is taken, $\cos(\alpha_r)$ will occur as a multiplicative constant. Since, for $\alpha_r \leq 10^\circ$, then $\cos \alpha_r \geq 0.985$; the effect is small enough to be neglected in the situations of interest in this work.

2.6.3 Propagation Effects

The ray picture of electromagnetic wave propagation is useful within the interference region.* However, buildings, aircraft structures and other obstacles present problems that are often best approached with wave theory. Another situation in which the application of ray theory may have to be re-examined with care is when the terrain reflection area is within the near field of one of the antennas, such as might occur in the case when $\tilde{h}_t \gg \tilde{h}_r$. Chapter 2 of Kerr [1] deals extensively with the conditions required for the application of ray theory, and to a much lesser extent, portions of Reed and Russell [7] (e.g., see 5.10 of [7]) do also.

2.6.4 Antenna Effects

The spatial and frequency diversity techniques described in subsections 2.2.3 and 2.2.4 are constructed so as to be independent of the probable variations of the antenna gain patterns with spatial direction in the first case and frequency in the second case. However, the potential occurrence of fades of various depths in the absence of diversity are dependent upon the practical antenna gain pattern variations. By determining these potential occurrences, the benefit of diversity usage can be better assessed. When there are antenna gain variations, Eq. (4) must be rewritten as

$$E = E_d g_d \{1 + R(g_r/g_d) \exp [j(\varphi_s + \varphi_L)]\} \quad (42)$$

* This region was described earlier as occurring between the beginning of the far field of the transmitting antenna and out to near the radio horizon.

where g_d and g_r are the gains of the receiving antenna in the directions of the direct and reflected ray paths respectively. Some numerical values will be used to indicate the effect of (g_r/g_d) . If $g_r/g_d < 0.7$, then 10 db fades cannot occur and the amount of fade protection gained by diversity technique usage is limited. If $g_r/g_d < 0.3$, then 3 db fades cannot occur and the need for diversity techniques is questionable. On the other hand, if $g_r/g_d > 1$, the amount of fade protection gained by diversity technique usage is greater than for isotropic antennas.

Another circumstance of concern is when the multiple antennas used in a spatial diversity system do not exhibit identical gain patterns. It is implicit in the analysis presented earlier that the direct signal strength is the same at all the antenna elements in the antenna system. Differences in the signal strength must be accounted for in practice in the design of the diversity combining network.

2.6.5 Diffuse Reflection Effects

When the terrain surface is rough, the diffuse component of the reflected waves exceeds in magnitude by far the specular component [2.3]. The amplitude and phase of the diffuse reflections vary in a statistical fashion; the conventional model being that the probability density function (PDF) for their phase is uniform (between 0 and 2π) and the PDF for their amplitude is a Rayleigh distribution [2]. When $h_r, h_t \ll d$, the average power contained in the diffuse component may be as high as 1/4 of the power reflected by the same surface if it were smooth. [2,3] Thus, the RMS electric field strength might

be as high as 1/2 of that of a wave reflected by the same surface if it were smooth.

In CW experiments, the time variations of the diffuse fluctuations appear noise like. However, in a pulsed signal experiment, the amplitude and phase of the diffuse signal may appear constant over the duration of a single pulse when that duration is sufficiently small. Thus, at a single antenna, 3 db fades and deeper ones can occur for some of the stronger diffuse reflections whose amplitudes lie in the tails of the PDF for the amplitudes. For example, in the satellite case where $\tilde{h}_t \gg \tilde{h}_r$, the average power in the diffuse component of reflection may be as high as 1/2 of the power reflected by the same surface if it were smooth [3]. In such a case, the RMS electric field strength would be 0.7 of that of a wave reflected by the same surface if it were smooth. In a case where the diffuse reflection varies slowly in time, relative to the signal duration, both of the diversity techniques under consideration would combat fades in the same manner as for the direct-specular ray interference.

2.6.6 Some Other Effects

In closing Section 2.5, two other points should be briefly noted. The first is that air frame shadowing of one or more of the antennas of a set can cause fading at the shadowed antennas. In this case, exposure to the direct wave (combined with non-effective terrain reflections), and not antenna diversity, as described in subsection 2.2.3 can cause an unfaded signal at the unshadowed antenna. During the course of an experiment, some form of diagnosis, such as the one discussed later in Section 3, must be used to clarify what is occurring.

The second observation is that discrete tones were used in the consideration of frequency diversity given in Subsection 2.2.4. The applicability of these results to spread spectrum systems which exploit a continuum of frequencies has not been investigated in this report, but from the results of Reference 15, it is expected that comparable results can be obtained with spread spectrum signalling.

SECTION 3
A MEASUREMENT PROGRAM TO EVALUATE ANTENNA HEIGHT DIVERSITY

Section 2 discussed and quantified the many advantages of spatial diversity with antenna elements separated in the vertical direction, particularly for low reflection angles. The present section discusses a measurement program to experimentally evaluate the application of vertical space diversity. This discussion will cover:

- (1) The measurements required.
- (2) The proposed receiver measurement equipment.
- (3) The proposed transmitter measurement equipment.
- (4) A list of further topics to be addressed.

3.1 MEASUREMENTS REQUIRED

In this section, the measurements required in assessing the usefulness of the antenna diversity are discussed in terms of:

- (1) Nature of the transmitter-receiver link.
- (2) Flight profile.
- (3) Number of antennas.
- (4) Number of frequencies.

The sections following discuss the electronic instrumentation for accomplishing the signal level measurements.

In view of the extensive previous investigations [1,4] of height diversity for a receiver located on the ground, it seems that the prime case of interest for these experiments is the case where the receiver is an aircraft. Height

diversity is best used for the lower altitude member of the communications link. This may be seen from Eq. (26) where if d_t , and $\Delta\phi_0$ are given, then the Δh required at the receiver is inversely proportional to the transmitter altitude. We propose two cases of transmitter altitude:

- (1) Transmitter altitude \gg receiver altitude.
- (2) Transmitter altitude = receiver altitude.

Although case (1) corresponds to a satellite-air link as well as to air-air links, the case of a satellite transmitter may not be of as much practical interest since by appropriate satellite positioning it may be possible to insure satellite elevation angles high enough to make R (and the multipath loss) quite low.

In Figures 13, 15, 22, and 23, the aircraft separations and receiver altitudes were shown at which spatial diversity with a vertical separation of 9 feet can be of value in reducing fades of greater than 10 db to a level no worse than 10 db. In Figures 12, 14, 20, and 21, the aircraft separations and receiver altitudes were shown at which spatial diversity can be useful in reducing fades of greater than 3 db to a level no worse than 3 db.

In planning flight profiles to demonstrate the usefulness of vertical antenna diversity it is clear that:

- (1) It is critically important that the aircraft operate over quite smooth terrain and keep at as low an altitude in the regions of interest as to minimize α_r (and hence minimize roughness).

- (2) When a region of significant multipath loss is encountered (i.e., ϕ is close to a multiple of 2π), the two aircraft should fly a path that minimizes changes in ϕ . Fresnel zone considerations (Appendix A) suggest that the best such path is one aircraft trailing the other.
- (3) For terrain - flight profile conditions close to the boundary of the regions shown in Figures 12 to 15 and 20 to 23, it may be easy to "miss" the region of significant degradation due to reflection.

Next, consider the number of antennas on the aircraft. From the development in Section 2 of this note, observe that the minimum reflection angle, α_r , (which in turn is related to the minimum value of h_t/d) at which antenna diversity can "significantly" change ϕ_L is directly proportional to Δh . Since surface roughness effects drop off as $(\sin \alpha_r)^{-2}$, it is clearly advantageous to work with the maximum possible Δh . Thus, it is desirable to have antennas as widely separated vertically as possible.

If only two antennas are used, it is clear from (13) that transmitter-receiver geometries exist for which the change in ϕ_L between the two antennas is a multiple of 2π , in which case antenna diversity does not alleviate the reflection multipath fades. In principle, this possibility can be alleviated by using additional antennas such that there exist vertical separations

$$h_k = (\Delta h_{\max}) \left(\frac{1}{M}\right)^k \quad k = 1, 2, 3, \dots, k_{\max} \quad (43)$$

where

$$M = \frac{2\pi - \delta\theta}{\delta\theta}$$

$\delta\theta$ = minimum amount by which ϕ_L must be changed to overcome a fade (at least $\pi/4$ for 3 db fades and .3 for 10 db fades)

k_{\max} is determined by the maximum α_r at which fades of the specified magnitude occur (see Appendix B).

Thus, if an objective of the experiment is to demonstrate that reflection multipath can always be alleviated by height diversity, it will generally be necessary to have additional antennas located to produce the height differences given by (43). At the very least, if the test aircraft permits a vertical separation considerably greater than that available on the aircraft of operation interest, it is desirable to have a third antenna located to yield a vertical separation typical of that achieved on the operational aircraft.

Another issue of practical interest involves the gain patterns of the receiving antennas. The theory outlined in the previous section assumes that the receiving antenna beam pattern is perfectly isotropic. In practice, this is not the case. If antennas in different locations have substantially different beam patterns at the angle of interest, but have overlapping regions in which antenna diversity is of use, then it is possible to demonstrate the

usefulness of antenna diversity as long as direct signal strength differences are taken into account. A practical problem that arises here is the fact that the arguments used in obtaining Figures 12 to 15 and 20 to 23 assume that one can utilize the diversity combining schemes described in Appendix E. If this diversity combining cannot be accomplished, the minimum reflection angle at which antenna diversity is of aid rises by about a factor of 2 and the regions in Figure 12 to 15 and 20 to 23 will change accordingly (however, for antenna separations of 18 feet, Figures 7 and 9 are still valid).

Although such gain patterns are available, we are not aware of any measurements at the frequencies, locations and type of airplane available for the test program. Thus, we suggest measuring the beam pattern of the installed receiving antennas before executing a flight test program so as to address the issues above.

Finally, we consider the number of frequencies to be used in the experiment. Although in principle only a single frequency is needed to assess antenna height diversity, we propose to consider use of two frequencies separated by at least 10-20 MHz. The rationale here is that use of two frequencies with a substantial frequency difference allows the use of frequency diversity as a diagnostic tool in assessing antenna diversity as follows: Since frequency diversity can alleviate ground reflection multipath on a single antenna, if a signal strength drop is not alleviated by frequency diversity, the fade is probably due to direct path shadowing by the aircraft structure. However, this

technique is limited, for a given receiver altitude \tilde{h}_r below some threshold values which depend on circumstances (e.g., see Figures 6 to 9), to some minimum reflection angles α_r below which the spatial diversity is effective but the frequency diversity is not. Hence, to use the above diagnostic tool, the flight profiles would have to be chosen so that either \tilde{h}_r is above the above-mentioned threshold values or the expected reflection angle of the specular reflection is not less than the above-mentioned minimum values. Conversely, if frequency diversity alleviates reflection multipath but height diversity does not, then it may be that the antenna gain patterns at the two physical locations are so different that antenna diversity is of little use. Since it is quite important that this last case be clearly separated from the previous case in assessing the usefulness of antenna diversity, the use of at least two frequencies seems necessary. The use of additional frequencies with spacings

$$\Delta f_k = (\Delta f_{\max}) \left(\frac{1}{M}\right)^k \quad (44)$$

where M is identical to that given after (43) is also desirable for the same reasons that we used in arriving at (43).

In using these frequencies as a diagnostic tool, it would be desirable to have all frequencies available simultaneously since R will vary as the reflection point moves along the earth. This of course, necessitates higher transmitter powers than would be required for single frequency operation. As a straw figure, we suggest three frequencies f_0 , $f_0 + 4$ MHz and $f_0 + 20$ MHz where f_0 is the base frequency at L band.

3.2 RECEIVER MEASUREMENT EQUIPMENT

In this section, the electronic instrumentation required in making the measurements indicated in the previous section are discussed. The equipment needs are most conveniently discussed if the receiver system is considered before the transmitter system.

In order to minimize overall system cost and complexity, it has been assumed:

- (1) It is sufficient to characterize the diversity performance by received signal power (e.g., no attempt will be made to estimate rf phase between antenna pairs).
- (2) Signal-to-noise ratios may be too low to permit the use of coherent estimation schemes (e.g., use of a phase locked loop).*
- (3) Banks of Doppler filters are not acceptable from the complexity viewpoint, particularly for inflight processing.
- (4) Moderate frequency stability (e.g., 1 part in 10^7) of the L-band carrier is easily achievable.
- (5) Data will be recorded in such a form that sophisticated (e.g., use of phase locked loops) post flight signal processing schemes will be possible should the conditions encountered require such schemes.
- (6) Inflight signal processing will suffice to demonstrate that acceptable data is being recorded as well as to provide an indication that the aircraft are in an "interesting" configuration.

* Although it should be noted that the recording approach proposed would permit the post flight use of such a scheme.

In Figures 28 to 31, the block diagrams of the proposed receiver and post flight processing are shown. Figure 28 indicates the on-board processing prior to recording on FM tape for a single antenna assuming that the transmitted signal is the sum of sinusoids at frequencies f_0 , $f_0 + f_1$ and $f_0 + f_2$ where $f_0 \approx 1.5$ GHz, $f_1 = 10$ to 20 MHz and $f_2 = f_1/5$. A low pass filter bandwidth was deemed adequate to encompass the uncertainty in received signal frequency, given:

- (1) Flight profiles where the aircraft fly one behind the other at very slowly changing separation. Such profiles would produce negligible Doppler shift. In some cases, it may be desirable to consider a stationary receiver (e.g., ground station), in which case the maximum Doppler shift would be:*

$$f_d = 1.5 \times 10^9 \frac{300 \text{ mph}}{186,000 \times 3,600 \text{ mph}} = 672 \text{ Hz} \quad (45)$$

- (2) Frequency stability of the center frequency f_0 is taken to be 1 part in 10^7 at the receiver and transmitter. Thus, the offset in frequency out of the IF is bounded by

$$f_{\text{offset}} \leq 2 \times 10^{-7} \times 1.5 \times 10^9 = 300 \text{ Hz} \quad (46)$$

- (3) Frequency stability of the diversity offset f_1 is taken to be one part in 10^7 at receiver and transmitter. For $f_1 = 20$ MHz, the f_{offset} for the signal at $f_0 + f_1$ above should be increased by

* This assumes a cruise speed of 300 mph, typical of a Convair 440.

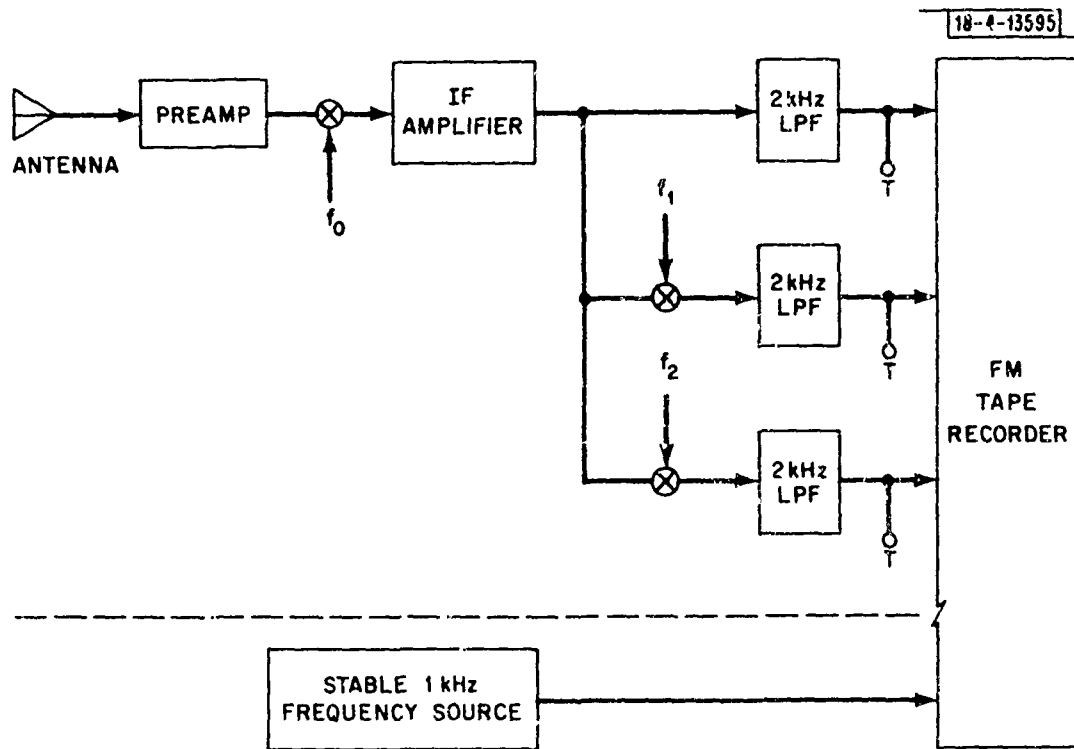


Fig. 28. In-flight received signal processing prior to recording.

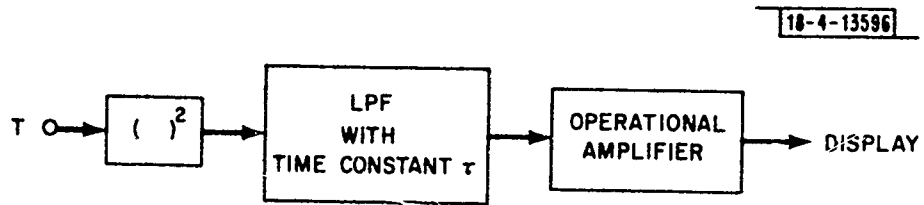


Fig. 29. In-flight received signal power monitoring.

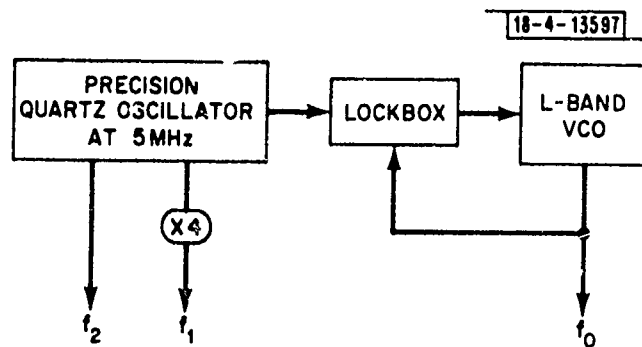


Fig. 30. Generation of tones for frequency diversity.

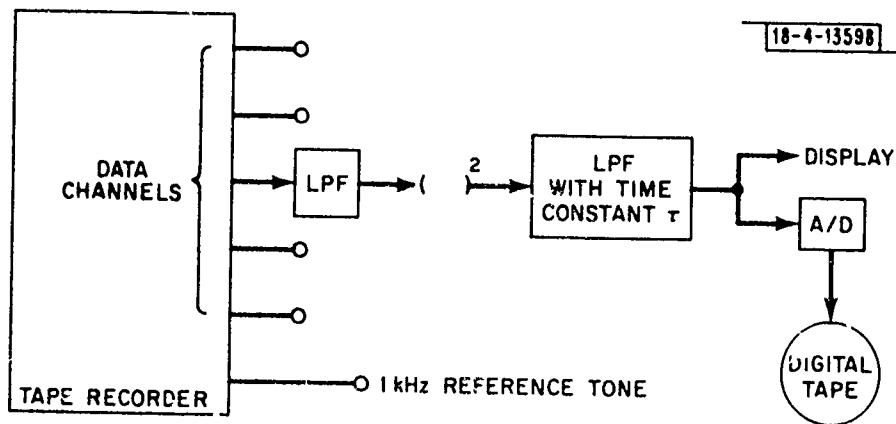


Fig. 31. Post-flight signal processing.

$$2 \times 10^{-7} \times 20 \times 10^6 = 4 \text{ Hz} \quad (47)$$

The stable sinusoidal source at the bottom of Figure 28 is intended to act as a timing reference on playback so that tape speed fluctuations will not degrade possible post flight frequency tracking.

We propose the use of a 14 channel (i.e., 1" tape width) FM analog tape recorder (which satisfies IRIG specifications) for the inflight preservation of the data. The data to be recorded should not have an enormous dynamic range (e.g., ≥ 30 db.) given reasonably alert onboard monitoring of the received signal levels. Operating at 7.5 inches per second (ips) (to give 40 db dynamic range in a 2.4 kHz bandwidth), a single data tape will last approximately 1.5 hours. Among the advantages of this scheme over digital recording:

- (1) Available off the shelf as a relatively inexpensive (\$14K) device that will operate in extreme environments.
- (2) Data tapes will last longer.
- (3) Analog recording is well coupled to the analog processing contemplated for the bulk of post flight signal processing (the very simple signal processing needed can be achieved much more quickly and inexpensively by analog means).
- (4) Voice channel on FM recorders allows convenient recording of auxiliary data.

By using a "standard" recording format, recorders can easily be substituted should a failure occur. Such tape recorders commonly come with multiples of seven channels; from the previous sections, it would seem that 10 channels would be used (3 antennas x 3 frequencies + ref. tone).

Figure 29 shows the inflight received signal estimation used to monitor receiving system performance and to allow continued adjustment of the aircraft geometry so as to maximize the "interesting" data. The operational amplifier is used to minimize current drain on the low pass filter being used as an approximation to an integrate-and-dump filter. There should be at least as many of these circuits onboard as there are antennas.

In Figure 30, it is suggested that the most convenient method of obtaining the desired frequencies f_0 , f_1 and f_2 is to derive them all from a single precise quartz oscillator. Note that in order to minimize the bandwidth of the filters in Figures 28 and 29, it is required that the transmitter and receiver frequency standards:

- (1) Each have long and short term stabilities on the order of 1 part in 10^7 .
- (2) Be identical to within 1 part in 10^7 in order that the net frequency offset be a part in 10^7 .

With current technology, economically matching and maintaining the frequencies apparently can only be accomplished with the precision quartz crystals available at 1 MHz and 5 MHz. The "lock box" shown in Figure 30 is a commonly used commercial device consisting of a mixer (to convert the 5 MHz to 1.5 GHz), an IF stage and a phase discriminator to provide the error input to the VCO.

Figure 31 indicates the "first-look" post flight processing. The energy level estimation circuit is identical to that of Figure 29. However, the utility of storing the output energy levels on a digital tape is indicated for use in detailed statistical analysis of the data.

3.3 TRANSMITTER MEASUREMENT EQUIPMENT

Having specified the receiver signal processing, we are now in a position to analyze the transmitter requirements. In Figure 32, a block diagram of the proposed transmitter system is shown. The quartz crystal oscillator "lock box" and voltage controlled oscillator (VCO) are utilized here for the same reasons that led to their use in the receiver front end as shown in Figure 30. The system shown uses double side band with a carrier power equal to that in the side bands to achieve the desired three tones with maximum spacing 20 MHz. Additional study into alternative approaches (e.g., FM or SSB) that might better utilize the characteristics of the L-band sources available seems warranted since the scheme suggested here is intended as a "straw man" to be used in a first pass cost sizing.

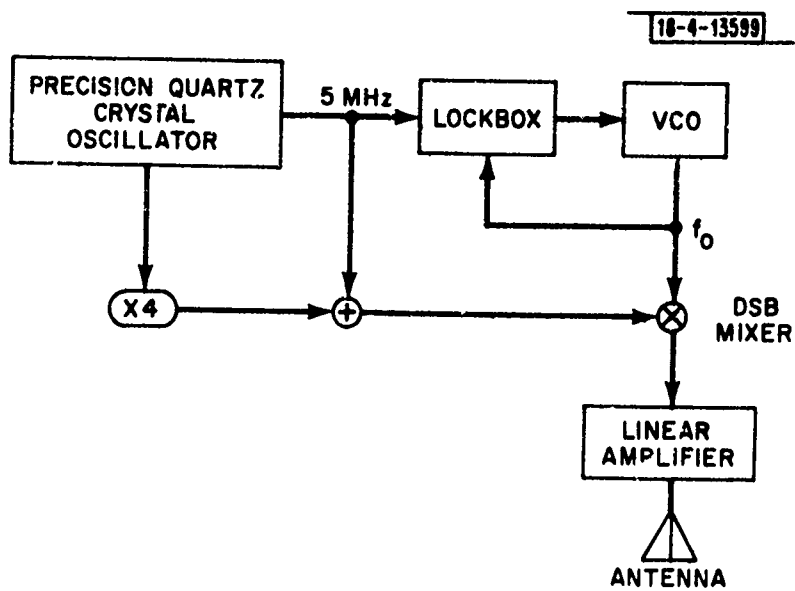


Fig. 32. Block diagram of transmitter.

The transmitter power required is a function of:

- (1) The desired statistical reliability of the received signal power estimates.
- (2) The receiver noise level.
- (3) The length of time over which the received signal power is stationary.

In Appendix C, formulas are presented that show the tradeoff between the three factors above. For fades of 3 db to 10 db, a 1 db 90% confidence limit seems quite reasonable while (from Figure 28) the bandwidth W is 2 kHz*. Thus, the key issue is the length of time T over which the received signal power should be stationary.

This depends on the rate of change of the transmitter-receiver-reflection point geometry as characterized by:

- (1) The fractional change in the first Fresnel zone over the time interval T .
- (2) The change in phase angle between direct and reflected rays due to aircraft geometry changes over the time interval T .

* It should be noted that post flight bandwidths of several 100 Hz are possible if the desired frequency stabilities are achieved and Doppler is negligible. Such a decrease in the bandwidth would yield better statistical reliability (e.g., a fourfold bandwidth decrease would yield .5 db 90% confidence limits.)

The fractional change in the first Fresnel zone is of interest since the reflection from the first Fresnel zone probably makes the major contribution to the reflected signal (see the discussion on pages 10-16 of [2]) and it is recognized that terrain changes may induce significant changes in the reflected signal. From Appendix A, it can be seen that the case $h_t = h_r$ yields the smallest ellipses. Taking $h_t = h_r = 1000$ feet, and $\alpha_r = 2^\circ$ as a "worst case," it is found that the time to move 10% of the first Fresnel zone at 300 mph (≈ 440 ft/sec) is the smaller of*

$$T_x = \frac{686.4}{440 \cos \theta + \delta \sin \theta} = \frac{15.6}{\cos \theta + \left(\frac{\delta}{440}\right) \sin \theta} \text{ seconds} \quad (48a)$$

$$T_y = \frac{23.9}{440 \sin \theta + \delta \cos \theta} = \frac{0.54}{\sin \theta + \left(\frac{\delta}{440}\right) \cos \theta} \text{ seconds} \quad (48b)$$

where θ is the heading angle of the aircraft velocity vector with respect to the line between the aircraft while δ is the cross track velocity error in ft/sec. Since $\delta < 440$, it is clear from (48) and (49) that one wishes to operate as close to $\theta = 0$ as is possible. Unfortunately, as $\theta \rightarrow 0$, the likelihood of antenna shielding by the aircraft body rises significantly. Thus, it seems reasonable to consider $\theta = 5^\circ$, in which case

$$T_x \approx 15.66 \text{ seconds} \quad (49a)$$

$$T_y \approx .620 \text{ seconds} \quad (49b)$$

* T_x = time to travel 10% of the major axis of the Fresnel ellipse.

T_y = time to travel 10% of the minor axis of the Fresnel ellipse.

Changes in the phase angle, ϕ , between the direct and reflected rays over the time interval T would induce diversity into the system above and beyond that which we are attempting to demonstrate. Thus, it is essential that the magnitude of these effects be carefully assessed. Writing Eq. (13) as

$$\Delta\phi = \frac{2\pi}{\lambda} h_r (2h_t/d) \quad (50)$$

we see that changes in the heights of the transmitter and receiver and/or changes in the transmitter-receiver distance will change ϕ . Differentiating (50) with respect to t

$$\frac{\partial\Delta\phi}{\partial t} = \frac{v_r}{\lambda} \left(\frac{2h_t}{d}\right) 2\pi + \frac{v_t}{\lambda} \left(\frac{2h_r}{d}\right) 2\pi - 2\pi (v_d) \left(\frac{2h_t}{d}\right) \left(\frac{h_r}{d}\right) \quad (51)$$

is obtained where

v_r = vertical velocity of the receiver

v_t = vertical velocity of the transmitter

v_d = velocity of one aircraft with respect to the other

It is now of interest to bound (51) assuming that the pilots will attempt to keep the aircraft altitudes constant and that the aircraft velocity vectors do not differ by more than 10° . Taking $v_r = v_t$ the sum of the first two terms is

$$\left(\frac{\partial \Delta \phi}{\partial t}\right)_1 = 4\pi \frac{v_r}{\lambda} \sin \alpha_r \quad (52)$$

Discussions with several private pilots suggest that an IFR aircraft will (at worst) have a 50 foot peak-to-peak barometric altitude oscillation with a period of approximately 10 seconds, thus suggesting

$$v_r \approx 25 \times 2\pi \times \frac{1}{10} = 15.7 \text{ ft/sec.} \quad (53)$$

Moreover, it is assumed that $\alpha_r \leq 10^\circ$ so as to minimize surface roughness. Using $\alpha_r = 10^\circ$ and the result of (53) with $\lambda = 1$,

$$\left(\frac{\partial \Delta \phi}{\partial t}\right)_1 \leq (2\pi) (4.9) \text{ radians/sec.} \quad (54)$$

is obtained. If the aircraft velocity vectors do not differ by more than 10° , then the third term in (52) is upper bounded by

$$\left|\left(\frac{\partial \Delta \phi}{\partial t}\right)_2\right| \leq (2\pi) (440 \sin 10^\circ) \left(\frac{1}{4} \sin^2 \alpha\right) \leq 2\pi (.6) \text{ radians/sec.} \quad (55)$$

Combining (54) and (55),

$$\frac{\partial \Delta \phi}{\partial t} \leq (2\pi) (5.5) \text{ radians/sec.}$$

is obtained. To insure that the net change in $\Delta\phi$ is less than 1.8° (corresponding to 10% of the minimum change to alleviate 10 db fades), it follows that

$$T \leq \frac{1.8}{(360)(5.5)} = 0.909 \text{ msec.} \quad (56)$$

Comparing this to Eqs. (48) and (49), it is clear that the control of transmitter and receiver altitude is the key constraint on the integration time.

Thus, it is worthwhile considering means of reducing it. Combining (52) and (55),

$$\left| \frac{\partial \Delta\phi}{\partial t} \right| \leq 2\pi(2v_r \sin \alpha_r + 110 \sin \theta \sin^2 \alpha_r)$$

is obtained from which it is clear that operating at very low α_r will aid considerably. For example, by working at $\alpha_r = 0.5^\circ$ (an angle that yields close to maximum receiver altitudes for 10 db fades), one obtains

$$T \leq 0.02 \text{ sec.}$$

In Table 4, we give the value of T and P_o/N_o (signal power-to-single sided noise spectral density ratio from Appendix C assuming 1 db 90% confidence levels and $W=2\text{kHz}$ for a variety of combinations of v_r and $(\alpha_r)_{\text{max}}$.

Table 4. T and P_0/N_0 Signal Power-To-Single Sided Noise Spectral Density Ratio.

v_r (ft/sec)	15.7			5			1		
$(\alpha_r)_{\max}$ ($^\circ$)	10 $^\circ$	3 $^\circ$.5 $^\circ$	10 $^\circ$	3 $^\circ$.5 $^\circ$	10 $^\circ$	3 $^\circ$.5 $^\circ$
T (msec)	.909	3.04	18.15	2.16	8.69	56.3	5.4	38.5	263.8
P_0/N_0 (db)	51.8*	46.6*	39.3	48.1*	42.2	36.05	44.2	36.4	30.1

*These values based on a Gaussian approximation that may not be valid for the WT product used.

The value for v_r given in Eq. (53) seems high since the peak acceleration would be

$$a_r \approx \frac{2\pi}{T} v_r = 9.86 \text{ ft/sec}^2 = 0.32 \text{ g}$$

which would be pretty noticeable. If the period of oscillation is held constant and it is assumed that $a_r \approx 0.1g$, then $v_r = 5 \text{ ft/sec}$. It is clear from the above that a more refined estimate of v_r based on the test aircraft to be used would be quite helpful.

For purposes of estimating the power budget, it is assumed that $P_o/N_o=40$ db as a representative SNR. In addition the power budget shown in Table 5 assumes:

- (1) Isotropic transmitting and receiving antennas.
- (2) A 200 mile aircraft separation.
- (3) 300°K receiver noise temperature.
- (4) The maximum fade depth to be estimated at the specified accuracy is 10 db.
- (5) All three tones are transmitted simultaneously .
- (6) Mixer losses, etc. have been incorporated into the excess path loss.

Table 5. Power Budget for Transmitter.

P_o/N_o	+ 40 db
Free space loss	+144 db
Excess path loss margin	+ 20 db
N_o	-199 db
Depth of fades	+ 10 db
Use of three simultaneous tones	<u>+ 5 db</u>
	+ 13 dbw = 20 watts

The fifth assumption deserves some additional discussion as there are some real advantages to operating in a time multiplexed manner:

- (1) From Appendix C, Example 1, it can be seen that the energy/noise density ratio required is given by an equation of the form

$$\frac{P_0 T}{N_0} = \frac{E}{N_0} = K_1 + \sqrt{K_2 + K_3(TW)}$$

where k_1 , k_2 and k_3 are constants given in Example 1 of Appendix C. Thus, using shorter integration times requires less signal energy. Hence, a time multiplexed system would require less signal power.

- (2) If the transmitter radiates only one tone at a time, the complexity of the transmitter may be reduced substantially.

On the other hand, time multiplexing will necessitate more complexity at the receiver in terms of synchronization systems. Also, since the primary interest in frequency diversity is as a tool in analyzing the antenna diversity results, it would be desirable to have the frequency diversity data all correspond to exactly the same aircraft - terrain geometry as a given antenna diversity measurement.

3.4 TOPICS TO BE ADDRESSED

There are a number of topics which have not been discussed here or deserve more attention than given here:

- (1) Antenna type and location - this issue should be addressed in specifics for each of the aircraft to be used. The issues raised in Section 3.1 with respect to beam pattern effects must be considered in this context.
- (2) Transmitter and receiver rf sections - a detailed design beyond the block diagrams presented here is required.
- (3) Flight profile and dynamics: Sections 3.1 to 3.3 have emphasized the importance of operating at low reflection angles (i.e., low receiver altitudes) with high positional stability in order to minimize transmitter power. Further investigations to better quantify flight profile errors are necessary before commencing transmitter procurement.
- (4) Diversity combining: in Appendix E we have discussed some diversity combining schemes which suggest that the phase change, $\Delta\phi_{L0}$, between direct and reflected rays required with an appropriate diversity combining scheme can be estimated from Figure 10. In practice, noise considerations and receiver complexity (especially for

frequency diversity) might dictate slightly larger phase shifts (e.g., wider antenna separations) than those considered here.

APPENDIX A

FRESNEL ZONE CONSIDERATIONS

In this Appendix we compute the length and width of the first Fresnel zone for the geometry shown in Figure A-1 at appropriate values of h_t , h_r , and α_r (note that h_t and h_r are heights above the tangent plane to the earth). In addition, we assume the earth can be modelled as a flat plane and that $d \gg h_t$ and h_r .

Then from Kerr [1] pages 412-415, we find that

$$\Delta x = d \frac{\sqrt{1 + \frac{4h_t h_r}{\lambda d}}}{1 + \frac{(h_t + h_r)^2}{\lambda d}} = d \frac{\sqrt{1 + \frac{4h_t h_r}{\lambda d}}}{1 + \left(\frac{h_t + h_r}{\lambda}\right) \sin \alpha_r} \quad (\text{A-1})$$

$$\Delta y = \sqrt{\lambda d} \sqrt{\frac{1 + \frac{4h_t h_r}{\lambda d}}{1 + \frac{(h_t + h_r)^2}{\lambda d}}} = \sqrt{\lambda d} \sqrt{\frac{1 + \frac{4h_t h_r}{\lambda d}}{1 + \left(\frac{h_t + h_r}{\lambda}\right) \sin \alpha_r}} \quad (\text{A-2})$$

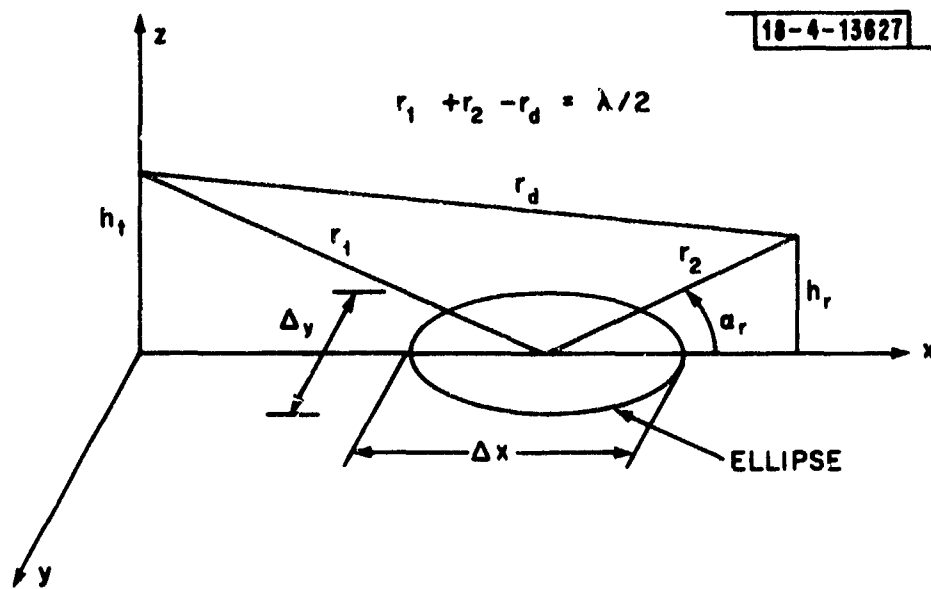


Fig. A-1. First Fresnel zone geometry for a flat reflecting plane.

If $h_t \gg h_r$ and $\lambda = 1$ ft, we obtain

$$\Delta x = d \frac{\sqrt{1 + 4h_r \sin \alpha_r}}{1 + h_t \sin \alpha_r} \approx 2d \frac{\sqrt{h_r / \sin \alpha_r}}{h_t} = \frac{2\sqrt{h_r / \sin \alpha_r}}{\sin \alpha_r} \quad (\text{A-3})$$

$$\Delta y = \sqrt{d \frac{1 + 4h_r \sin \alpha_r}{1 + h_t \sin \alpha_r}} = 2\sqrt{d} \sqrt{\frac{h_r}{h_t}} \approx 2\sqrt{h_r / \sin \alpha} \quad (\text{A-4})$$

where the approximations

$$1 + h_r \sin \alpha_r \approx h_r \sin \alpha_r$$

$$1 + h_t \sin \alpha_r \approx h_t \sin \alpha_r$$

seem good for a "typical" case of $h_t = 20,000$ ft, $h_r = 1,000$ ft and $\sin \alpha_r = 0.01$.

On the other hand, for $h_t = h_r$ we obtain

$$\Delta x = d \frac{\sqrt{1 + 2h_r \sin \alpha}}{1 + 2h_r \sin \alpha} \approx \frac{2h_r / \sin \alpha_r}{\sqrt{2h_r \sin \alpha_r}} = \sqrt{\frac{2h_r}{\sin \alpha_r}} \cdot \frac{1}{\sin \alpha_r} \quad (\text{A-5})$$

$$\Delta y = \sqrt{d} \sqrt{\frac{1 + 2h_r \sin \alpha}{1 + 2h_r \sin \alpha}} = \sqrt{d} = \sqrt{2h_r / \sin \alpha_r} \quad (\text{A-6})$$

In Tables A-1 and A-2 we evaluate (A-3) - (A-6) for several values of h_r and α_r .

Table A-1. Fresnel Zone Widths for $h_t > h_r$.

h_r (ft)	$\sin \alpha_r$	$\frac{1}{30}$		$\frac{1}{60}$		$\frac{1}{100}$	
		Δx (Mi)	Δy (ft)	Δx (Mi)	Δy (ft)	Δx (Mi)	Δy (ft)
500		1.3	329	3.7	239	8.5	447
1,000		1.8	337	5.2	465	12.0	632
2,000		2.6	478	7.4	658	17.0	894

Table A-2. Fresnel Zone Widths for $h_t = h_r$.

h_r (ft)	$\sin \alpha_r$	$\frac{1}{30}$		$\frac{1}{60}$		$\frac{1}{100}$	
		Δx (Mi)	Δy (ft)	Δx (Mi)	Δy (ft)	Δx (Mi)	Δy (ft)
500		.93	169	2.6	232	6.9	316
1,000		1.3	239	3.7	329	8.5	447
2,000		1.8	337	5.2	465	12.0	632

APPENDIX B

OPTIMUM SPACING OF ANTENNAS (FREQUENCIES) IN A HEIGHT (DISCRETE TONE) DIVERSITY SYSTEM

In this Appendix, we show that the antennas (frequencies) in a height (discrete tone) diversity system should be logarithmically spaced in order to efficiently alleviate ground reflection multipath fades over a wide range of transmitter-receiver geometries. We recall from the body of the report that both height and frequency diversity rely on changing ϕ_L , the net phase lag of the reflected signal with respect to the direct signal so that the sum of ϕ_L and ϕ_s , the phase change on reflection, is no longer close to an odd multiple of π . In particular, a vertical separation Δh_r between two antennas gives a phase change

$$\Delta\phi_L = \frac{4\pi h_t f}{cd} \Delta h_r \quad (B-1)$$

while a frequency change of Δf between two tones gives

$$\Delta\phi_L = \frac{4\pi h_r h_t}{cd} \Delta f \quad (B-2)$$

The need for additional vertical separations (or frequency changes) arises from the possibility that the transmitter-receiver geometry is such that the phase change achieved may be close to a multiple of 2π .

We will now demonstrate that in principle, the possibility that the net phase shift is too close to 2π can be alleviated by using either:

- (1) Additional antennas such that there exist vertical separations

$$\Delta h_k = (\Delta h_{\max}) \left(\frac{1}{M}\right)^k \quad k = 1, 2, 3, \dots, k_{\max} \quad (\text{B-3})$$

- (2) Additional tones such that there exist frequency separations

$$\Delta f_k = (\Delta f_{\max}) \left(\frac{1}{M}\right)^k \quad k = 1, 2, 3, \dots, k_{\max} \quad (\text{B-4})$$

where Δh_{\max} = maximum usable vertical separation

Δf_{\max} = maximum usable frequency separation

$$M = \frac{2\pi - \delta\theta}{\delta\theta} \quad (\text{B-5})$$

$\delta\theta$ = minimum amount by which ϕ_L must be changed
to overcome a fade

k_{\max} is determined by the region over which fades of
the specified magnitude occur.

First, we note that both (B-1) and (B-2) are in the form

$$\Delta\phi_L = Gx \quad (\text{B-6})$$

where G represents the transmitter-receiver geometry and x is the quantity we vary to obtain diversity. Next, we define a function

$$q_x(G) = \begin{cases} 1 & \text{if } \delta\theta \leq \Delta\varphi_L \text{ modulo } 2\pi \leq 2\pi - \delta\theta, \\ & \text{i.e., the diversity is effective} \\ 0 & \text{otherwise} \end{cases} \quad (\text{B-7})$$

In Figure B-1, we see that for a given x , $q_x(G)$ is a periodic function of G . If we have m separations (either frequency or vertical), then we can define a function

$$\begin{aligned} q_{\text{sum}}(G) &= q_{x_1}(G) \cup q_{x_2}(G) \cup \dots \cup q_{x_m}(G) && (\text{B-8}) \\ &= 1 \text{ if diversity is effective} \\ &= 0 \text{ otherwise} \end{aligned}$$

where \cup denotes the logical or operator.

From (B-8), we see that $q_{\text{sum}}(G)$ must be zero until $G = \delta\theta/x_{\text{max}}$. Our objective is then to choose additional separations $\{x_i\}$ such that $q_{\text{sum}}(G)$ is 1 over as great an additional region as possible. As shown in Figure B-2, choosing

$$x_1 = x_{\text{max}}/M$$

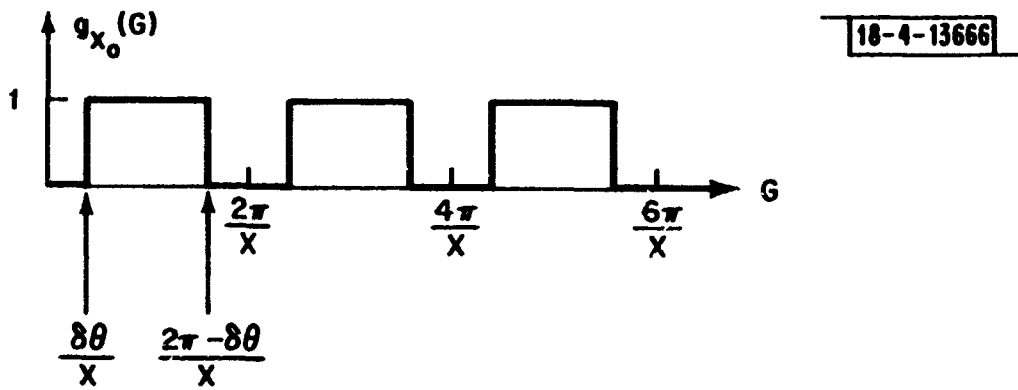


Fig. B-1. Region of diversity usefulness vs generalized transmitter-receiver geometry.

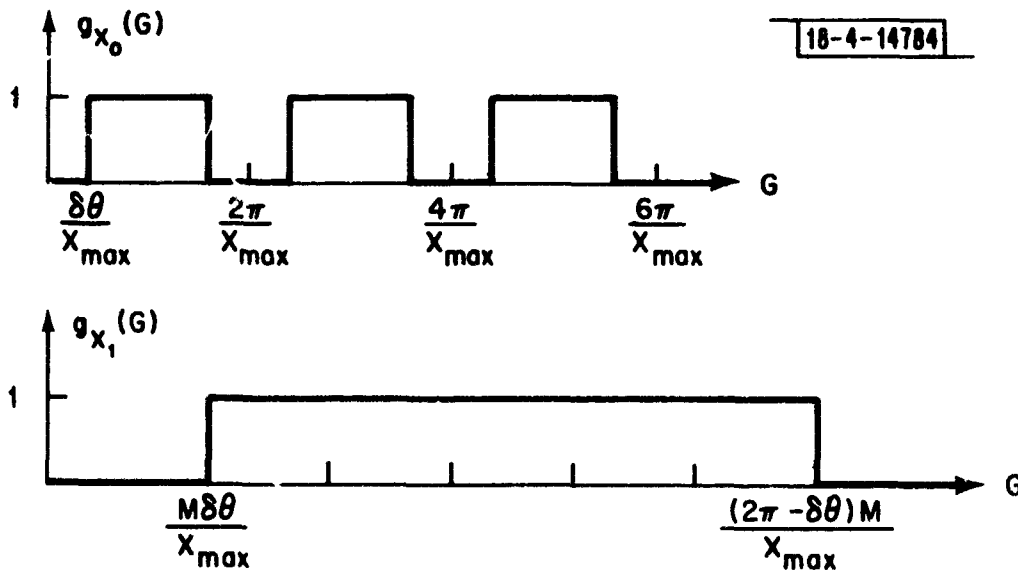


Fig. B-2. Region of diversity usefulness vs generalized transmitter-receiver geometry with logarithmic separations.

insures that $q_{\text{sum}}(G)$ is 1 out to $G = \frac{(2\pi - \delta\theta)M}{x_{\text{max}}}$. By induction, we see that by choosing

$$x_k = x_{\text{max}}/M^k$$

we insure that $q_{\text{sum}}(G)$ is 1 out to $G = \left(\frac{2\pi - \delta\theta}{x_{\text{max}}}\right)M^k$. From the text, we recall that there is generally a maximum value of G , G_{max} , above which fades of the specified magnitude cannot occur. This implies that setting

$$k_{\text{max}} = 1 + \log_m \left(\frac{G_{\text{max}} x_{\text{max}}}{2\pi} \right)$$

will insure that diversity improvement is obtained over the full range of transmitter-receiver geometries for which improvement can be obtained.

APPENDIX C

STATISTICAL ASPECTS OF ESTIMATING THE RESULTANT SIGNAL POWER

In this Appendix, we establish the tradeoff between signal power, noise levels and integration time to achieve a desired accuracy in the estimate of resultant signal power using the filter-square-integrate system shown in Figure C-1. We recall that the signal $y(t)$ out of the band pass filter is given by

$$y(t) = \sqrt{2P_0} \cos(\omega_d t + \phi) + n(t) \quad (C-1)$$

where P_0 is the power in the resultant signal and $n(t)$ is the Gaussian noise with mean square value $N_0 W$ obtained by passing white Gaussian noise of (single sided) spectral density N_0 through the bandpass filter with transfer function $H(\omega)$ and bandwidth

$$W = \int_0^{\infty} |H(\omega)|^2 d\omega \quad (C-2)$$

In the absence of the WGN, it is easy to see that the system of Figure C-1 generates an estimate \hat{P}_0 identically equal to P_0 as long as the bandpass filter

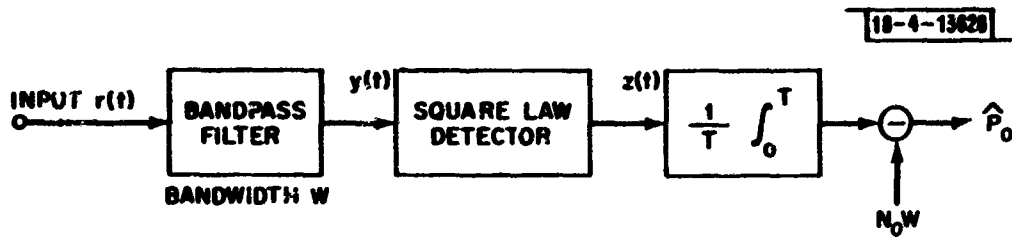


Figure C-1. Receiver to estimate the resultant signal power.

has unity gain at ω_d . We now consider the statistical characteristics of the estimate \hat{P}_0 when WGN is present assuming an ideal bandpass filter (e.g., unity gain from 0 to W and zero gain at frequencies above W). It is straightforward to show that for $\omega_d \neq 0$ and $\omega_d T \gg 1$.

$$\hat{P}_0 = \frac{1}{T} \int_0^T y^2(t) dt - N_0 W = P_0 + \sqrt{8P_0} \int_0^T n(t) \cos(\omega_d t + \phi) dt + \frac{1}{T} \int_0^T n^2(t) dt - N_0 W \quad (C-3)$$

From (C-3) using the fact that $n(t)$ is a zero mean Gaussian random process it is straightforward to show that the estimate is unbiased. i.e.,

$$E[\hat{P}_0] = P_0$$

Computing the variance and/or probability distribution of \hat{P}_0 directly from (C-5) gets quite messy,¹ and it is convenient to make the following approximation to the integral in (C-3) based on assuming an ideal band pass filter and using a sampled data representation for $y(t)$:

$$\hat{P}_0 = \frac{1}{T} \int_0^T y^2(t) dt - N_0 W \approx \frac{1}{M} \sum_{k=1}^M y^2\left(\frac{kT}{M}\right) - N_0 W \quad (C-4)$$

where

$$\frac{T}{M} = \frac{1}{2W}$$

$$y\left(\frac{kT}{M}\right) = \sqrt{2P_0} \cos(\omega_d kT + \eta) + n(kT) \quad (C-5)$$

Since the $n(kT)$ are independent, identically distributed random variables, the variance of the sum in (C-4) is the sum of the variances of the individual $y^2(kT/M)$, i.e.,

$$\text{Var}[\hat{P}_0] = \frac{1}{M} = \sum_{k=1}^M [8P_0 N_0 W \cos^2(\omega_d kT + \eta) + 2(N_0 W)^2] \quad (C-6)$$

¹ It should be noted that the distribution of \hat{P}_0 is not given by Marcum's Q function that appears in random phase communications channel calculations. The difference arises because we do not attempt to track Doppler (or use a bank of Doppler filters) in our estimation scheme.

$$= \frac{1}{M} [4P_0 N_0 W + 2(N_0 W)^2]$$

$$= \frac{1}{2WT} [4P_0 N_0 W + 2(N_0 W)^2]$$

By assuming that $M(=2WT)$ is large enough such that \hat{P}_0 has a Gaussian distribution, one can get an estimate of the signal power required to achieve the desired accuracy as follows:

(1) Define $u_k = y^2(kT/M)$

(2) Then the central limit theorem states that

$$P \left\{ a \leq \frac{\sum_k u_k - E(u_k)}{\sqrt{\sum_k \text{Var}(u_k)}} \leq b \right\} = \frac{1}{\sqrt{2\pi}} \int_a^b e^{-x^2/2} dx \quad (C-7)$$

(3) By direct substitution from (C-3) and (C-6), it follows that

$$\frac{\sum_k u_k - E(u_k)}{\sqrt{\sum_k \text{Var}(u_k)}} = \frac{\hat{P}_0 - P_0}{\frac{1}{\sqrt{M}} [4P_0 N_0 W + 2(N_0 W)^2]^{1/2}} \quad (C-8)$$

(4) For a confidence level of $1 - \epsilon$, the usual procedure is to take $\gamma = b = -a > 0$ such that

$$\epsilon/2 = \frac{1}{\sqrt{2\pi}} \int_{\gamma}^{\infty} e^{-x^2/2} dx \quad (C-9)$$

- (5) Given $1 - \epsilon$, we determine γ from (C-9). Next, it is desirable to determine the db deviation in \hat{P}_0 from P_0 that corresponds to the two values of γ . This is given by

$$10 \log_{10} (\hat{P}_0/P_0) = 10 \log_{10} \left[1 \pm \frac{\sqrt{4P_0 N_0 + 2N_0^2 W}}{P_0 \sqrt{2T}} \right] \quad (C-10)$$

- (6) Using (C-10), we can readily determine the tradeoff between P_0 , N_0 , W and T to achieve the desired accuracy as expressed by confidence limits.

Example

We want to achieve 90% confidence limits of ± 1 db. From (C-10), we see that this necessitates

$$\frac{\sqrt{4P_0 N_0 + 2N_0^2 W}}{P_0 \sqrt{2T}} \leq 0.20$$

Moreover, from tables of the Gaussian distribution (C-9), we find that $\gamma=1.65$. Thus, for this case, the minimum value of P_0 is defined by

$$\frac{P_0 \sqrt{2T}}{\sqrt{4P_0 N_0 + 2N_0^2 W}} = \frac{(1.65)}{(.20)} = 8.25$$

or alternatively

$$P_0 = \frac{4N_0 + \sqrt{16N_0^2 + N_0^2 WT(4)(2)(1/8.25)^2(2)}}{[4T/(8.25)^2]}$$

$$\frac{P_0}{N_0} = \frac{68.06 [1 + \sqrt{1 + .0147(WT)}]}{T}$$

Thus, for $W = \text{kHz}$ and $T = 1 \text{ second}$:

$$\frac{P_0}{N_0} = 524 \quad \text{i.e., } 27.2 \text{ db}$$

When WT is not large enough to justify use of the Gaussian approximation to \hat{P}_0 , the situation becomes more involved insofar as determining confidence limits goes. If one defines

$$u_k = v^2(kT/M)$$

$$a_k = \sqrt{2P_0} \cos(\omega_d k \frac{T}{M} + \phi)$$

$$\sigma^2 = N_0 W$$

then the density function of u_k is given by

$$p(u_k) = \frac{1}{\sqrt{2\pi u_k \sigma^2}} \left[e^{-(\sqrt{u_k} - a_k)^2 / 2\sigma^2} + e^{-(\sqrt{u_k} + a_k)^2 / 2\sigma^2} \right] \quad (C-11)$$

and the distribution of \hat{P}_0 determined by a M fold convolution of (C-11) followed by averaging over ϕ . Somewhat more appealing are bounds based on the moment generating function of u_k :

$$M(u_k|\phi) = (1 - 2s\sigma^2)^{1/2} \left[\exp a_k^2 \left(s + \frac{2s^2\sigma^2}{1 - 2s\sigma^2} \right) \right] \quad (C-12)$$

from which we find that the semi-invariant moment generating function of \hat{P}_0 is given by

$$\mu(s|\phi) = -\frac{M}{2} \ln \left(1 - 2 \frac{s\sigma^2}{M} \right) + \frac{1}{2} \sum P_0 \left[s + \frac{2s^2\sigma^2}{M - 2s\sigma^2} \right] - sN_0W \quad (C-13)$$

Given M , P_0 , σ^2 and confidence limit $\epsilon/2$, one then chooses $s > 0$ to give the smallest value of $\gamma > P_0$ such that

$$\epsilon/2 = \exp [\mu(s) - s\gamma] \quad (C-14)$$

The value of γ found in (C-14) is the upper confidence limit; the lower limit can be found by choosing $s < 0$ to give the largest value of $\gamma < P_0$ such that (C-14) is satisfied.

In the above, we have assumed that the square law detector does not average over the phase of $w_d t$. However, if

$$y(t) = \sqrt{2P_0} \cos[(w_0 + w_d)t + \phi] + n(t)$$

with $w_0 \gg W$ then in many cases the output of the square law detector is proportional to the square of the envelope of $y(t)$. This case has been examined in exhaustive detail by Marcum, Helstrom [10] and Chadwick [11] who show that the probability density of \hat{P}_0 is given by

$$p(\hat{P}_0) = \frac{1}{2\sigma^2} \left(\frac{\hat{P}_0}{2P_0}\right)^{(M-1)/2} \exp\left[-\frac{1}{2\sigma^2}(\hat{P}_0 + 2MP_0)\right] I_{M-1}\left[\frac{M\sqrt{2P_0\hat{P}_0}}{\sigma}\right] \quad (C-15)$$

where

$$\begin{aligned} M &= 2WT \\ \sigma^2 &= N_0 W \\ I_{M-1} &= M-1^{\text{th}} \text{ order Bessel function} \end{aligned}$$

For small values of M , explicit expressions for the distribution function of \hat{P}_0 in terms of Marcum's Q function and the modified Bessel functions may be the most accurate means of proceeding. For large M , Helstrom (see pages 177-180 of [10]) has demonstrated that the Gaussian approximation to the density in (C-15) is quite good. Since the squared envelope has the same statistics as the system described earlier after we take into account the fact that the squared envelope estimate is too large by a factor of 2, the procedure and formulas outlined in (C-7) - (C-10) may still be used.

APPENDIX D

A FIRST-ORDER MODEL OF MULTIPATH REFLECTIONS FROM NONSMOOTH SURFACES

D.1 INTRODUCTION

This Appendix presents a first-order model to provide engineering estimates of the power reflection from nonsmooth terrain. Exact theoretical results are not available for the general reflection case [1]. Approximate expressions have been examined and those presented were selected because (a) they fit reasonably well much of the available data, and (b) their analytic simplicity is in keeping with their probable relative accuracy. It has been observed by Beckmann and Spizzichino [2], Durlach [9], Moore [10], and others in surveys of the literature that much of the experimental data available or their interpretations are controversial or in some way deficient. However, there is sufficient acceptable data [2,3,7,9-14] to estimate certain important effects, which are presented in this note.

D.1.1 Basic Concepts

There are several ways of approaching the description of electromagnetic field scattering from nonsmooth surfaces. It is convenient to build up the

desired description by first considering simpler situations. Thus, consider first a plane electromagnetic wave incident on a smooth planar surface. Assume the incident plane wave is a simple uniform (TEM*) wave. This is the canonic plane wave form from which arbitrary nonuniform plane waves can be synthesized. This incident plane wave may be further usefully decomposed into two simpler cases. In the first case, called horizontal polarization, the electric vector is parallel to the reflecting surface. In the second case, called vertical polarization, the magnetic vector is parallel to the reflecting surface. The magnitude of the reflected electric field strength e_r is proportional to the magnitude of the incident electric field strength e_i , $e_r = R_0^+ e_i$ where R_0^+ is the classical Fresnel reflection coefficient for a smooth planar surface. Here the "+" and "-" superscripts indicate vertical and horizontal polarization. For time-harmonic fields $e_i = E_i \exp(j\omega t)$, $e_r = E_r \exp(j\omega t)$, the formulas are

$$R_0^+ = \frac{\left| \epsilon_r^2 \sin\gamma - \sqrt{\epsilon_r^2 - \cos^2\gamma} \right|}{\left| \epsilon_r^2 \sin\gamma + \sqrt{\epsilon_r^2 - \cos^2\gamma} \right|} \exp(j\phi_s^+) \quad (D-1)$$

and

$$R_0^- = \frac{\left| \sin\gamma - \sqrt{\epsilon_r^2 - \cos^2\gamma} \right|}{\left| \sin\gamma + \sqrt{\epsilon_r^2 - \cos^2\gamma} \right|} \exp(j\phi_s^-) \quad (D-2)$$

* A TEM wave has its electric and magnetic vectors perpendicular to each other and the direction of wave propagation.

where

$$\epsilon_r = \frac{\epsilon}{\epsilon_0} - 60 j\lambda\sigma \quad (D-3)$$

ϵ and σ are the dielectric constant and conductivity (mho/meter) of the terrain, ϵ_0 is the dielectric constant of free space, λ is the free space wavelength (in meters) of the wave incident on the reflecting surface, at angle of γ with respect to the surface. It has been assumed that the relative magnetic permeability is unity. The angle of reflection, γ_r^* , always equals the angle of incidence, γ_i , in the simple smooth planar surface case.

The next step of generalization is to take into account the roughness of the surface. Usually, the geometry of the rough surface is modelled for convenience by a sample function of some random distribution which for most purposes can be characterized by a small number of parameters. This avoids the necessity of describing the size, shape and location of all the troughs and peaks in the actual surface. If the surface geometry changes with time (e.g., as does the surface of a rough sea) or if a transmitter**and/or receiver motion, the reflected electric field will require a more complex description than has been given so far. One approach is to model the phenomena from the equation

$$E_r = (\rho_s + \rho_r) R_0^\dagger E_i = (R_s + R_r) E_i \quad (D-4)$$

* The angle between the direction of propagation of the reflected wave and the surface.

** Assumed at this point in the discussion to be far enough away from the surface so that the incident wave on the surface is a plane wave.

where ρ_s and ρ_r represent a deterministic and a random process, $R_s = \rho_s R_0^+$ is the specular reflection coefficient, $R_r = \rho_r R_0^+$ is the diffuse reflection coefficient, and ρ_s and ρ_r are called scattering coefficients. In the present model $\bar{\rho}_r = 0$ and the deterministic portion of the reflected waves satisfies $\gamma_r = \gamma$. The angles of incidence and reflection are now measured between the direction of the appropriate wave propagation and the planar mean surface as illustrated in Figure D-1. R_0^+ is calculated for this mean surface. This model is not grossly different from others in the literature and leads to conclusions that match reasonably well the experimental results. From the preceding, it follows that the reflected power varies as

$$\overline{|E_r|^2} = (|\rho_s|^2 + \overline{|\rho_r|^2}) |R_0^+|^2 |E_1|^2 \quad (D-5)$$

since terms like $\bar{\rho}_r \hat{\rho}_s = 0$. The caret symbol represents complex conjugation and $|\dots|$ represents the absolute value of the bracketed quantity. Eq. (D-5) yields a convenient decomposition of power as the sum of deterministic and random constituents.

The next step of generalization takes the effect of the terrain curvature into account in the reflection process by means of a divergence factor D . To do this, transmitters and receivers at finite distances r_1 and r_2 from a point of reflection must be considered. This is most simply done by considering the electromagnetic energy radiated outward from the transmitter along trajectories called ray paths. The rays traversing these paths are locally plane waves and reflect from surfaces according to the same formulas as plane waves. The

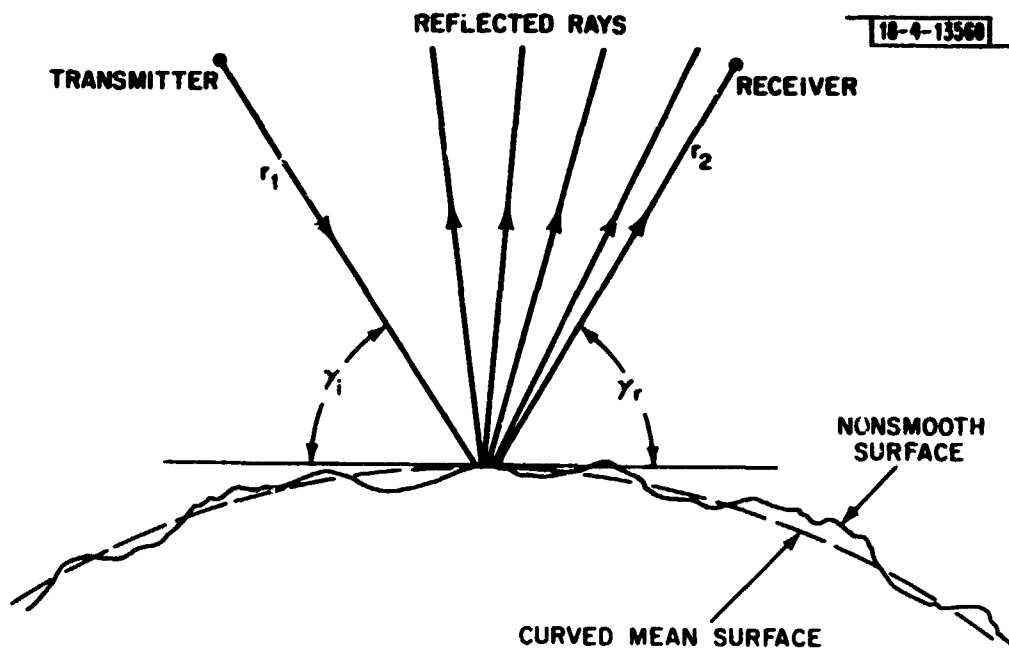


Fig. D-1. A representation of rough surface scattering.

geometry of these ray paths is determined by the variations in refractive index of the medium in which they exist. In free space, ray paths are straight lines while in the atmosphere they are usually curved lines. A pencil of rays emitted by a transmitter which intersects a convex curved surface is reflected as a second pencil of rays which diverge more rapidly than the first. This is what factor D measures. It is customarily used only in describing the deterministic reflected waves (for which the model requires $\gamma_i = \gamma_r = \gamma$) by replacing R_0^+ by DR_0^+ . D is given by [2]

$$D = D_0 \left[1 + \frac{2r_1 r_2}{R(r_1 + r_2)} \right]^{-1/2} \quad (D-6)$$

where

$$D_0 = \left[1 + \frac{2r_1 r_2}{R(r_1 + r_2) \sin \gamma} \right]^{-1/2} \quad (D-7)$$

and R is the radius of the earth in the present discussion. Setting $r_1 = Ar_2$, Eq. D-6 becomes

$$D = D_0 \left[1 + \frac{2r_2}{R} \left(\frac{A}{1+A} \right) \right]^{-1/2} \quad (D-8)$$

Since

$$\frac{1}{2} \leq \frac{A}{1+A} \leq 1 \quad (\text{for } 1 \leq A < \infty), \quad (D-9)$$

and typically

$$\frac{2r_2}{R} \ll 1. \quad (D-10)$$

Eq. (6) reduces to (for reflections from the earth's surface)

$$D \approx D_0 \quad (D-11)$$

for $\sin\gamma$ of the order of $2r_1r_2/R(r_1+r_2)$. For planar incident waves D is obtained by letting $r_1 \rightarrow \infty$ in which case

$$D \approx \left[1 + \frac{2r_2}{R\sin\gamma} \right]^{-1/2} \quad (D-12)$$

for $\sin\gamma$ of the order of $2r_2/R$. To account for the curvature of the ray paths in the lower atmosphere the customary approximation is to use 4/3 of the earth's radius for R [2]. For nonsmooth curved terrain the mean surfaces are chosen as curved, as was illustrated in Figure D-1.

To maintain consistency with common usage the deterministic constituent the reflected rays will be called the specular rays, and ρ_s will be called the specular scattering coefficient. The random constituent of the reflected rays will be called the diffuse rays, and ρ_r will be called the diffuse scattering coefficient. However, in relating different discussions of reflections from nonsmooth surfaces in the literature there are small differences in definitions and basic models.

From the above theoretical model of the reflection process from nonsmooth surfaces, a number of general predictions can be made about the results of experiments. Some of these are as follows. In CW experiments (e.g., stationary transmitting and receiving antennas over a nonsmooth sea) the reflected waves would consist of two constituents. The deterministic portion is commonly called the coherent component. The phase of the received coherent signal would be constant. The diffuse portion is commonly called the incoherent or noise-like component. The phase of the received incoherent component would be random. In experiments using pulsed signals it is possible for the pulses to be of sufficiently short duration so that the reflection geometry changes negligibly throughout the duration of the pulse. In this case, the diffuse rays may not change appreciably during the pulse and could not be treated as noise-like during the pulse interval. However, considered over many pulses, this constituent may slowly change in a random fashion.

D.2 SPECULAR REFLECTION

In this section, the assumptions underlying the calculation of nonsmooth surface scattering will be listed. The theoretical result for specular reflection described and the relation of experimental results to the latter result will be discussed. It is found that the theoretical result, listed in this section, for the specular scattering coefficient is adequate to model the experimental results.

For simplicity consider the one-dimensional case when the surface is given by a random stationary Gaussian process $\zeta(x)$. For a given x , $\zeta(x)$ is a random variable taking on values Z with a PDF (probability density function) of $p(Z)$.

For $x=x_1$ and $x=x_2$ we write

$$\zeta_1 = \zeta(x_1) \quad , \quad \zeta_2 = \zeta(x_2) \quad (D-13)$$

The autocorrelation coefficient $c(\tau)$, $\tau=x_1-x_2$, for a Gaussian process is given by [2]

$$c(\tau) = \frac{\overline{\zeta_1 \zeta_2}}{\overline{\zeta_1^2}} \quad (D-14)$$

which has the property that $c(\tau)$ decreases monotonously from its maximum value $c(0)=1$ to its minimum value $c(\infty)=0$. The distance in which $c(\tau)$ drops to the value e^{-1} is the important parameter L , generally called the "correlation distance." In most analyses $c(\tau)$ is chosen somewhat arbitrarily to be

$$c(\tau) = \exp(-\tau^2/L^2) \quad (D-15)$$

although the approximate relation $c(\tau) \approx \exp(-|\tau|/L)$ was found by one autocorrelation study, using contour maps [13], to be more accurate. Another parameter of considerable significance is the root-mean-square height of the surface irregularities

$$\sigma = (\overline{\zeta^2})^{1/2} \quad (D-16)$$

A commonly used model of a nonsmooth planar surface is a sample function of a Gaussian random process with a reference surface of zero mean, i.e., $\bar{\zeta}=0$.

Results are derived [2] by use of the following assumptions:

- (1) The Gaussian random process is stationary.
- (2) Multiple scattering of the waves can be neglected.
- (3) Shadowing of some surface patches by other surface irregularities can be neglected.
- (4) The incident electromagnetic wave is a plane wave.
- (5) The scattered wave is received at a point sufficiently removed from the patch of surface which has scattered it so that this wave may also be considered plane.
- (6) The linear dimensions of the scattering surface are large compared to a wavelength λ .
- (7) The correlation distance is small compared to the linear dimensions of the scattering surface, but large compared to λ .
- (8) The radius of curvature of the surface irregularities are sufficiently large compared to λ so that the classical Kirchhoff approximation of the boundary conditions on the electromagnetic fields [2] at the surface may be used.
- (9) The reflecting surface is the surface of a perfect conductor.

A result derived by [2] from the above for specular reflection is for the average of the square of the absolute value of the specular scattering

coefficient. We shall use the preceding result as our mathematical model for ρ_s , i.e.,

$$|\rho_s|^2 = \exp(-g)$$
$$g = (4\pi\sigma\sin\gamma/\lambda)^2 \quad (D-17)$$

which is independent of L . The quantity \sqrt{g} (with or without the factor of 4π) is often referred to as the "apparent surface roughness." At the end of the derivation in [2] referred to above, a heuristic argument is given (see pp. 97-98 of [2]) that the same result applies to the surface of a lossy dielectric. The data to be presented supports this point of view.

Eq. (D-17) is plotted as the solid curve in Figure D-2 along with data points deduced from the work of many independent experiments, from Figure 14.1 of [2].

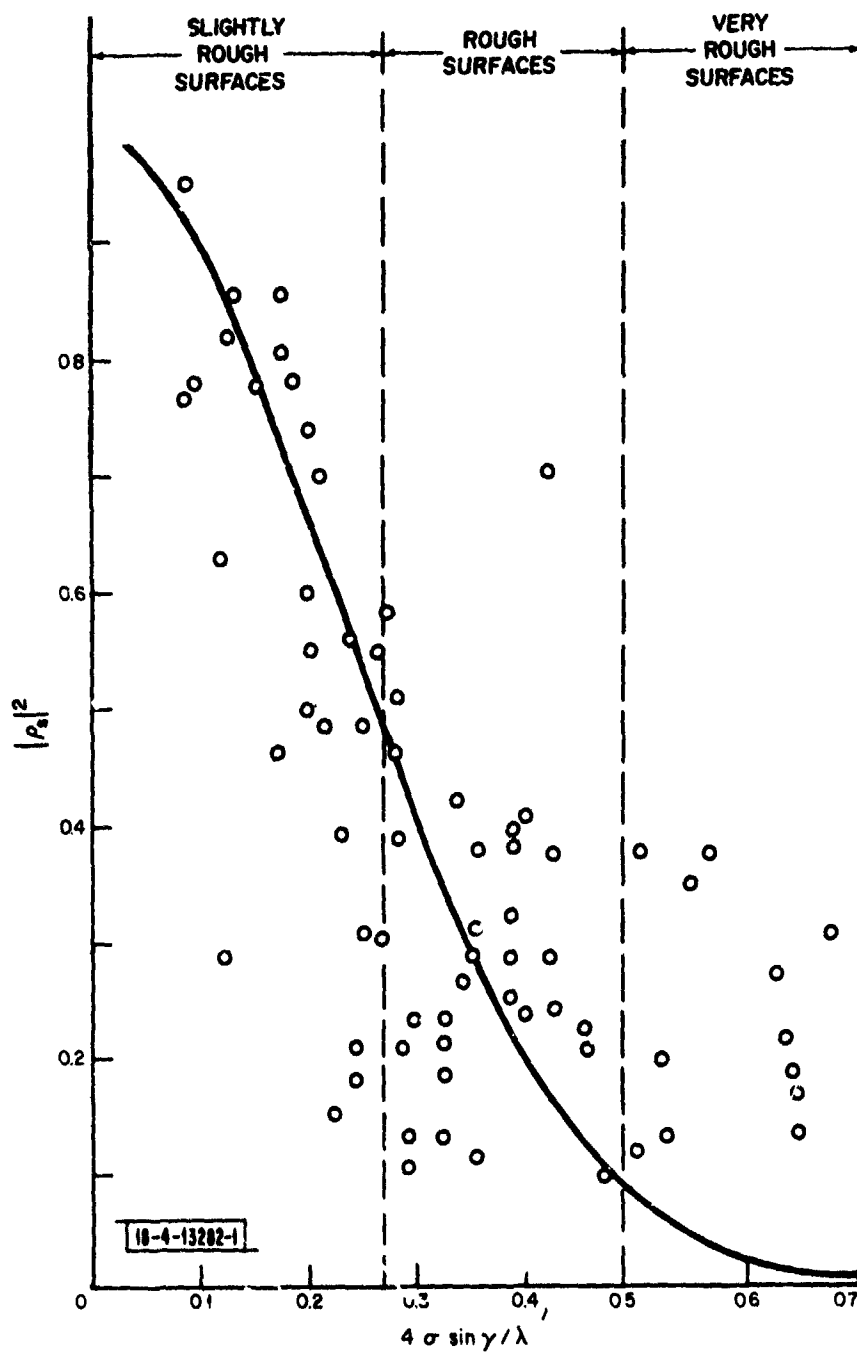


Fig. D-2. Roughness factor as a function of roughness and elevation angle.

Spizzichino [2] regards the scattering of the data points as due to several reasons:

- (1) The data are often given with little precision.
- (2) The measurement of R_s is often inaccurate, especially near 0 and 1.
- (3) There is inaccuracy in evaluation of R_0 .
- (4) The evaluation of σ is often even more inaccurate.
- (5) Most points with $\Delta\phi > 0.4\pi$ very probably correspond to diffuse scattering or to a combination of specular and diffuse scattering since the authors of the data sometimes give values without making it clear to which of the two types it corresponds.

Nevertheless, the data is considered [2] to substantiate the theoretical result of Eq. (D-17). It is pointed out in [2] that the data points in Figure D-1 were obtained by different measurement techniques used over land and over sea, in plane and hilly country; and in different climates, countries, and continents. This, indeed, adds great generality to the results,

Further strong support for the above point of view, and justification for Eq. (D-17), is given by the data on coherent reflection in Refs. [11,12] of which the data in [12] is reproduced below in Figure D-3. From our earlier comments this data should measure the specular scattering coefficient and is plotted in that manner. The solid line represents $\exp(-g/2)$, and the horizontal coordinate $\alpha\gamma/\lambda = \sigma \sin\gamma/\lambda$.

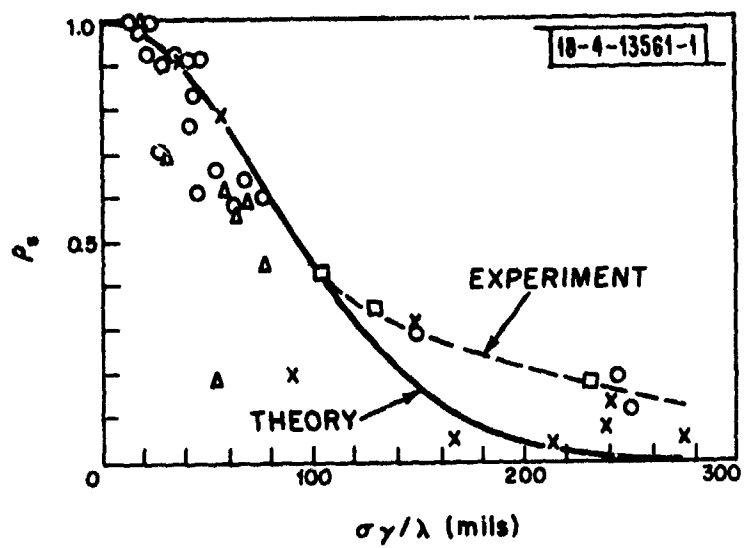


Fig. D-3. The specular scattering coefficient vs apparent ocean roughness.

There are portions of the curve in Figure D-3 which go below the data points. The author [3] observes that this departure begins at precisely that point at which the curve of incoherent reflected field strength vs. apparent surface roughness changes character and conjectures that a single mechanism* is responsible for these phenomena. There has been no further work published, to the knowledge of the present author, which investigates this conjecture.

D.3 DIFFUSE REFLECTIONS

There are the results of a number of experiments which can serve as useful guides for constructing a first-order model for diffuse reflections. The data described in Section 15.2 of [2] (which includes data taken at 1 GHz), which is taken by Spizzichino as verification of the theory given in Section 12.4.3 of [2], suggests that for very rough surfaces

$$\left(\overline{|\rho_r|^2} \right)^{1/2} = (\rho_r)_{\text{RMS}} \approx 0.35 \pm 0.15 \quad (\text{D-18})$$

i.e., ρ_r is a number, independent of $\sigma \sin \gamma / \lambda$ (the apparent surface roughness), and independent of the relative position of the receiving antenna. The distribution of $(\rho_r)_{\text{RMS}}$ from a variety of experiments are shown on page 336 of [2].

Eq.(D-18) gives an asymptotic result for $(\rho_r)_{\text{RMS}}$ for "large" $4\pi\sigma \sin \gamma / \lambda$.

$(\rho_r)_{\text{RMS}}$ for "low" and "intermediate" values of $4\pi\sigma \sin \gamma / \lambda$ can be estimated reasonably well from the data on incoherent scatter discussed by Beard, Katz,

* Multiple scattering, which is neglected in the derivation of Eq. (D-17).

and Spetner [11], and by Beard [3,12] which is illustrated in Figure D-4. The vertical coordinate of the original figure in [12] has been rewritten in our present notation $(\rho_r)_{\text{RMS}}$. These data were taken over water under varying sea-state conditions and at various frequencies. The solid curve represents a good estimate for a first-order model. If a transmitting and receiving antenna were in relative motion over a rough soil it is plausible to assume that the diffuse multipath would have a similar character to that measured by fixed antennas over a time-varying nonsmooth sea.

We have been unable, to date, to find a theoretical result which predicts the data on $(\rho_r)_{\text{RMS}}$. A simplified, heuristic derivation is offered in a footnote on page 340 of [2] but the description is too brief and ambiguous to reconstruct. As a heuristic alternative, one useful simple first-order model is given by

$$\overline{|\rho_r|^2} = 0.25[1 - \exp(-g)] \quad (\text{D-19})$$

Calculations from this simple model are compared with the mean value of Beard's data [3] are illustrated in Figure D-5. Although the curves for the model and for the experimental data do not correspond in all details, the first does predict the trend of the second with reasonable accuracy in the slightly rough surface and rough surface cases and will yield the correct asymptotic value for very rough surfaces. The geometry is such that the altitudes of the transmitting and receiving antennas are small compared to their separations.

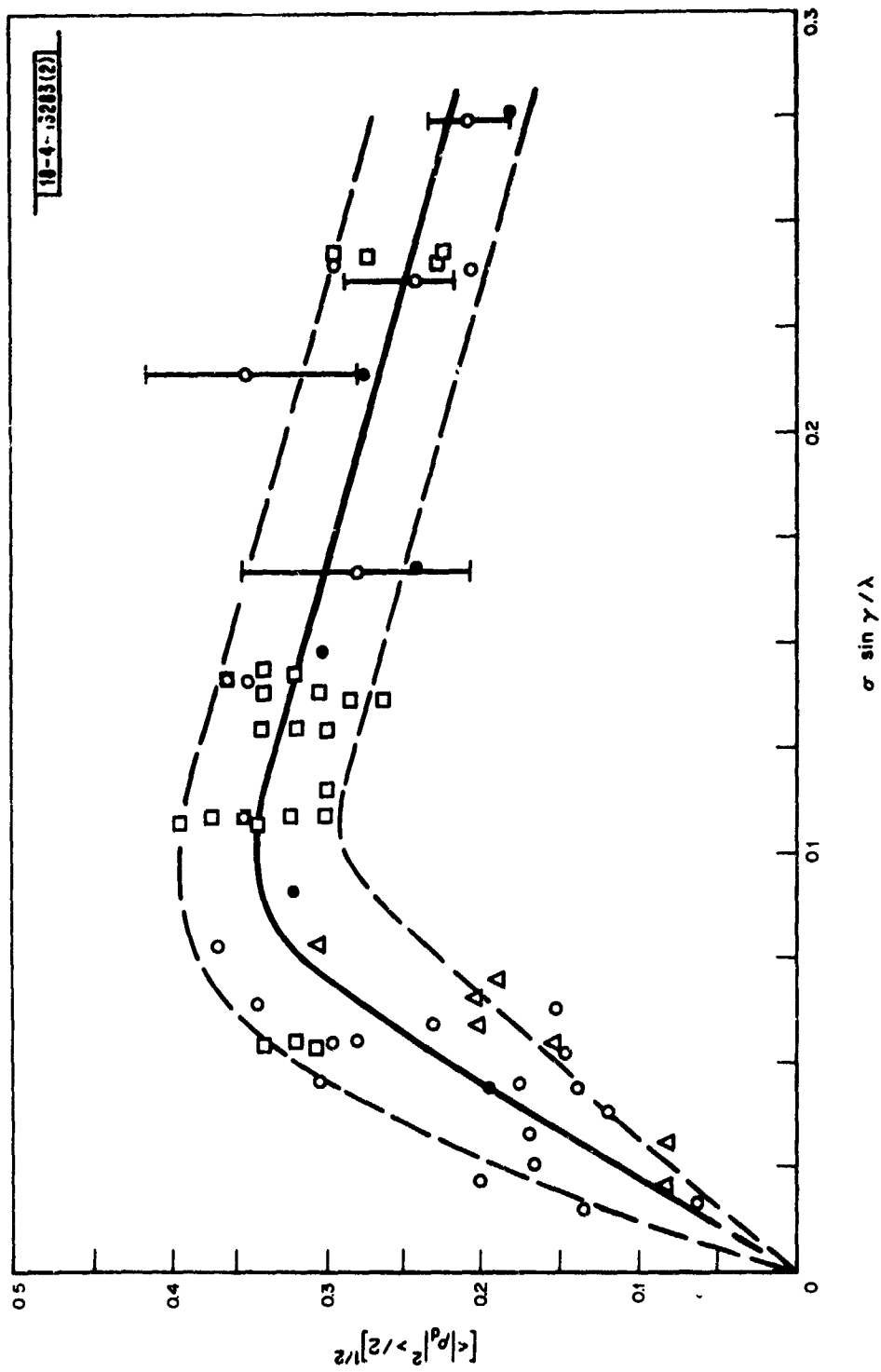


Fig. D-4. The RMS value of diffuse scattering coefficient vs apparent occur roughness (from data in [5]).

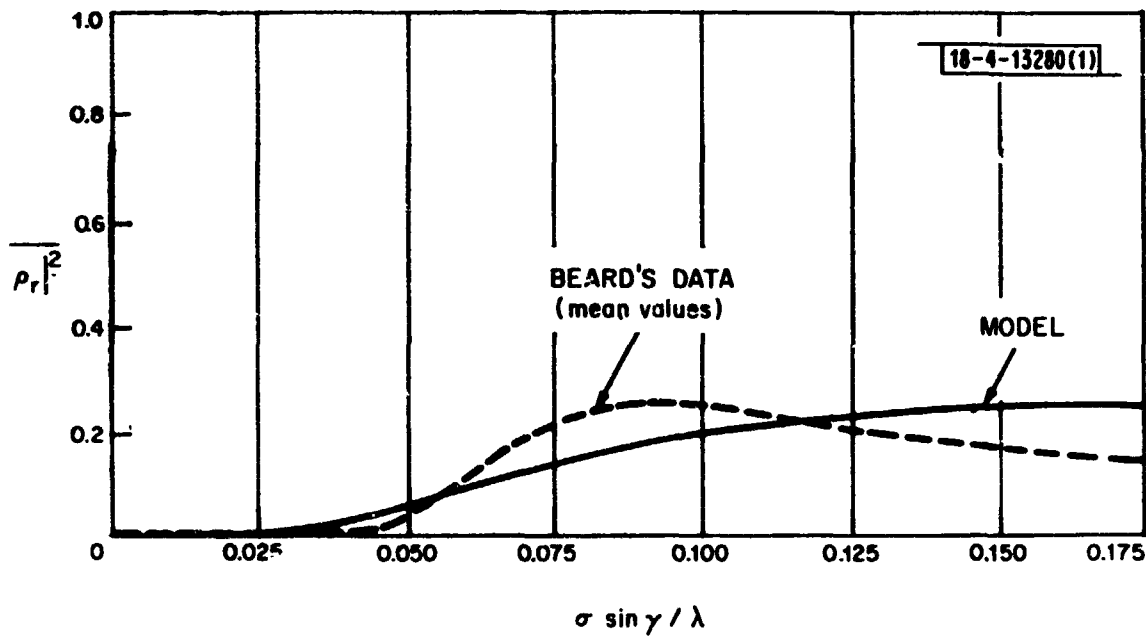


Fig. D-5. The scattering coefficient of diffuse power reflected vs apparent surface roughness.

From all of the preceding, a composite figure may be constructed for the scattering coefficients of the specular and diffuse reflected power. This is shown in Figure D-6.

The preceding holds when the altitudes of the transmitting and receiving antennas are small compared to the distance between them. In the satellite-aircraft case, Jordan finds theoretically [14] from the asymptotic evaluation of the appropriate integral*, that the diffusely reflected power is

$$P_r = D^2 |R_0|^2 (1 - e^{-g}) P_i \quad (D-20)$$

where P_i is the incident power. However, the experimental results reported in [14] show smaller values of P_r than indicated by Eq. (D-20) but larger than that modelled by Eq. (D-19). From the data in [14] the $\overline{|p_r|^2}$ curve in Figure D-7 was constructed. This data may be simply modelled by

$$\overline{|p_r|^2} = 0.5 [1 - \exp(-g)]^2 \quad (D-21)$$

* Private communication.

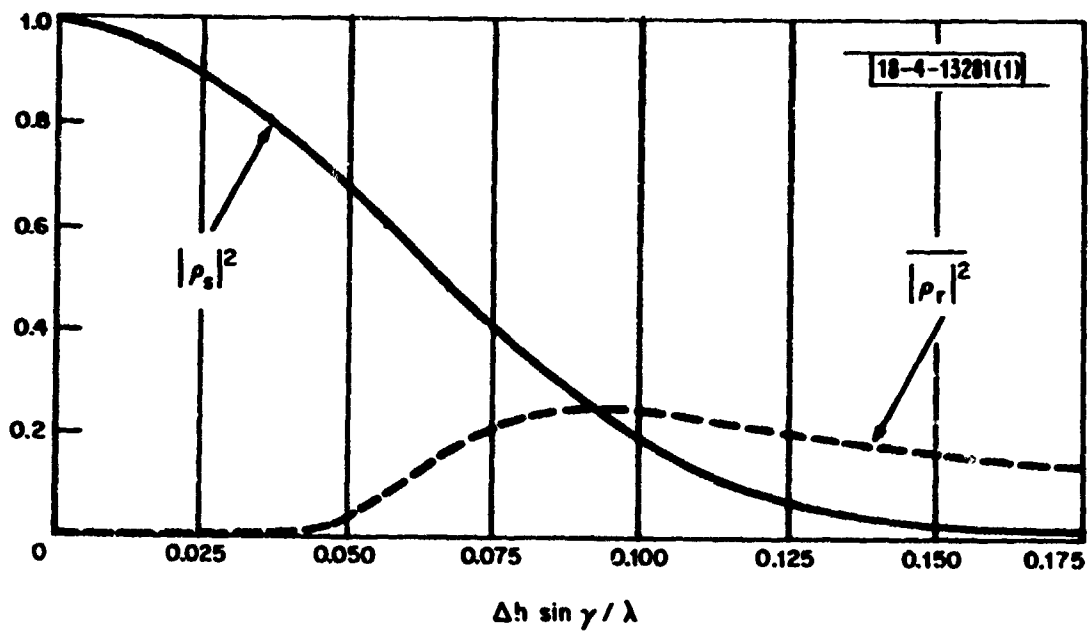


Fig. D-6. The scattering coefficient model for specular $|\rho_s|^2$ and diffuse $|\rho_r|^2$, power reflection.

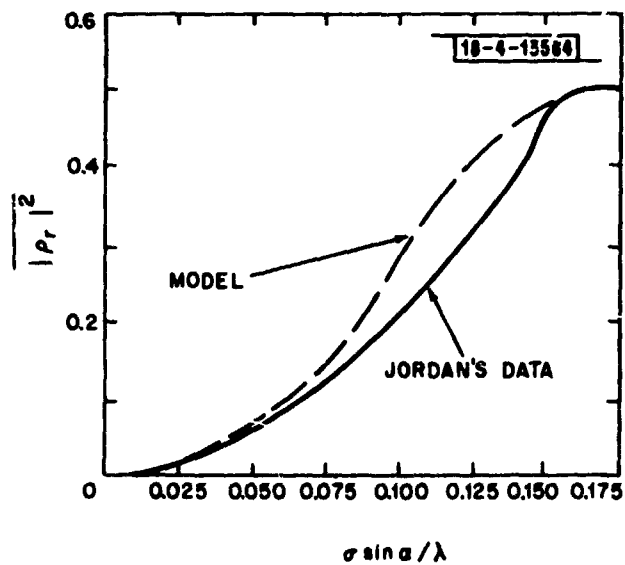


Fig. D-7. The diffuse scattering coefficient vs apparent surface roughness for satellite-aircraft geometries. The data from fig. 11 of reference 9 was used to construct the smooth curve. The model is from Eq. 21.

APPENDIX E

COMBINING OF DIVERSITY OUTPUTS

In this Appendix we discuss some methods of suitably combining the antenna (frequency diversity) outputs so as to alleviate ground reflection multipath fading. Our objective here is to demonstrate that the change $\Delta\phi_{L0}$ in the direct-reflected signal phase [cf (4) and (13)] given by Figure 10 ($\Delta\phi_{L0} = \sin^{-1} \rho$ where the fade margin = $20 \log_{10} \rho$) suffices for situations other than that shown in Figure 10.

First, we observe that if no combining of the antenna outputs is accomplished, then situations can arise in which a value of $\Delta\phi_{L0}$ twice that in Figure 10 is required. As an example of this, we consider Figure E-1. If the angle β between E_r and E_d is $-\Delta\phi_{L0} + \epsilon$ (where $\epsilon \ll \Delta\phi_{L0}$) at the lowest antenna of the set of antennas, then it is not sufficient for Δh_r to be such that there is $\Delta\phi_{L0}$ relative phase lag between E_r and E_d at a higher antenna because this would not insure that the desired fade margin is obtained. Rather, Δh_r would have to be such that there is $2\Delta\phi_{L0}\epsilon$ relative phase lag between E_r and E_d at the higher antenna to obtain the desired fade margin.

However, with suitable combining of the two antenna outputs, it is possible, in principle, to achieve alleviation of fading with the value of $\Delta\phi_{L0}$ given by Figure 10. One such scheme (suggested by the results in [8]) assumes that a good estimate of the relative phase between the diversity (e.g. antenna) outputs can be obtained such that the rf vector outputs can be combined in phase

(e.g., by use of a ferrite phase shifter). With this scheme utilized for the case illustrated in Figure E-1, analysis shows that the minimum phase lag required, is slightly less (typically 1%) than that required in Figure 10.

A somewhat simpler scheme for combining antenna outputs is shown in Figure E-2. This system achieves performance quite comparable to that phase estimation scheme discussed above. For example, at a 10 db fade margin, the system shown in Figure E-2 requires a $\Delta\phi_{L0}$ 15% larger than that given by Figure 10 (thus, necessitating an antenna separation 15% larger for fixed geometry or alleviation down to angles 15% larger). For a 3 db fade margin, the value of $\Delta\phi_{L0}$ would be 27% larger than that given by Figure 10.

In view of the closeness of the value of $\Delta\phi_{L0}$ based on Figure 10 to the values required for the above combining schemes, it was decided to use the $\Delta\phi_{L0}$ values obtained from Figure 10 for the numerical calculations. However, we should note two limitations of our diversity combining analysis:

- (1) For communications applications, the diversity scheme should alleviate all reductions in signal-to-noise ratio (SNR) below the specified fade margin rather than simply reductions in signal level. The extent to which the combining schemes discussed above achieve the desired SNR improvement will depend on the details of the particular receiver equipment being utilized.
- (2) With frequency diversity, the above combining schemes may be difficult to implement operationally. If this is the case and no other suitable combining schemes are

18-4-14772

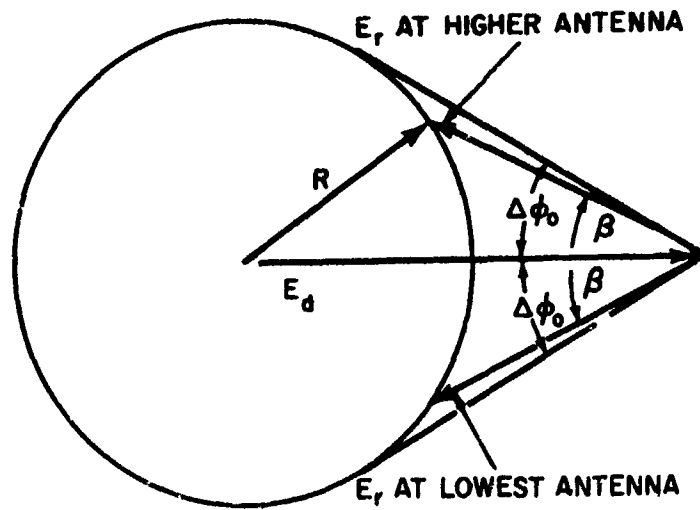


Fig. E-1. The geometry of direct and reflected electric fields at the lowest antenna and at a higher antenna.

UPPER
ANTENNA

18-4-14752

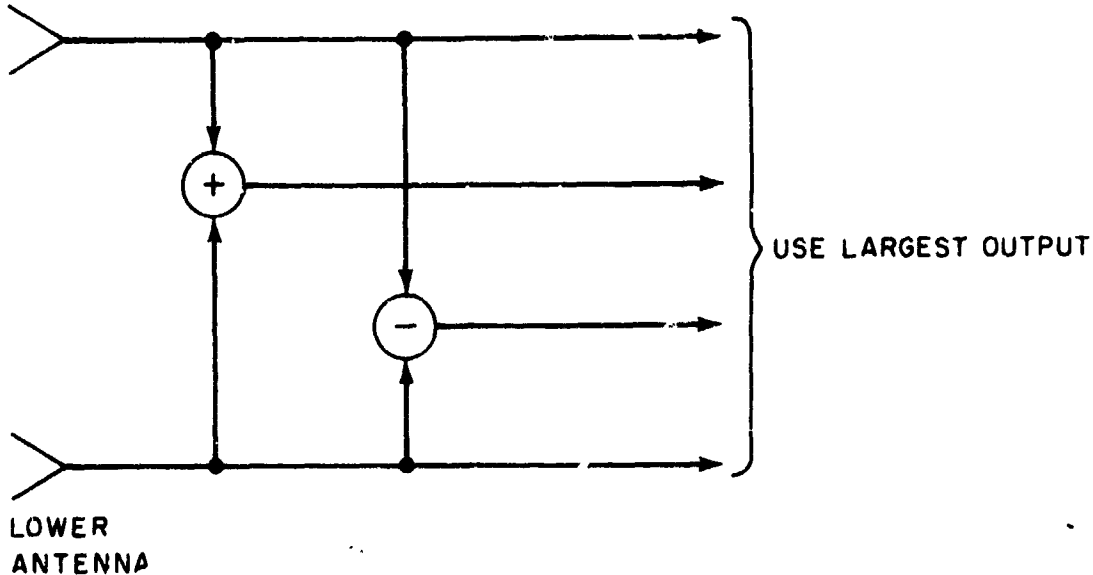


Fig. E-2. Possible antenna diversity combining scheme.

utilized, then the value of $\Delta\phi_{L0}$ used for frequency diversity [in (29)] would have to be twice that used for antenna diversity. Thus, one would have to use a $\Delta f = 20$ MHz to achieve the improvement shown here for $\Delta f = 10$ MHz.

REFERENCES

- [1] D. E. Kerr, editor of Propagation of Short Radio Waves, (McGraw-Hill, New York, 1951).
- [2] P. Beckmann and A. Spizzichino, The Scattering of Electromagnetic Waves from Rough Surfaces, (Macmillan, New York, 1963).
- [3] C. I. Beard, "Behavior of Non-Rayleigh Statistics of Microwave Forward Scatter from a Random Water Surface," IEEE Trans. Antennas Propag., AP-15, 649 (1967).
- [4] M. I. Skolnik, "Sea Echo," Chap. 26 in Radar Handbook, M. I. Skolnik, ed. (McGraw-Hill, New York, 1970).
- [5] B. R. Bean and E. J. Dutton, Radio Meteorology, Monograph 92, (National Bureau of Standards, Boulder, Colorado, 1966).
- [6] M. S. Wong, "Refraction Anomalies in Airborne Propagation," Proc. IRE, 46, 1628 (1958).
- [7] H. R. Reed, and C. M. Russell, Ultra High Frequency Propagation, (Chapman and Hall, London, 1965).
- [8] A. Johnson, "Test Report on UHF Airborne Antenna Combiner," Air Force Avionics Laboratory, Report AA1 TM-72-4, (February 1972).
- [9] N. I. Durlach, "Influence of the Earth's Surface on Radar," Technical Report 373, Lincoln Laboratory, M.I.T., 18 January 1965, DDC AD-627635.
- [10] R. K. Moore, "Ground Echo," Chap. 25 in Radar Handbook, M. I. Skolnik, (McGraw-Hill, New York, 1970).
- [11] C. I. Beard, I. Katz, and L. M. Spetner, "Phenomenological Vector Model of Microwave Reflection from the Ocean," IRE Trans. Antennas Propag., AP-4, 162 (1956).
- [12] C. I. Beard, "Coherent and Incoherent Scattering of Microwave from the Ocean," IRE Trans. Antennas Propag., AP-9, 470 (1961).
- [13] H. S. Hayre and R. K. Moore, "Theoretical Scattering Coefficient for Near Vertical Incidence from Contour Maps," J. Res. Natl. Bur. Std. 68D, 427 (1961).
- [14] K. L. Jordan, Jr., "Multipath Characteristics in a Satellite-Aircraft Link at 230 MHz," NATO TACSATCOM Scientific Group Mtg., London, 15-19 September 1969.
- [15] J. L. Katz, "Performance of Spread Spectrum Modulation in a Multipath Environment," Technical Note 1972-28, Lincoln Laboratory, M.I.T. (21 July 1972), DDC AD-747481.